UNIVERSITÁ DEGLI STUDI DI PADOVA

FACOLTÁ DI INGEGNERIA

DIPARTIMENTO DI INGEGNERIA MECCANICA, SETTORE MATERIALI

CORSO DI LAUREA MAGISTRALE IN INGEGNERIA DEI MATERIALI

TESI DI LAUREA

NEW ORGANIC-INORGANIC SOL-GEL RESISTS FOR MICRO AND NANOIMPRINTING

Relatore: Dott.essa GIOVANNA BRUSATIN

Correlatore: Dr. VAIDA AUZELYTE

Laureanda: Agnese Virginia Savegnago

Matr. n. 602408

Anno Accademico 2010/2011

Ai miei fratelli Giovanni e Giacomo

Fatti non foste a viver come bruti, ma per seguir virtute e canoscenza.

(Divina Commedia, Inferno, Canto XXVI)

INDEX

INTRODUCTION

The research activity on new lithographic resist materials, alternative to widespread used polymeric systems, has known increasing development in recent years, in particular as regards the synthesis of sol–gel resists with innovative properties and suitable to avoid a material sacrificial use in the lithographic process and to satisfy specific performance demands (i.e. refractive index, porosity, etc.).

The sol–gel synthesis is an economic, relatively fast and effective method for a film realization. Among the most attractive features of a sol–gel processing, it is worth to mention the low process temperatures (typically <200 °C), the possibility to obtain large surface coatings, homogeneous multicomponent oxide films and the relatively cheap experimental setups required for material synthesis and deposition. In particular titanium dioxide (TiO_2) sol-gel materials have been extensively investigated for its potential application in solar cells, optical waveguides, photonic crystals and gas sensors. One of the hindrances for miniaturization of these devices is the lack of an easy and reliable way of TiO_2 patterning. Conventional methods such as photolithography, electron beam lithography or ion beam lithography can be used for the fabrication of nanopatterned TiO_2 thin films, but they are too costly to use in many applications. Furthermore, a number of drawbacks remain, such as low throughput and unsuitability of these methods for large-area patterning. Many research efforts have been directed towards other lithographic techniques as nanoimprint lithography (NIL). Nanoimprint lithography (NIL) is a promising technique for generating nano- and microstructures. However, its progress is closely linked to the availability of suitable resist materials. In fact, although nanoimprint lithography is a well-established technique for patterning organic materials, it has not found a *niche* in direct patterning of inorganic compounds, especially oxides. This is primarily due to the fact that these are hard materials and do not have a workable softening point.

There are two major challenges in the direct imprinting of sol–gel materials. Firstly, sol-gel precursors have high surface energy thus requiring a good mold release system, and secondly, the solvent in the sol-gel material, which helps to ‘soften’ it for the imprint process, gets trapped in the imprinted structures, resulting in poor demolding and incomplete filling of the precursor material inside the mold.

In this study new hybrid organic-inorganic TiO_2 sol-gel materials with high TiO_2 content (more than 50% respect silicon dioxide (SiO_2) content) are synthesized, characterized and

micro-/nano-patterned using thermal nanoimprint lithography.

Two different preparation methods are elaborated to produce hybrid TiO_2 sol-gel materials. In the first approach TiO_2 domains are incorporated into organic resin using the sol–gel method (in-situ synthesis). This process is based on the hydrolysis and condensation of precursors such as metal alkoxides to prepare network-like hybrid materials. The second approach to prepare TiO_2 hybrid materials is incorporating commercial purchased anatase TiO_2 nanoparticles into organic resins (ex-situ synthesis). By exposing these two materials to the UV light, it is possible to obtain crack-free purely inorganic films, having a thickness up to few micrometers using only one spin-coating step. The spin-coated films have been characterized using UV-vis and FTIR spectroscopy, profilometry, X-ray diffraction and ellipsometry to evaluate their physical and structural properties. Viscosity studies have been performed to understand the rheology during imprinting. While scanning electron microscope (SEM) and AFM have been utilized to analyze imprint results.

Fabrication of micro and nanostructures of hybrid TiO_2 in-situ and ex-situ sol-gel materials by thermal nanoimprint lithography has been demonstrated. Using mold copies made by Ormostamp®, ordered arrays less than 100nm wide lines and dots are created.

1. NANOTECHNOLOGY

A novel branch of technology, nanotechnology, arose in 1959 when Richard Feynman gave his famous talk at the annual meeting of the American Physical Society at the California Institute of Technology entitled "There is plenty of room at the bottom: an invitation to enter a new field of physics". With this visionary talk, Feynman anticipated a large spectrum of field that are now well established such as electron and ion beam fabrication, nanoimprinting lithography (NIL), quantum electronics, projection electron microscopy, nano- and micro-electromechanical systems (NEMS/MEMS) [1].

The word "nanotechnology" was used for the first time in 1974 by Taniguchi when he wanted to describe the technology which was operating in the nanometer range. The main goal of nanotechnology (which operates in the scale of 1-100nm) is to fabricate and use structures, devices, and systems that have innovative properties and functions due to their small or intermediate size. In general there are two different approaches for nanostructure fabrication. The first one, called the "top-down approach", includes different techniques (e.g. electron beam lithography, photolithography and NIL) which are focused on a progressive reduction of dimensions. The second approach, the "bottom-up approach", uses techniques (e.g. molecular self-assembly, carbon nanotube synthesis) in which nanostructures are assembled out of smaller units, like atoms or molecules [1]. In the following paragraphs, the "top-down approach", and in particular the micro- and nano lithography, will be specifically dealt with.

Several nanofabrication techniques are reported in the literature, but only a small percentage of them have the potential to be viable in volume manufacturing since manufacturing viability requires that the patterning approach have the following attributes [2]:

- Long-range order in nanostructures: this includes control of size of patterns and the location of the patterns with respect to an ideal grid.
- Patterning of arbitrary structures with varying pattern densities: a general-purpose lithography approach should be able to print varying types of features with varying pattern densities.
- Suited for fabricating highly integrated devices.
- Low process defectivity to achieve high overall product yield.

- Large area, high-throughput processes: this is critical for achieving acceptable data transfer rates in the manufacturing process to achieve cost-effective device manufacturing.

1.1. NANOLITHOGRAPHY

Nanolithography is the branch of nanotechnology concerned with the study and application of fabricating nanometer-scale structures. The miniaturization of objects and device components down to the micron- and nanometer-scale, and the development of methods to fabricate them, presents one of the main technological trends of the last decade. Various lithographic techniques ranging from conventional methods (called also photon-based top-down patterning techniques e.g. photolithography, electron beam lithography, X-rays) to unconventional ones (e.g. nanoimprint lithography) are used to create small features. In their turn, the “traditional” lithographic methods are divided into processes that use electromagnetic radiation (photolithography, EUV, XRL) and those which use "particles", whether electrons or ions (EBL, FIB). The main goal of lithography is to create a desired pattern in a resist layer and subsequent transfer of the pattern into or onto the underlying substrate. The basic steps of a lithographic process are schematically illustrated in Fig. 1.

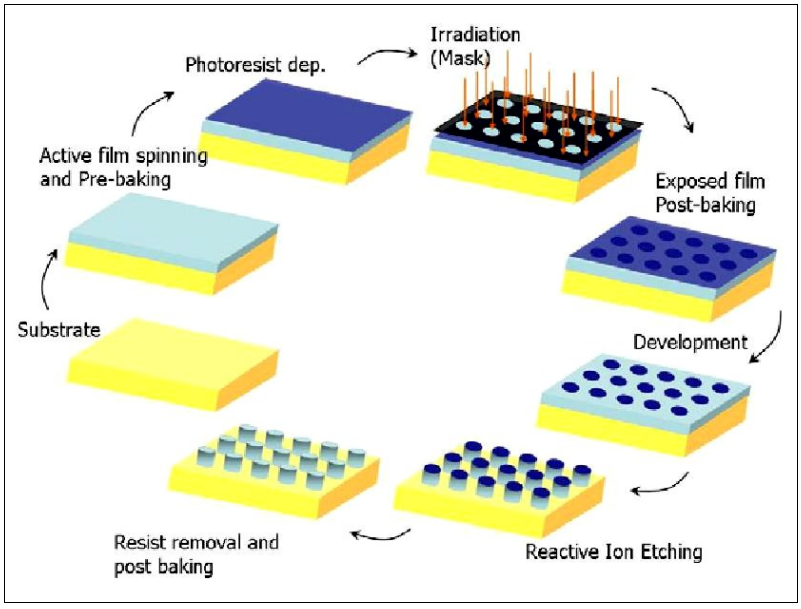

Fig. 1 Scheme of a conventional lithographic process.

First, the substrate (often silicon) is cleaned using chemical baths or plasma procedures in order to remove contaminants which may lead to poor adhesion or defects formation in the resist layer. In the next step, a resist layer is spin coated onto the substrate from a solution containing the resist dissolved in an appropriate casting solvent. After this, the sample is baked on a hotplate in order to remove the excess solvent from the resist and to thermally anneal residual stress in the resist built up during the spinning session. This step is referred to as a post-apply-bake (PAB). Next, assuming EBL, the sample is e-beam irradiated causing chemical changes in the exposed area which influence the solubility of the exposed area relative to the unexposed area of the resist in a developing solvent. Following e-beam exposure, the sample is baked again to either thermally anneal the exposed regions, in order to reduce unwanted chemical changes that might have been caused within the resist layer during the exposure, or to promote further chemical changes in the exposed or unexposed area. This step is referred to as a post-exposure-bake (PEB). Subsequently, the sample is developed through spray, puddle or immersion methods. A resist can have a negative or positive tone depending on whether the unexposed or the exposed regions are removed from the substrate during the development process. Usual the patterns obtained are transferred into or onto the substrate by using techniques such as etching of lift-off. Finally, the resist structures are removed via a liquid stripping process or dry oxygen plasma etch without altering properties of the layers beneath the resist [1].

1.2. CONVENTIONAL LITHOGRAPHIC METHODS

Top-down patterning with photolithography has been the workhorse of the semiconductor industry over 30 years. In addition to its continued improvement in resolution, the appeal of photolithography has been its long-range order, precision overlay, and its extremely high data transfer efficiency making it attractive in the manufacturing of large scale integrated devices. Extreme ultraviolet lithography (EUV) at 13,2nm (soft X-ray) wavelengths is being developed by the semiconductor industry to provide patterning capability of arbitrary nanostructures [2]. In addition to EUV, other high-throughput next generation lithography silicon IC fabrication techniques must be considered: X-ray lithography (XRL), electron beam lithography (EBL) and focused ion beam lithography (FIB).

1.2.1. Photolithography

Photolithography (or “optical lithography) uses light to transfer a geometric pattern from a photomask to a light-sensitive chemical photoresist on the substrate. The light shines through the photomask, which blocks it in some areas and lets it pass in others (Fig. 2). Typically photolithography uses ultraviolet light (UV light is electromagnetic radiation with a wavelength shorter than that of visible light, but longer than X-rays, in the range 10nm to 400nm, and energies from 3eV to 124eV).

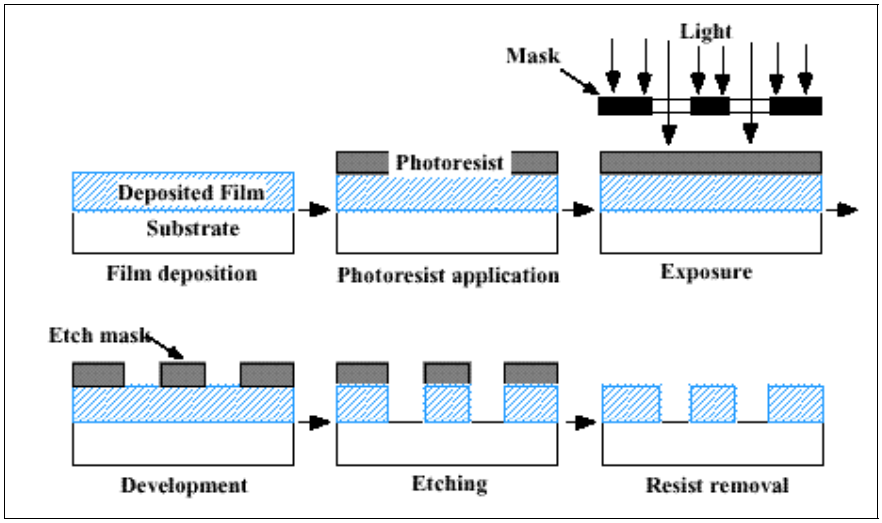

Fig. 2 Principal steps of a photolithography process.

Historically, ultraviolet light is produced by gas-discharge lamps using mercury, sometimes in combination with noble gases such as xenon. These lamps produce light across a broad spectrum with several strong peaks in the ultraviolet range. This spectrum is filtered to select a single spectral line, usually the "g-line" (436nm) or "i-line" (365nm). Generally, changing wavelength is not a trivial matter, as the method of generating the new wavelength is completely different, and the absorption characteristics of materials change. Furthermore, insulating materials such as silicon dioxide (SiO_2), when exposed to photons with energy greater than the band gap, release free electrons and holes which subsequently cause surface charging.

A mask or "photomask" is a square glass plate with a patterned emulsion of metal film on one side. The mask is aligned with the wafer, so that the pattern can be transferred onto the wafer surface. Each mask after the first one must be aligned to the previous pattern. Once the mask

has been accurately aligned with the pattern on the wafer's surface, the photoresist is exposed through the pattern on the mask with a high intensity ultraviolet light. There are three primary exposure methods: contact, proximity, and projection (Fig. 3).

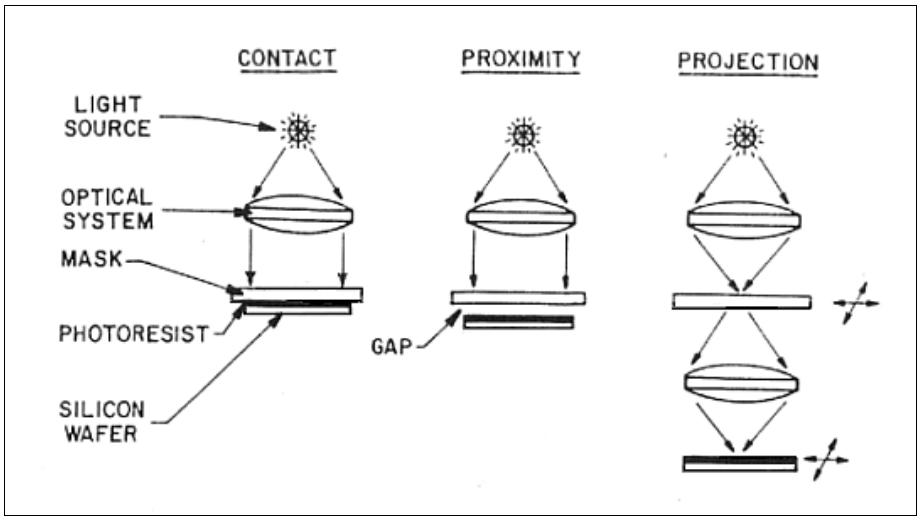

Fig. 3 Different exposure methods in photolithography.

Contact Printing. In contact printing, the resist-coated silicon wafer is brought into physical contact with the glass photomask. The wafer is held on a vacuum chuck, and the whole assembly rises until the wafer and mask contact each other. The photoresist is exposed with UV light while the wafer is in contact position with the mask. Because of the contact between the resist and mask, very high resolution is possible in contact printing. The problem with contact printing is that debris, trapped between the resist and the mask, can damage the mask and cause defects in the pattern.

Proximity Printing. The proximity exposure method is similar to contact printing except that a small gap, 10 to 25μm wide, is maintained between the wafer and the mask during exposure. This gap minimizes (but may not eliminate) mask damage.

Projection Printing. Projection printing, avoids mask damage entirely. An image of the patterns on the mask is projected onto the resist-coated wafer, which is many centimeters away. In order to achieve high resolution, only a small portion of the mask is imaged. This small image field is scanned or stepped over the surface of the wafer.

The most important figure of merit in the manufacture of integrated circuits is the critical dimension (CD). The critical dimension is the smallest feature that it is possible to pattern on

the surface. The ability to project a clear image of a small feature onto the wafer is limited by the wavelength of the light that is used, and the ability of the reduction lens system to capture enough diffraction orders from the illuminated mask. The minimum feature size that a projection system can print is given approximately by: $CD = k_1 \cdot \lambda / NA$, where CD is the minimum feature size, k_1 is a coefficient that encapsulates process-related factors, λ is the wavelength of light and NA is the numerical aperture of the lens as seen from the wafer. From this equation, to reduce the critical dimension of a lithography system, it is necessary: change the wavelength of the source, increase the numerical aperture (NA) or reduce k_1. An example of photonic patterns made by photolithography is shown in Fig. 4.

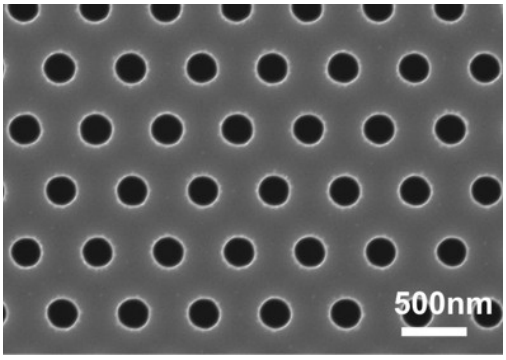

Fig. 4 SEM image of photonic patterns with hexagonal symmetry made of photolithography. Top-down image of 600nm-period hexagonal hole array etched to a depth of about 800nm in silicon.

1.2.2. Extreme UV lithography (EUV)

Extreme ultraviolet lithography is a next-generation lithography technology using an extreme ultraviolet radiation wavelength (generally defined to be electromagnetic radiation in the part of the electromagnetic spectrum spanning wavelengths from 120nm down to 10nm, and therefore having photons with energies from 10eV up to 124eV). For this selective wavelength, the radiation is obtained from laser induced plasma or synchrotron radiation. In fact neutral atoms or condensed matter cannot emit EUV radiation. The Xe or Sn plasma sources for EUV lithography are either discharge-produced or laser-produced [3].

All matter absorbs EUV radiation. Hence, EUV lithography needs to take place in a vacuum. All the optical elements, including the photomask, must make use of defect-free Mo/Si multilayer which acts to reflect light by means of interlayer interference; any one of these mirrors will absorb around 30% of the incident light.

The EUV systems contain at least two condenser multilayer mirrors, six projection multilayer mirrors, and a multilayer object (mask). Since the optics already absorbs 96% of the available EUV light, the ideal EUV source will need to be sufficiently bright. EUV source development has focused on plasmas generated by laser or discharge pulses. The mirror responsible for collecting the light is directly exposed to the plasma and is therefore vulnerable to damage from the high-energy ions and other debris. An example of 50nm-lines patterned by EUV is reported in Fig. 5.

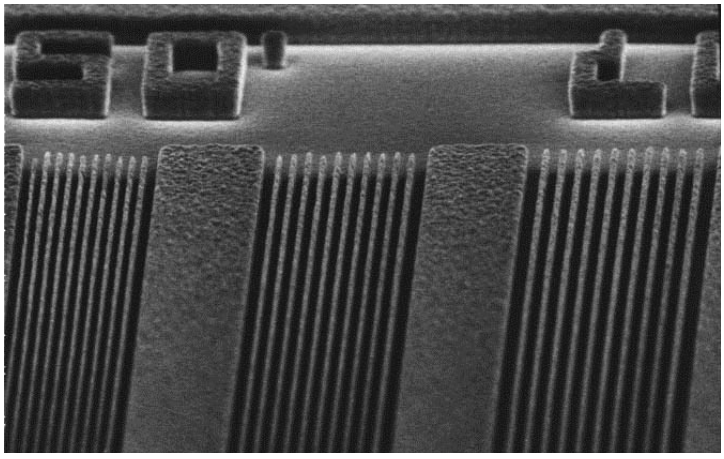

Fig. 5 SEM image of 50nm-lines patterned by extreme ultraviolet lithography.

The advantage of extreme UV lithography relies on its projection configuration and its high potentiality for several generation manufacturing. However, there are still many technological challenges to be overcome, including mask optimization, fabrication of high precision optical elements as well as engineering issues such as alignment, system metrology and feedback control.

1.2.3. X-ray lithography (XRL)

X-ray lithography uses X-rays (wavelength range from 0.5 to 4nm-soft X-ray) to transfer a geometric pattern from a mask to a light-sensitive chemical photoresist on the substrate. Having short wavelengths, X-rays overcome the diffraction limits of optical lithography, allowing smaller feature sizes. Because it's difficult to use optical diffraction components for imaging in the X-ray regime, X-ray lithography is carried out as a simple 1:1 shadow projection technique with a proximity gap between mask and substrate. The X-rays illuminate

a mask placed in proximity of a resist-coated wafer [4].

Exposure can be done with synchrotron radiation or laser-induced plasma source.

The mask consists of an X-ray absorber, typically of gold or compounds of tantalum or tungsten, on a membrane that is transparent to X-rays, typically of silicon carbide or diamond.

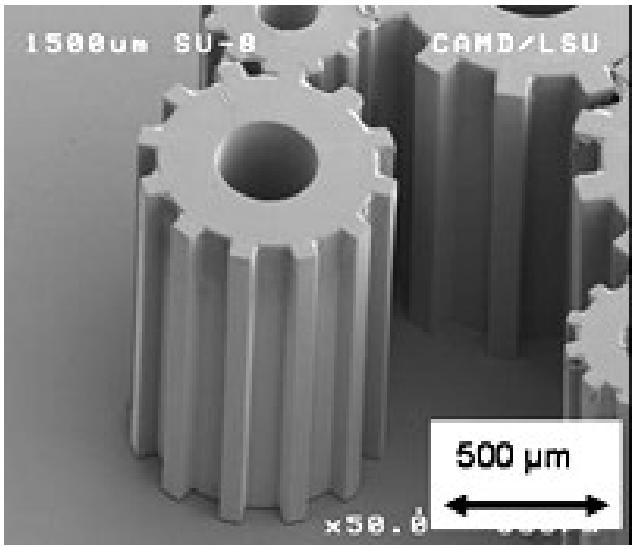

Fig. 6 A polymer microstructure patterned by X-ray lithography.

The X-ray lithography is nearly ready for industrial use, but some technical issues remain open, such as the mechanical and radiation stability of the mask, the availability of high throughput e-beam system for mask making and the reliability of high accuracy alignment.

1.2.4. Electron beam lithography (EBL)

Electron beam lithography provides excellent resolution due to the small wavelength and a small probe size, whereas the resolution in optical lithography starts to become limited by the wavelength of the light that is used for exposure. The main drawback of EBL is that it is slow and too expensive for volume manufacturing. The main characteristics an e-beam pattern generator should have are: a small spot size (down to a few nm), low cost (high throughput), high yield and the ability to write reproducible structures over large areas. There are two main e-beam writing strategies: projection printing and direct writing. In projection printing, a large e-beam pattern is projected parallel through a mask onto a resist coated substrate by using g a high-precision lens system. In direct writing, a small e-beam spot is moved with respect to the

wafer to expose the wafer one pixel at a time, eliminating the expensive and time-consuming production of the masks [5].

A typical e-beam system consists of a column of electron optics for forming and controlling the electron beam, a sample stage and control electronics. The column includes principally an electron source, magnetic lenses, a beam blanker and a mechanism for deflecting the beam. Depending on the design, e-beam energy varies in the range of 1-100keV with a spot size down to a few nanometers.

SEM images of multi-layer line-array patterned using EBL are shown in the figure below.

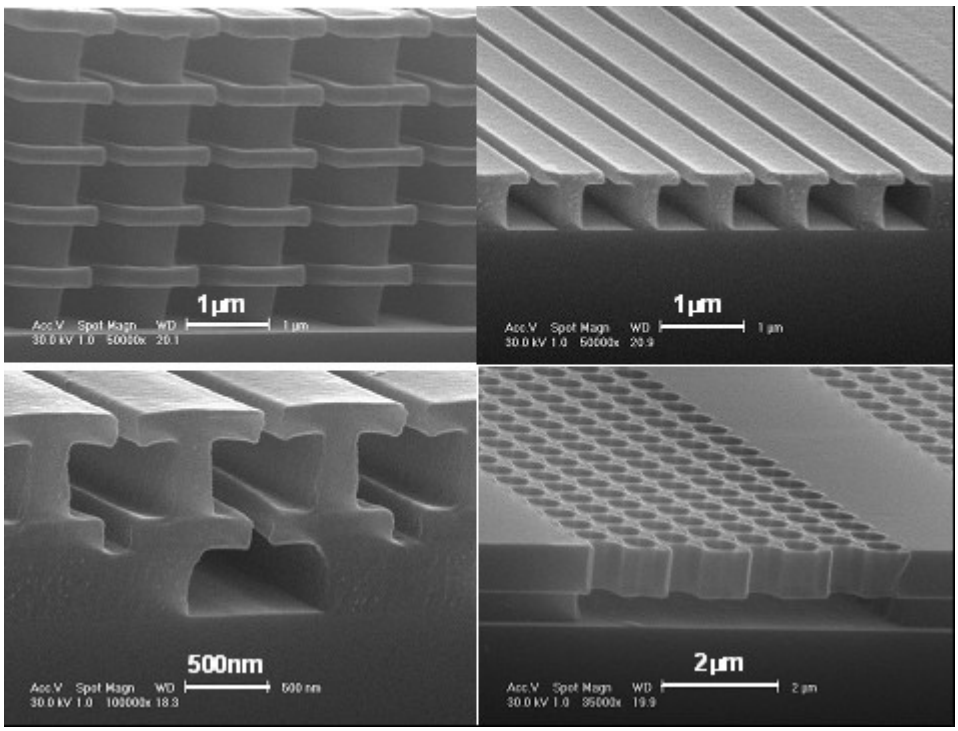

Fig. 7 SEM images of multi-layer line-array structures made of electron-beam sensitive polymers. These structures can serve as 3D photonic crystals (upper-left image) and quasi-3D suspending slab photonic crystals (lower-right image). The structures were fabricated by e-beam lithography with single- step 100keV-exposure, and multiple-development steps [6].

In a resist, electrons undergo small angle forward scattering and some back-scattering events coming from the substrate. The forward scattering tends to broaden the initial beam diameter, whereas the back-scattering can spread over a large volume. During this process, the electrons are continuously slowing down, providing a cascade of low-energy electrons (secondary electrons) which are responsible for the resist reaction. Finally, the dose distribution looks like

a sharp peak of the forward contribution superimposed with a back-scattered fog. The secondary electron-induced resist reaction can be polymerization, polymer cross-linking or chain scissor as well as more complex processes.

Most exposures are performed with high-energy electrons (between 50 and 100keV) because they provide high resolution. In fact, the higher the energies, the smaller the minimum feature size is obtainable. The back-scattered electrons from the substrate cause exposure of areas in the proximity of the intended pattern (proximity effect), which in most cases can be corrected. In e-beam lithography at low energy (between 2 and 20keV), the penetration depth of electrons is limited. In this case, electrons will lose almost all their energy in the resist layer, increasing the exposure efficiency and the throughput of the lithography tool, but at the expense of a high resolution. Also, the proximity effect is reduced due to the miniaturization of the electron scattering effect from the substrate. Still there are several disadvantages when using low acceleration voltages, for example an increase in the beam size, the requirement to use very thin resist layers or charging effects. If a thick resist layer is used, it is possible that electrons (which have a low penetration depth at low voltage) expose only a fraction of the resist thickness. During the development process, the unexposed underlying resist layer might be dissolved leading to a pattering failure [1].

The most important properties that an e-beam resist (and more generally all lithographic resist) must have in order to become a suitable candidate for nanolithography are [1]:

Electron dose is the number of electrons per unit area required to achieve the desired chemical response in the resist. Each lithographic process has an optimum dose which represents the dose at which the measured linewidth after development is equal to the designed linewidth. When a pattern is exposed at lower doses compared to the optimum (underexposure), the actual structure width is smaller than the designed structure width. The main consequence of overexposure (dose higher than the optimum dose) is a widening of the pattern size. In general, the electron dose should be low in order to achieve high sensitivity and throughput.

Process latitude. The process latitude (PL) represents the change in the critical dimension (CD) for a given change in the exposure dose and it is given by the following expression: $PL(\%)=100(D_{[+10\%]}-D_{[-10\%]})/D_{[0\%]}$ where $D_{[0\%]}$ represents the optimum dose and $D_{[\pm 10\%]}$ are the doses corresponding to a 10% increase or decrease in the feature size.

Contrast and sensitivity. In general, the e-beam resist is characterized by contrast curves, which can be easily obtained by plotting the remaining thickness after the development process versus the electron dose. An ideal resist should have both a high contrast and a high sensitivity. Unfortunately, in reality, an increase in one of these parameters leads to a decrease in the other, and vice versa. A high sensitivity will provide a high throughput (e.g. reduction of the writing time), but in general it leads to a shallower slope for the contrast curve, hence a lower contrast.

Contrast (γ) is defined as the slope of the linear portion of the falling edge (positive resist) of the remaining resist thickness versus log(dose) curve: $\gamma=1/\log (D_1/D_2)$ where D_1 is the maximum dose at which still no film is lost and D_2 is the minimum dose at which all the resist thickness is lost. The sensitivity is defined as the dose for which all of the resist is removed (D_2).

Line edge roughness (LER). For nanolithography, the LER should be as small as possible in order to avoid pattern distortion or deterioration of the resolution. The LER is caused by various factors which range from the lithographic system (dose fluctuation, mask roughness) to resist materials and the development process. Nevertheless, the main cause for LER is represented by the polymer aggregates which are naturally present in all resist layers. The presence of the polymer aggregates causes uneven dissolution rates between the aggregates and the surroundings area, due to the density difference between these two regions. The surrounding areas of the aggregates, which have a lower density than the polymer aggregates, are quickly and complete dissolved. After that, the aggregated polymers are extracted from the surface, although it is possible that the dose is too low to achieve complete development. A higher dose might limit the effect of the aggregates but it cannot complete eliminate the trapping of the aggregates at the edge of the pattern. At the edge of the pattern, aggregates are not extracted and remain trapped in the sidewall after development process. This is due to the low dose received by the sidewalls, impeding the dissolution of the areas which surround the aggregates. As a consequence, the shapes of the polymer aggregates appear at the edge of the pattern, causing LER. One way to overcome this limitation for nanolithography is to use resist with small molecular size which implies small aggregated polymers.

Resolution. The resolution (i.e. the capability of resolving very small features) of e-beam resists should also be high. Therefore, the resist should be very thin to minimize electron

scattering, which is the resolution-limiting factor when very small structures are desired. In general, the patterned structures are lines and the repeating distance between adjacent features is called "the pitch". The lines can be classified into isolated (when the designed feature width is much smaller than the pitch) or lines and spaces (when the designed feature width is equal or bigger than the pitch). When the pitch of the features decreases, achieving high resolution becomes a real challenge.

Line width control and the reproducibility is the ability to maintain the same feature size across an entire sample and from one substrate to another, respectively, when the electron dose is kept constant.

Etch resistance represents the ability of the resist to withstand an etching process and it is probably the most difficult requirement to achieve for a resist. After development, the pattern is usually transferred into the underlying layer or substrate by either a wet or dry etch process. Although wet etching offers high throughput and good selectivity, it can also cause a loss of adhesion of the resist, due to the interaction between the etchant solution and the resist itself. Moreover, wet etching is isotropic which means that the etching rate is equal in all directions. As a consequence, under-etching will not only alter the size of the transferred pattern, but will also lose the vertical, anisotropic sidewalls. All these problems seem to be solved by using a dry etching process. In this case, a vertical profile is obtained, resulting in exact replication of the pattern in the underlying layer or substrate.

Process window. It is well known that the resolution is limited by various factors such as baking temperature, resist material, delay time between baking and exposure, electron dose and the development process. The process window is just an indication of how much these factors can be varied without causing any appreciable loss in resolution or distortion of the pattern. If a resist has a wide process window for a certain factor mentioned above, that means that this factor might be varied, but that it will not cause a major change in the resulting pattern.

1.2.5. Focused ion-beam lithography (FIB)

Focused ion beam lithography is analogous to electron beam lithography, it scans an ion beam, instead of electrons beam, across a surface to form a pattern. The ion beam may be used for directly sputtering the surface, or may induce chemical reactions in the exposed top

layer.

The ion source is typically made of a sharp W-tip coated with liquid metal. In addition, a mass separator is used as an aperture to select one type of ion.

As the ions penetrate the material, they loose their energy at a rate of several order of magnitude higher than of electrons because of their heavy masses. As a consequence, the penetration of ions and thus the back-scattering-caused proximity effects, are much more reduced compared to that of electrons. The heavier the ions, the smaller is their penetration depth. In practice, light ions such as H^+, He^{++}, Li^+ and Be^{++} are employed for lithography. The drawback of FIB is its limited writing speed, due to the fact that the ion beam current density is one or two order of magnitude smaller than the electrons beams, although the resists are generally more sensitive to ions.

Example of a photonic device fabricated using FIB is reported in Fig. 8.

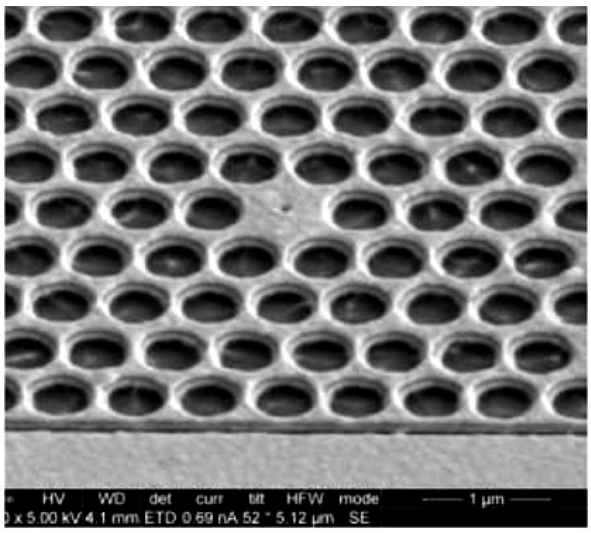

Fig. 8 A plasmonic-polariton crystal device fabricated using a focused ion beam system [7].

1.3. NON CONVENTIONAL LITHOGRAPHIC METHODS

The ability to fabricate structures from the micro- to the nanoscale with high precision in a wide variety of materials is of crucial importance to the advancement of micro- and nanotechnology. Critical issues, such as resolution, reliability, speed and overlay accuracy, they all need to be addressed in order to develop a new lithography methodologies for

industrially relevant processes. As compared to optical methods, these new techniques achieve their nanoscale patterning resolution using mechanical means and have the potential to achieve nanoscale replication at a low cost.

The most well-known non-conventional techniques are: soft lithography, thermal and UV imprinting process. The thermal and UV imprinting processes are also known with the generic name of nanoimprint lithography (NIL).

In general nanoimprint lithography is a process in which a mold (also called a template) is pressed into a deformable material to form a pattern. The material is then hardened so that when the mold is removed, the topography of the mold is transferred into the material.

NIL offers several advantages over other traditional lithographic techniques. First, because NIL is a mechanical process, the resolution is not limited by the diffraction of the light or the photoresist chemistry and development, as in optical lithography. Instead, the resolution of NIL depends on the minimum template feature size that can be fabricated. Additionally, because NIL tools do not require complex optics and sophisticated light sources, these tools are typically less expensive than optical system. NIL also offers a potential cost savings in the number of process steps requires to build a device through the ability to imprint both functional materials and 3-D structures [8]. More details about NIL will follow in the next chapters.

The soft-lithography is based on the use of an elastomeric stamp that is patterned with a relief structure on its surface [9]. The mold is generally made with a very flexible material such as polydimethylsiloxane (PDMS). There are a variety of related techniques using PDMS masters including micro-contact printing (μCP), micro-transfer molding (μTM) and micro-molding in capillaries (MIMIC). In μCP, for example, “ink” adhering to the raised features of a polymer mold is transferred to a substrate using intimate contact of the soft mold and the substrate. This layer acts as an etch mask for subsequent etch processes. Specifically, microcontact printing uses the relief patterns on a stamp to form patterns of self-assembled monolayers (SAMs) of ink on the surface of a substrate through conformal contact. Stamps are obtained from a master patterned by electron beam lithography, by casting and curing an elastomeric material: polymethylsiloxane (PDMS). Inking of the stamp occurs through the application of a thiol solution either by immersion or coating. The highly hydrophobic PDMS material allows the ink to be diffused into the bulk of the stamp, which means the thiols reside not only

on the surface, but also in the bulk of the stamp material. This diffusion into the bulk creates an ink reservoir for multiple prints. The stamp is let dry until no liquid is visible. Then the stamp is put into physical contact with the substrate and the thiol solution is transferred to the substrate. The thiol is area-selectively transferred to the surface based on the features of the stamp. During the transfer the carbon chains of the thiol align with each other to create a hydrophobic self-assembling monolayer (SAM). The resolution of microcontact lithography is limited by the mold feature size and the diffusion of the ink molecules around the contact portions [9].

Finally there are other non-conventional techniques that go under the category of proximity probe lithography. The proximity probe lithography refers to a new class of surface modification techniques, based on either scanning tunneling microscope (STM) or atomic force microscope (AFM) [10]. All these techniques employ a sharp probe tip placed in the close proximity of the sample surface with a feedback loop for distance regulation. Tunneling current across the tip and the sample surface is used for STM whereas optical methods are employed to monitor the vertical movement of the AFM cantilever.

A great diversity of material modification mechanism can be involved in proximity probe lithography. In STM lithography, short current pulses are generated for atomic deposition, extraction or displacement. In AFM lithography, a metalized AFM tip can be used for current pulse generation, allowing selective oxidation, resist exposure, field ionization, field-induced evaporation, indentation, chemical etching, as well as precursor decomposition.

2. NANOIMPRINT LITHOGRAPHY (NIL)

Nanoimprint is an emerging lithographic technology that promises high-throughput patterning of nanostructures. Based on mechanical embossing principle, nanoimprint techniques can achieve pattern resolutions beyond limitations set by light diffraction or beam scatterings in other conventional techniques. Molding techniques based on imprint processes make use of the differences between the mechanical properties of a structured stamp and a molding material. NIL was first reported as thermoplastic molding, and is therefore often referred to as hot embossing lithography (HEL).

In 2003 NIL was accepted by ITRS (International Technology Roadmap for Semiconductors) as the next generation lithography candidate and found its way to the road map for the 32nm node and beyond, scheduled for industrial manufacturing in 2013 [11].

Normally the principal elements required for NIL are (i) a mold with predefined surface relief nanostructures, and (ii) a suitable resist material that can be deformed and hardened to preserve the shape of the impression. Usually, the resist material is applied on the top of a substrate. The schematic of a NIL process is shown in Fig. 9.

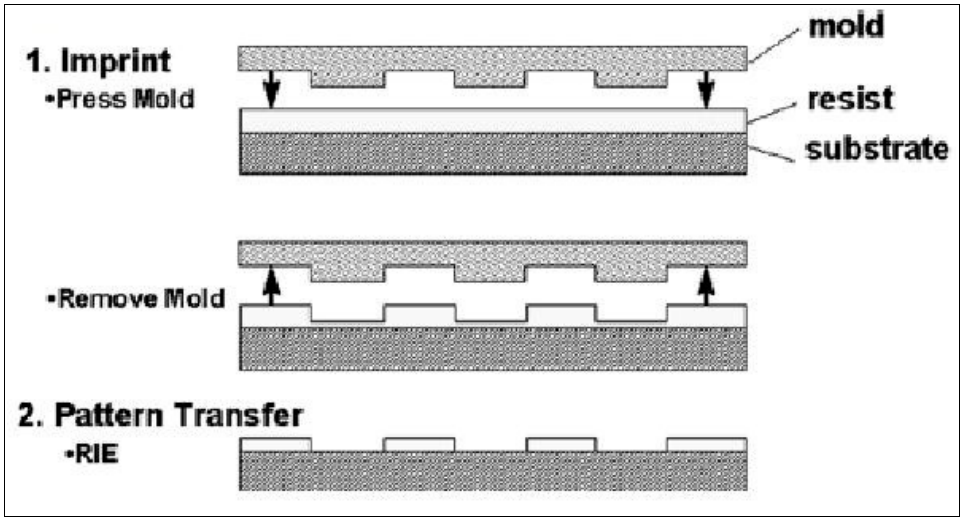

Fig. 9 Schematic of the NIL process. (1) Imprinting using a mold to create a thickness contrast in a resit, followed by mold removal and (2) pattern transfer using anisotropic etching to remove residue resist in the compressed areas.

The first stage of the NIL process is the molding of a thin thermoplastic film using a hard

master. During a process cycle the resist material is made viscous by heating, and shaped by applying pressure. The thermoplastic film is compressed between the stamp and the substrate and the viscous polymer is forced to flow into the cavities of the mold, conforming exactly to the surface relief of he stamp. When the cavities of the stamps are filled, the polymer is cooled down, while the pressure is maintained. The molten structure is then frozen. After relieving the pressure, the stamp can be retrieved (demolded) without damage, and reused for the next molding cycle. In a second step, the thickness profile of the polymer can be used as a resist for pattern transfer. For this, the residual layer remaining in the thin areas of the resist has to be removed, which is done by homogeneously thinning down the resist in an (ideally) anisotropic etching process. In this way, process windows are opened to the substrate and the polymer can be used as a masking layer.

With the integration of light sources into imprint machines, UV-NIL was developed for photo-curable resists. The basic difference between UV-NIL and thermal (T-) NIL is that a resin, which is liquid a room temperature, is shaped by a moderate pressure, which is then crosslinked and hardened by curing using UV radiation, all the processes have their specific advantages, e.g. while UV-NIL can be performed at room temperature, hot embossing is low cost since nontransparent stamps can be used [12]. The major characteristics of the process are summarized in Tab. 1.

Type of NIL / properties	**NIL (T-NIL) hot embossing**	**UV-NIL UV-imprint**
basic process sequence (see Figs. 8.3 and 8.6)	1) spin-coat thermoplastic film 2) place stamp on film 3) heat until viscous 4) emboss at high pressure 5) cool until solid 6) demold stamp	1) dispense liquid resin 2) parallel alignment of stamp with defined gap 3) imprint at low pressure 4) expose with UV light through stamp and crosslink 5) demold stamp
Pressure p	20–100 bar	0–5 bar
Temperature T_{mold}	100–200 °C	20 °C (ambient)
Temperature T_{demold}	20–80 °C	20 °C (ambient)
Resist	solid, thermoplastic $T_g \approx 60$–100 °C	liquid, UV-curable
Viscosity η	10^3–10^7 Pas	10^{-2}–10^{-3} Pas
Stamp material	Si, SiO_2 opaque	glass, SiO_2 transparent
Stamp area	full wafer, > 200 mm diameter	25×25cm^2, limited by control of gap
Stamp contact	facilitated by bending	planarization layer
Embossing time	from seconds to minutes	< 1 min (per exposure)
Advantage	low-cost large-area equipment and stamps	low viscosity, low pressure, alignment through stamp
Challenge	process time, thermal expansion due to thermal cycle	step and repeat needed for large areas
Development needed	alignment, residual layer homogeneity	material variety
Hybrid approaches	thermoset resists: embossing and curing before demolding	thermoplastic resists: hot molding and UV-curing before demolding
Advantage	low temperature variation cycle: demolding at high temperature possible	solid resist: full-wafer single imprint possible

Tab. 1 Comparison of hot embossing and UV imprinting, with typical parameters of current processes [12].

The resolution of NIL is determined by the mechanical strength of the mold and polymer. Many experiments have indicated that with suitable resist and mold, the resolution of NIL can be below 5nm, in general, the small holes in a resist are much easier to imprint than the small resist pillars, because the small pillars can easily tear off during the mold separation and are extremely difficult to image.

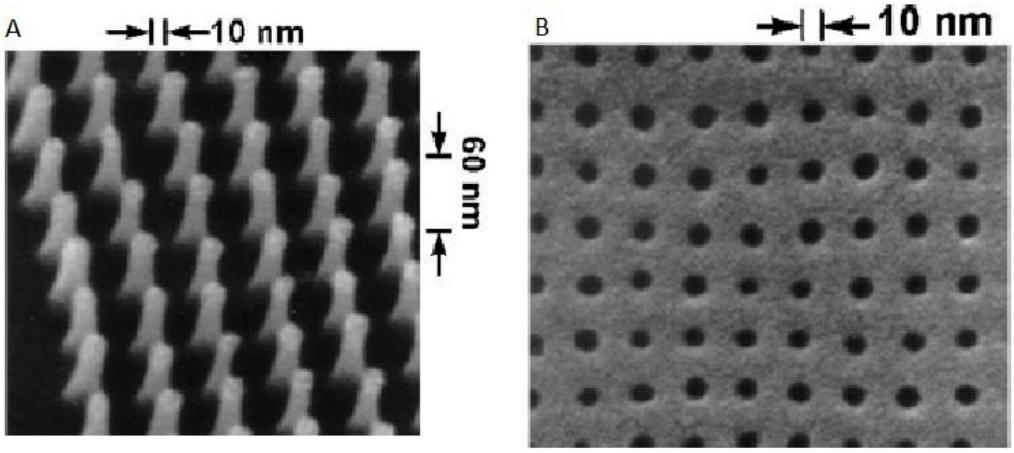

Fig. 10 (A) SEM image of a fabricated mold with a 10nm diameter array. (B) SEM image of hole array imprinted in PDMS by using such a mold [13].

2.1. NIL RESISTS

Imprint materials that are used to form the pattern on the substrate can be one of two kinds: (1) a sacrificial imprint resist, where the material is used as an etch mask to create patterns in a substrate (similar to photoresists in optical lithography) or (2) a functional imprint material, where the imprinted material directly becomes part of a device. Functional materials are more difficult to design as they have to satisfy both the imprint process constraints for achieving a high-fidelity nanopattern, and satisfy the properties required by the device over the course of the life of the device [2].

Traditionally in NIL processes thermoplastic materials are used, whose mechanical properties can be repeatedly and reversibly changed from a solid into a viscous state by simply varying the temperature. The rheological processes described later for thermoplastic materials can be considered to be similar to thermoset or UV-curable materials as long as the thermomechanical properties can be changed without affecting the chemicals ones.

Because imprint lithography makes a conformal replica of the surface relief patters by mechanical embossing, the resist materials used in imprinting need to be easily deformable under an applied pressure and should have a sufficient mechanical strength as well as a good mold-releasing properties to maintain their structural integrity during the demolding process.

Two material properties are important for the imprinting process. The resist material should have a Young's modulus lower than that of the mold during imprinting. The low modulus of the resist material is necessary for it to be deformed by the mold. To complete the imprinting process within a practical time frame, the resist material should also have a sufficiently low viscosity [13].

2.1.1. Thermoplastic resists

In NIL, typically a thermoplastic material is used as the imprint resist. During the imprint step, the resist is heated to a temperature above its glass transition temperature. At that temperature, the resist becomes a viscous liquid and can flow and, therefore, can be readily deformed into shape of the mold. This specific temperature (T_g) is chosen because above it both requirements mentioned in the previous paragraph can be met simultaneously. In fact above T_g both Young's modulus an the viscosity will drop by several orders of magnitude compared to their respective values at room temperature.

In practice, the suitable imprint temperature is, normally, chosen 70-80°C above the material's glass transition temperature (T_g). This choice can be explained by considering the typical deformation behavior of a thermoplastic polymer as a function of the temperature. At a temperature below T_g, the major contribution to the deformation comes from the elongation of the atomic distance, and the deformation is ideal elastic. Moreover the magnitude of deformation is very small. Above T_g, local motion of chain segments takes place. However, the entire chains are still fixed by the temporary network entanglements. A rubber-elastic plateau region exists beyond T_g, where a relative large deformation may occur due to extension of chain segments fixed between entanglements points in the rubbery state the deformation will recover after the force is released. Finally, with a further increase in temperature, the viscous liquid flow state is reached. In this region motion of entire chains takes place and the polymer flows by chain sliding. The deformation is irreversible, which makes it the right temperature range for NIL patterning. A good imprinting result can be

acquired when the imprinting temperature is set to be higher than the flow temperature (T_f) of the polymer. Empirically an optimal imprinting temperature is found 70-80°C above T_g of the material used.

Since the T_g is the onset temperature for molecular motion of polymers, factors that increase the energy required for molecular motion (e.g. intermolecular forces, inter-chain steric hindrance and bulky and stiff side groups) also increase the Tg value; those factors that decrease the energy requirements (e.g. flexible bonds and flexible side groups) decrease the T_g.

For many applications, it is desirable to use a lower temperature in processing. A reduction in temperature has to be compensated by corresponding increases in imprinting pressure and time to obtain satisfactory results.

The viscosity of a polymer material not only depends on the temperature, but also depends strongly on the polymer's molecular weight, M_w, relative to the so-called critical molecular weight (M_c) of a given polymer. The polymer molecular weight is important because it determines many physical properties (e.g. glass transition temperature, mechanical properties such as stiffness, strength, viscoelasticity and viscosity).

In comparison to methods like electron beam lithography (EBL), where nanoscale polymer structure can be produced by irradiation-induced chain scissor, the polymer chains are only moved and deformed during molding, thus keeping their chemical properties such as the molecular weight.

The Mc value can be interpreted as the molecular weight at which a temporary network of entanglements spans macroscopic dimensions. In practice, low-molecular-weight polymers with Mw<Mc can be imprinted at lower temperatures, lower pressures, or within shorter times. However, the absence of such a network of entanglements may leads to more brittle behavior, and could result in the fracture of the imprinted polymer features during the mold-separation step [14].

The high temperatures and pressures required for nanoimprinting of thermoplastic materials could limit the throughput and application scope of the NIL technique. In addition, the thermal expansion mismatch between the mold and the substrate often presents an obstacle for pattern overlay over large substrates.

2.1.2. New imprintable materials

The resist material is generally regarded as one of the challenges of this technique because the material has to fulfill several requirements such as low viscosity, low adhesion to the mold, good adhesion to the substrate, modest imprint temperature and pressure and high etch resistance to allow pattern transfer into the substrate. In general, resist materials are applied onto the surface of the substrate by spinning techniques and are dried to form a thin uniform layer of thickness depending on application and the resolution (minimum feature size) required. Currently, a great opportunity exists for developing new materials and polymer formulations that are more suitable for nanoimprint applications. Up to now, researchers have mostly used commercial thermal plastic materials, e.g. poly(methylmethacrylate) (PMMA) and polystyrene (PS), as NIL resists. Obviously, these materials are not optimized at all for the special requirements of the NIL process. For example one critical requirement of the candidate polymers used in imprinting based lithography is that they should provide excellent mould releasing properties during the de-moulding process and at the same time should not compromise the adhesion of the mould to the substrate. Commercially available polymer materials can hardly satisfy these seemingly contradictory requirements. Although the mould surface is treated normally with a low surface energy surfactant, when imprinting high density or high aspect ratio patterns, the imprinted polymer tends to adhere to the mould, creating pattern defects that are not acceptable for many applications. Block copolymer materials that have dual surface properties through microphase segregation can be exploited to solve this problem. In addition, a higher dry etching resistance is highly desirable if the imprinted polymer pattern is to be used as a dry etching mask for further pattern transfer. Adding a Si-containing material in the polymer formulation could be an effective method [14].

Siloxane copolymers

Of special interest are the PDMS–organic block or graft copolymers. In contrast to PMMA, and organic polymers in general, siloxane copolymers exhibit significant differences by virtue of the highly open, flexible, and mobile Si–O–Si backbone [13]. These include a low surface energy, low *T*g, and a high thermal stability. Furthermore, it is known that these copolymers undergo a microphase segregation above their *T*gs because of the unfavorable enthalpy of mixing. When cast or hot-pressed onto a high-surface-energy substrate such as silicon, glass, or metal the copolymer film forms an air/polymer interface enriched with lower-surface-

energy component (PDMS block), and a polymer/substrate interface dominated by the higher-surfaceenergy component (organic block). The dual surface character makes these copolymers excellent candidate materials for NIL: they allow easy mold–resist separation and at the same time they exhibit good adhesion to the substrate. This duality is not possible with homopolymers. Siloxane copolymers offer another advantage over homopolymers, in that they have a strongly improved etching resistance because of the high Si content and the high strength of the Si–O bond.

Fast Thermally Curable Liquid Resists

The thermal plastic polymers used in NIL become viscous fluids when heated above their *T*g values; however, the viscosity of heated polymers typically remains high, and thus the imprinting process requires significant pressures [13]. As discussed previously these thermoplastic resists normally have a high tendency to stick to the mold, which seriously affects the fidelity and quality of the pattern definition. Furthermore, they do not offer the necessary etch resistance. Thermally curable monomers are an alternative to thermal plastics. These liquid materials can be imprinted in a short period of time at low pressures and temperatures. PDMS-type materials are a class of thermally curable materials widely used by many research groups. A fast, thermal-curable liquid resist is based on the same hydrosilylation chemistry of siloxane polymers and consists of two principal chemical components: a vinyl-terminated PDMS polymer, a silyl-hydride-based (Si–H) dimethylsiloxane crosslinker. The high Si content in this polymer system guarantees that the resist has a high etching resistance in RIE processes. Moreover by changing the molecular weight of the precursor and the percentage of silyl-hydride groups in the crosslinker, the Young modulus of the cured material can be tuned. The short time required for curing the material and the fast crosslinking time satisfies the need for high-speed patterning in practical applications.

Hybrids organic-inorganic resists

Some particular applications (e.g. optical waveguides) require thicker patterns, in the order of one micrometer. Alternative materials were proposed to meet this criterion, such as organically modified ceramic (ORMOCER®) [15]. The relative proportions of the structural elements determine the material properties. ORMOCER®s are hybrid polymer materials

synthesized by the sol-gel process. This process starts by building up an inorganic network through controlled hydrolysis and condensation of organically modified Si alkoxides. In a subsequent step the polymerizable groups, which are fixed to the inorganic network, react with each other in a thermal or UV-initiated process. In this two-stage process an inorganic-organic copolymer is synthesized. In addition it is possible to use organically modified Si alkoxides, which do not enter into any organic polymerization reaction and thereby contribute to an organic functionalization of the inorganic network. The properties are controlled by the choice of base materials, by how the inorganic polycondensation reaction is conducted, and by controlling the linking reactions which lead to the construction of the organic network. ORMOCER®s have a lower elastic modulus and are more ductile than inorganics, so shaping the precursor into the mold is easier, while cracking occurs less easily during the embossing step.

2.2. NIL MOLDS

The mold used in NIL can essentially be any type of solid material that has a high strength and durability. The molds or stamps are normally made in silicon, dielectric materials (e.g. silicon dioxide or silicon nitride), metals (e.g. nickel), or polymeric materials that have a sufficient Young modulus [14].

The properties of these hard molds contrast those of elastomeric stamps used in soft lithography, and are essential for producing nanoscale features because the protrusion patterns on the mold should not deform, buckle, or collapse during imprinting, even at elevated temperatures. In this manner, preservation of the shape and aspect ratio as well as faithful pattern definition is guaranteed.

Considerations for selecting mold materials include hardness, compatibility with traditional microfabrication processing and thermal expansion coefficient of the material. The thermal coefficient is especially important in thermal NIL, where temperature over 100°C is typically required in the imprinting step. A thermal mismatch between the mold and the substrate could result in pattern distortions or a stress build-up during cooling cycle, which would effect the pattern fidelity. In this regard, a Si mold and Si substrate make a very good pair for the NIL

process.

Any kind of process generating a surface profile in a hard material can be used to fabricate stamps (molds) for NIL. The fabrication of an hard mold involves a lithographic process and a reactive ion etching (RIE). For the lithographic step, one can choose from UV lithography for microscale and larger features, electron-beam lithography for very small features or NIL itself. If high resolution features on a large area are needed the time and therefore the fabrication costs for such a stamp quickly increases dramatically. The use of working stamps for imprinting, i.e. copies of original masters, is mandatory due to the high costs of original stamps and the danger of degradation of these masters in the imprinting process. The UV-curable Ormostamp material from Micro Resist Technology® was tested as a material for working stamps with success [16].

Bending of stamps

In hot embossing lithography, the stamp is often considered as a hard tool which is inflexible over millimeter distance. However, this is true only for special cases. e.g. when density and sizes of stamp protrusions are homogeneous over the whole stamp surface. Significant bending may occur when dust particle of some μm diameter are present between the stamp and the substrate. Because of the high Young's modulus of the stamp, the equilibration mechanism (often a thin layer of silicone behind the stamp) is not able to achieve a conformal contact of the stamp with the polymer and consequently structures are not embossed in the vicinity of these particles [12].

For the ideal case where no significant bending would occur, e.g. by using a thick rigid stamp or small grating areas, the overall sinking of the stamp would be determined by the largest stamp protrusion, in this case the surrounding area. In the ideal case of a grating covering the whole stamp surface, the molding process would be determined by the grating protrusions.

For a typical case where the grating is surrounded by a large unstructured area, stamp bending results in an inhomogeneous residual layer.

The profile of the transition areas between the center and the border regions are due to bending. In Fig. 11, the effect of transition areas on the quality of pattern transfer is schematically shown. Care must be taken with the amount or resist thinned down during the removal of the residual layer in order to ensure complete transfer of the grating (section 5b).

Under- and over- thinning will result in a loss of the grating structure (section 5a and 5c). For large differences in height in the transition region, i.e. large bending, complete transfer of cavities is impossible. A few additional protrusions or cavities can be added in order to keep in transition area out of the grating structure. This should be placed in the vicinity of nanostructures, with intercavity distance smaller than typical transition distances. The additional cavities also ensure better flow of the polymer and shorter embossing time.

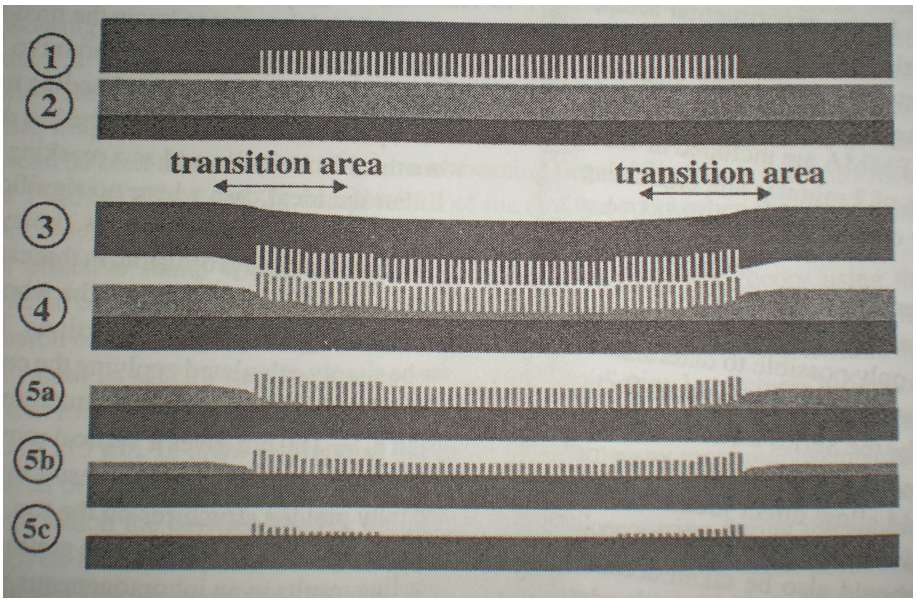

Fig. 11 Schematic view of the molding of a large array of nanocavities surrounded by large stamp structure. Stamp (1) and resist (2) before embossing. (3) Local bending of the stamp during molding. (4) Resist after embossing with inhomogeneous residual layer. (5a) to (5c) show different state of resist thinning. (5b) is the state where complete pattern transfer is possible [17].

Mold surface preparation

A mold for imprint lithography typically has a high density of nanoscale protrusion features on its surface. This effectively increases the total surface area that contacts the imprinted polymer, leading to strong adhesion of the imprinted polymer to the mold. This effect can easily be seen by the sticking of a resist material to a mold without any special treatment. Solutions to this problems are (I) incorporating an internal release agent into the resist formulation, (ii) applying a low-surface-energy coating to the mold to reduce its surface energy, and (iii) choosing a mold material with an intrinsically low surface energy.

The most widely adopted approach is to form a self-assembled monolayer of a fluorosilane release agent on the mold surface (e.g. 1H,1H,2H,2H-perfluorodecyl-thrichlorosilane), either

by a solution phase or a vapor-phase reaction. Vapor phase coating has been shown to provide better imprint results for nanoscale features because it avoids the difficulty of liquid wetting of the nanoscale trench features on the mold. This approach can be readily applied to oxide surfaces, or to Si surfaces that have been oxidized with a piranha soak to generate required terminal hydroxyl groups. Silanization of oxidized silicon with a $RSiCl_3$ precursor begins with hydrolysis of the polar head group, which converts the Si–Cl bonds to Si–OH (silanol) groups. The silanol groups generated, which are strongly attracted to the hydrophilic surface of oxided silicon, condense and react with the hydroxyl group on the surface as well as other monomer silanol group to form networks of covalent siloxane bonds, Si–O–Si. Such covalent bonding makes the surfactant coating layer chemically and thermally stable.

2.3. NANORHEOLOGHY

For a deeper insight into the embossing process and the problems occurring during processing, knoledge about the mechanical propertie of the material is indispensable. Rheological aspects are of the highest importance for the processing of the thermoplastic materials.

2.3.1. Theory of the squeeze flow

During embossing the linear movement of a stamp is transferred into a complex squeeze flow of viscous material. In the thin polymer films used in NIL, a small vertical displacement of the stamp results in a large lateral flow. The two surfaces of the stamp and the substrate have to come entirely into contact with each other and maintain this contact until the desired residual layer thickness is reached.

Before embossing, the polymer film has a initial thickness h_0 and the depth of the micro-relief is h_r. For a fully inserted stamp, the film thickness under the single stamp protrusions is $h_f \equiv h(t_f)$. A simple model for the squeezed polymer flow underneath the stamp protrusion is obtained by treating the polymer as an incompressible liquid of constant viscosity, and solving the Navier-Stokes equation with non slip boundary conditions at the stamp and substrate surfaces. According to this model, given for line-shaped stamp protrusions and cavities, it is

possible to find the following expression, known as Stefan's equation, for the film thickness *h(t)* when a constant imprint force *F* per length is applied to the stamp protrusion [12]:

$$\frac{1}{h^2(t)} = \frac{1}{h_0^2} + \frac{2F}{\eta_0 L s^3} t$$

where η_0 is the zero shear viscosity, *s* the protrusion width and *L* the protrusion length. Inserting the final thickness $h_f \equiv h(t_f)$ in the previous relation, gives the embossing time:

$$t_f = \frac{\eta_0 L s^3}{2F}\left(\frac{1}{h_f^2} - \frac{1}{h_0^2}\right)$$

For many practical cases, where a constant pressure under each stamp protrusion $p=F/(sL)$ is assumed, this formula gives:

$$t_f = \frac{\eta_0 s^2}{2p}\left(\frac{1}{h_f^2} - \frac{1}{h_{02}}\right)$$

As a direct consequence of the Stefan's equation it can be seen that, for the same, small (narrow) stamp protrusions will sink faster than the large (wide) ones. The stamp geometry can therefore optimized by reducing the dimensions of contusions.

While stamps with nano-protusions would allow fast embossing of some seconds, using standard NIL process parameters, protrusions of some hundreds of microns would already increase embossing times to some hours. The strong dependance of the embossing time on the pressing area has the consequence that, for fully inserted stamp relief (full contact over the total stamp area), the flow practically stops (Fig. 12).

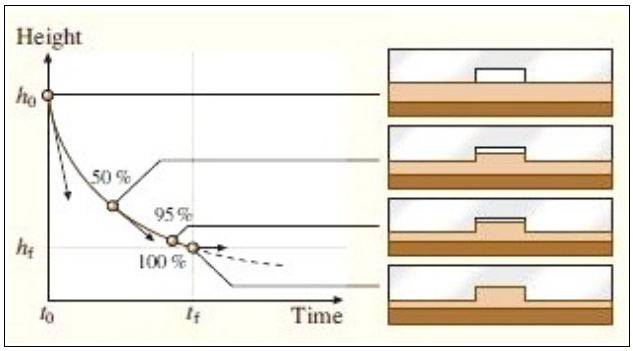

Fig. 12 Schematics of the squeeze flow of a compressed polymer film into the cavity.

The stamp geometry can therefore be optimized by reducing the dimensions of the protrusions. The array in Fig. 13a is equivalent to the microcavity in Fig. 13b, which has the

same volume as the total volume of the cavity array. The fill factor, i.e. ratio of area covered by cavities to the total stamp area, should be kept constant, both locally (at the length scale corresponding to the cavity dimensions) and also across the wafer, i.e., for large stamp protrusions, to ensure better flow of the polymer and shorter embossing times. For this purpose, additional protrusions and cavities can be placed in intermediate areas not needed for the device function, or structures repeated several times.

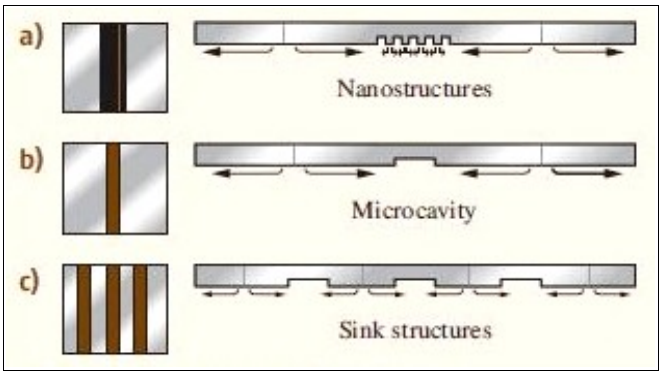

Fig. 13 Comparison of the squeeze flow for nano and micro cavities.

Consider a general situation where the mold consists of a combination of nanoscale patterns next to some large-scale patterns. If the mold and the substrate remain flat during imprinting, the mold relief patterns penetrate into the resist layer on the substrate in a parallel fashion as shown in Fig. 14(a). Because of the viscous polymer flow, the large-scale protrusions on the mold cannot penetrate the polymer film fully in a time frame that is practical for NIL. Not only will this cause incomplete polymer molding of large-scale patterns, it will also affect the nanoscale patterns in close proximity to the large-scale features, yielding a shallower resist pattern than that on the mold. On the other hand, if either the mold or the substrate can bend under a high pressure during imprinting, such that a conformal contact can be made at the polymer resist layer as shown in Fig. 14(b), the same feature height can be achieved for both large-scale and nanoscale patterns. However, due to mold bending, the nanoscale relief patterns penetrate deeper into the resist layer than with the large patterns, leading to a thinner residue layer in the nanoscale pattern region than that in the large pattern region. Fig. 14(c) is an example where nanopatterns are next to the large structures on the mold. The displaced polymer cannot reach the center of the nanopattern region, leaving the center of the nanopatterns formed incompletely.

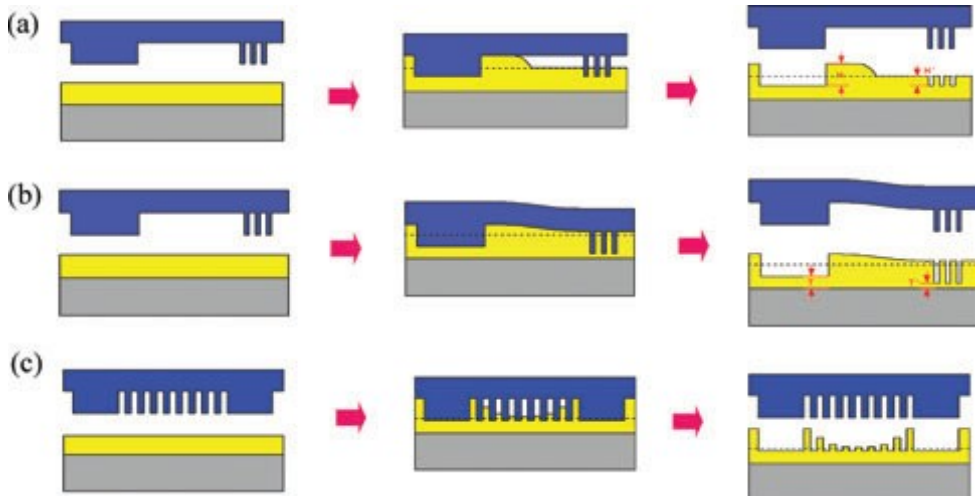

Fig. 14 Several defect generation mechanisms in NIL that occur when mold contains complex patterns. The high viscosity prevents total displacement of the polymer under the large size patterns, which affects the imprint of nearby nanoscale patterns (*a*) and (*b*). Insufficient polymer flow over a large distance causes incomplete filling of nanoscale trenches (c) [9].

Hirai et al. were the first to investigate the polymer deformation process by numerical simulations [18]. They have studied the pressure required for successful imprinting and the filling rate into the grooves of the mold as a function of the aspect ratio of the pattern, the initial thickness of the polymer, and the duty cycle of the structure for a periodic pattern. It was found that the required pressure increased not only for high-aspect-ratio patterns, but for low-aspect-ratio patterns as well. This is because for wide trenches the pressure is not evenly distributed as a result of the polymer flow resistance, and the polymers fill in from the edges with a slower filling rate than at the center of the cavity. The pressure also increases when the initial thickness of the polymer film decreases to less than twice the mold depth. This again can be attributed to the increased resistance of polymer flow in the confined nanofluidic channels formed between the mold protrusion and the substrate surface.

2.3.2. Effect of polymer film thickness and mold geometry on polymer flow in the imprinting stage

Several recent studies [19-21] have investigated the impact of polymer material properties, mold geometry, and process conditions on polymer deformation, and further studied the impact of the polymer deformation mode on the replication time. When the polymer flows vertically into an open cavity during imprinting, the polymer can deform as a single peak centered in the cavity, or as a dual peak, where each peak remains close to the vertical

sidewalls, depending upon the geometry. Fig. 16 shows the effect of rectangular cavity width (*W*) and film thickness on polymer deformation. As cavity width increases, the deformation mode changes from single peak to dual peak deformation. The polymer deformation also transitions from single to dual peak as the initial polymer film thickness decreases. For the largest cavity widths and thinnest polymer layers, the two peaks are highly localized near the vertical cavity walls and do not interact. In addition high shear along the indenter sidewall reduces the peak distance from sidewall, causing slightly smaller peak distance from sidewall for smaller indenter widths (*S*) than larger indenter widths. The polymer peak also spreads laterally slightly more for larger cavity height than smaller cavity heights (h_c).

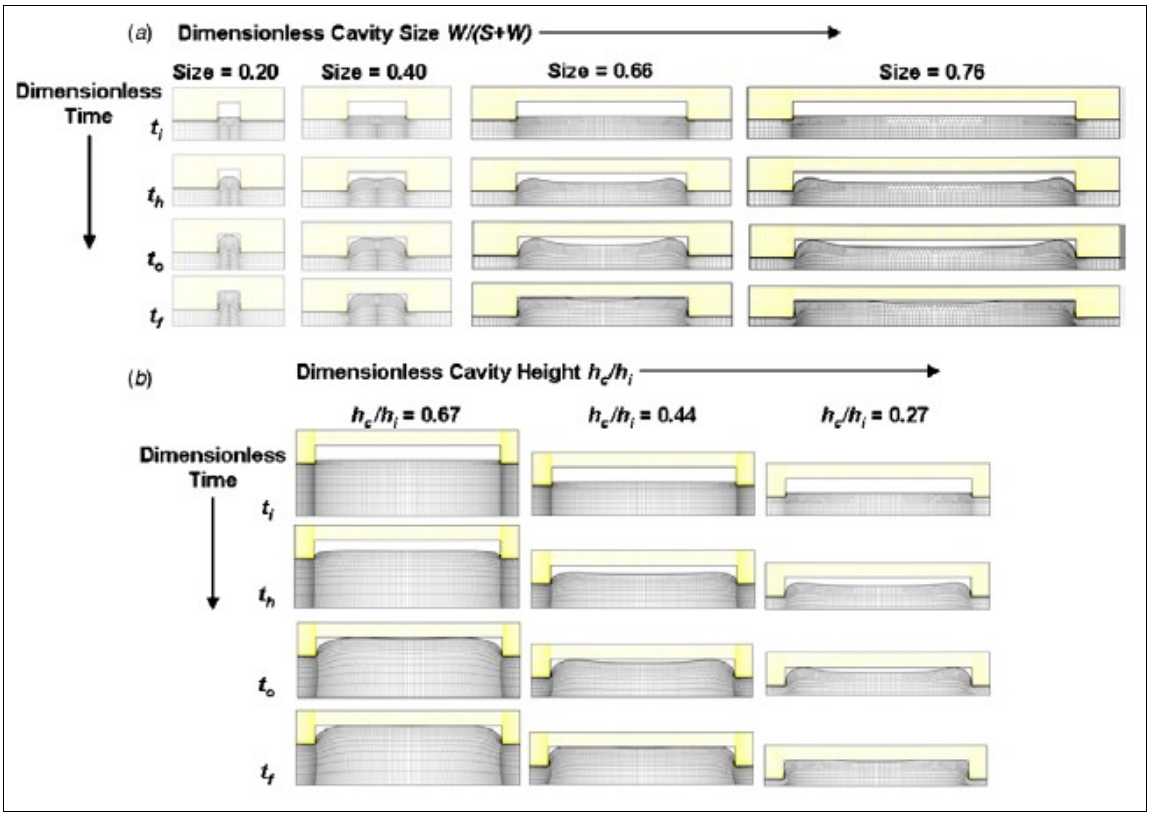

Fig. 15 Deformation profile for (a) increasing cavity width holding indenter wodth and film thickness constant and (b) decreasing film thickness holding cavity geometry constant [19].

Fig. 16 shows the impact of rectangular cavity geometry and film thickness on fill times for a viscous Newtonian fluid. In general, wider cavities fill faster than narrower cavities, and taller cavities on thin polymer films fill slower than shorter cavities on thick polymer films. In all cases, single versus dual peak deformation mode affects cavity filling time. In both single and dual peak flow, it is possible to increase cavity width (*W*) and/or decrease indenter width (*S*)

to promote shear. In general, taller cavities fill slower than shorter cavities. The wider the cavities reach filling onset more rapidly than narrower cavities but the overall filling time is not necessarily governed by cavity width.

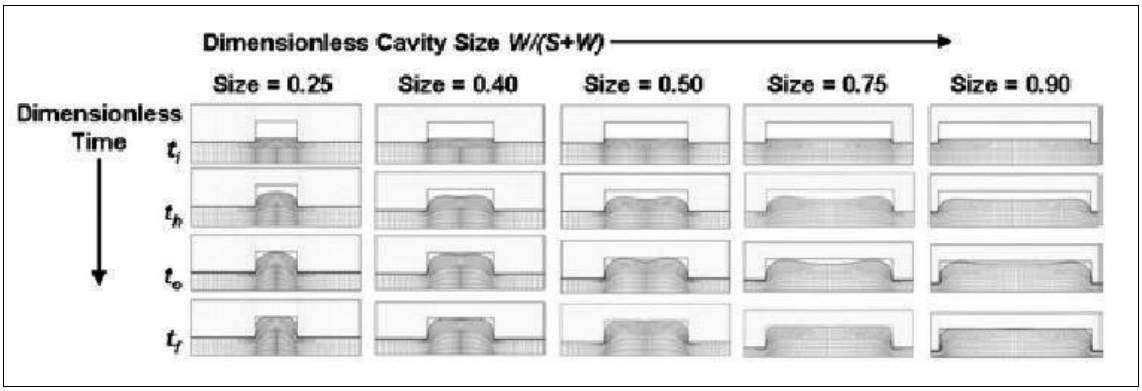

Fig. 16 Impact of indenter width and cavity height to film thickness ratio on cavity filling [19].

The ratio of cavity width to film thickness modulates single peak versus dual peak cavity filling, regardless of the absolute size of the features and the pressure or temperature applied during imprinting. In general, when the ratio of cavity half width to initial polymer film thickness is less than unit, the polymer deform as dual peaks. The cavity is filled faster for a geometry at the single/dual-peak threshold, with increasing filling times for conditions that deviate from this threshold.

2.3.3. Effect of polymer film thickness and mold geometry on velocity field in the imprinting stage

Another important factor to consider for better understanding the nanoimprint process is the study of the velocity fields, including the lateral and vertical velocity. The study of the velocity field is significant because it can directly describe the mode of the polymer deformation, which is the key role to determine the mechanism of nanoimprint forming. The lateral velocity profiles describe the fluid flow between two walls. On the other hand, the vertical velocity profiles are the fluid flow between the polyer resist and air existing in cavity display and can be used to visualize the polymer deformation directly [20]. In the figure below, it shows that before the flow front contact to the roof of cavity, all lateral velocities at the flow front have the same flow trends for any time step, in which the lateral velocity increases with increasing distance from the cavity center until it reaches the maximum value

near the cavity sidewall. On the other hand, before the flow front contact to the roof of cavity, there are two different flow trends of the vertical velocity. One is that the vertical velocity at the flow front increases with decreasing distance from the cavity center, while the other is that the vertical velocity increases with increasing distance from the cavity center until it reaches the maximum value near the cavity sidewall. Once the vertical and lateral velocities have the same flow trend, their maximum values occur near the sidewall, which can deposit more polymers around the sidewall. As a result, the dual-peak deformation is formed (Fig. 17A). On the other hand, when the vertical and lateral velocities have different flow trends the single-peak deformation appears since the larger vertical velocity brings the polymer to the cavity center (Fig. 17B).

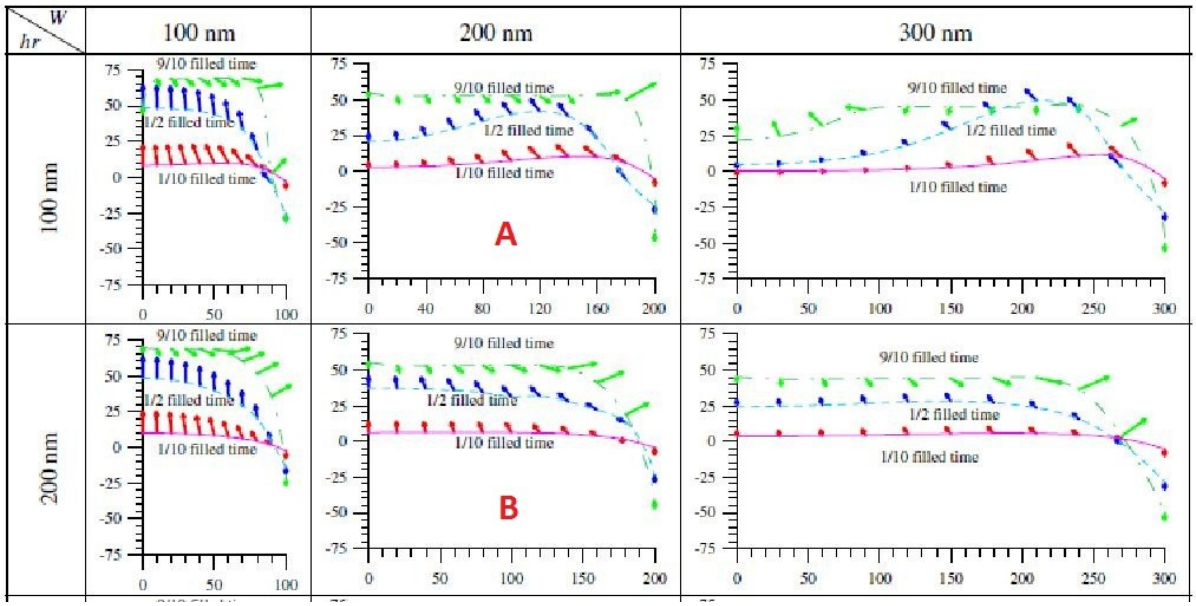

Fig.17 The velocity vector at the flow front with various time steps for various half cavity widths when indenter width is 200nm [20].

2.4. DEMOLDING

During demolding the stamp is detached from the molded structure by a vertical movement of the stamp. If fully molded, the thickness profile exhibits the inverse tone of the relief of the stamp surface.

Deformation can also occur while the polymer is in its solid state. Distortion or damaging of the molded structure during this step can occur as a result of different effects such as adhesion at the surface, friction due to surface roughness and trapping of the polymer due to the

negative slopes cavity sidewalls. If the side walls of the stamp cavities are not completely flat, then the polymer will locally interlock with the mold. As a result the polymer structures or parts of the wall profile are either ripped away or deformed during demolding and for small width, high aspect ratio structures the shear results in a stretching of the total structure when the stamp is pulled away [11]. The deformation or stretching of the polymer should generally be avoided by ensuring a good quality of the cavity side walls with no undercuts and very smooth surfaces. A reduction in the friction during demolding is also possible by adding a demolding agent to the polymer or by use of an improved anti-adhesive layer on the stamp.

According to the considerations of previous paragraphs, there are different areas of optimization [12]:

1. Initial film thickness. Process times to mold thin polymer layers can be reduced by simply using a high initial layer thickness. The reason for this is easy to understand: for thicker films the squeeze polymer can flow more freely in the central plane of the film unaffected by the friction at the boundaries. Care must be taken where a high initial thickness usually results in an unacceptable residual thickness, i.e. too high for further pattern transfer.
2. Molding temperature. High molding temperatures can lower polymer viscosities and reduce times to fill the mold cavities. However in current embossing setups, the relative high heat capacities and the low heating and cooling rates often limit embossing time. This is because the stack of mold and polymer, as well as the substrate and heating plates of the press have to be heated and cooled. Furthermore, unwanted temperature effects may occur such as a decomposition of the polymer or changes in the electronic, chemical or mechanical properties of the underlying substrate or stamp. For a good replication fidelity, often processes are preferred where all the stack elements are kept in thermal equilibrium during the temperature cycle, consequently leading to long embossing time.
3. Stamp geometry. The distance of lateral polymer flow should kept as small as possible. Stamp cavities and protrusion should be distributed homogeneously over the entire stamp area i.e. the fill factor should be kept constant in order to limit the displacement of polymer in the vicinity of each structure. This reduced the tendency

for incomplete filling and variation of residual layer thickness over the surface area. Often an equilibration mechanism such as a thin silicone mattress (e.g. PDMS) is used to equilibrate pressure inhomogeneities due to the thickness variation in the mold or the press setup.

4. Demolding. It seems likely that any reasonable structure present on a stamp can be molded, by using sufficient heat (assuring low viscosity), pressure (assuring sufficient flow) and time. For high aspect ratio structures, demolding become a critical step in the replication process. High aspect ratio structures can be realized if molds with vertical sidewalls are used. Here, adhesion, imperfections of the walls and roughness in conjunction with lateral deformation due to the different thermal expansion of mold, polymer and substrate might lead to interlocking of high friction during demolding. Anti-adhesion layers on the mold can reduce friction forces, but will become less effective as the cavities become very small and only a few polymer chains have to be extracted from a cavity.

3. HYBRID ORGANIC-INORGANIC SOL-GEL MATERIALS

The sol-gel process, which is mainly based on inorganic polymerization reactions, is a chemical synthesis method initially used for the preparation of inorganic materials such as glasses and ceramics. Its unique low-temperature processing characteristic also provides unique opportunities to make pure and well-controlled composition organic/inorganic hybrid materials through the incorporation of low molecular weight and oligomeric/polymeric organic molecules with appropriate inorganic moieties [22].

The major driving forces behind the intense activities in this area are the new and different properties of the nanocomposites which the traditional macroscale composites and conventional materials do not have. Unlike the traditional composite materials which have macroscale domain size of millimeter and even micrometer scale, most of the organic/inorganic hybrid materials are nanoscopic, with the physical constraint of several nanometers, typically 1-100nm, as the minimum size of the components or phases. This size effect modulates the properties of nanophased materials, for example (1) thermal behavior, melting points or T_g can be shifted for tens of degree or canceled, (2) mechanical properties change, (3) rheological behavior and stability of solutions and dispersions vary because the viscosity of polymeric solutions are strongly dependent on the molecular mass while the stability of colloidal solutions is dependent on the mass of the particles. (4) Electronic properties are easily changed by the size of the domains, especially when the objects are in the nanometer range.

3.1. GENERAL BACKGROUND OF SOL-GEL CHEMISTRY

Hybrid organic/inorganic sol-gel materials can be prepared by two approaches. Organic molecules can be just embedded into an inorganic material, or vice versa. Alternatively, the organic and the inorganic groupings can be linked by stable chemical bonds. The latter approach required precursors in which the organic group (R) is bonded to the oxide-forming element (M) in a hydrolytically stable way. The general process is outlined in Eq. 1 for metal alkoxide, the most commonly used type of precursors in sol-gel processes.

$$xRM(OR')_n + yM(OR')_m + zH_2O \rightarrow R_qMO_p + wR'OH \quad \text{(Eq. 1)}$$

There is a huge variety of possibilities for the modification of organic-inorganic hybrid

materials:

- Variation of the element *M*. In principle, any element *M* for which compounds suitable for sol-gel processing is available can be used for the formation of the inorganic structures.
- Variation of the organic group *R*. the choice of the organic group *R* is nearly unlimited. The only condition is that the group id hydrolitically stable or reacts with water in a controlled way. The crucial question is the hydrolytic stability of the *M-R* link.
- Variation of *x:y* (Eq. 1), the ratio between the substituted an unsubstituted precursor. With decreasing *x*, the hybrid materials become "more inorganic", and vice versa. The case *y*=0 corresponds to a one-component system with $RM(OR')_n$ as the only precursor.

The organic group *R* can have different functions: the most general is that of a network modifier. If an alkoxy group in $M(OR')_m$ is replaced by one or more hydrolytically stable group *R*, the degree of cross-linking of the oxide network, formed during sol-gel processing, decreases. A more challenging possibility is the use of precursors in which the organic group *R* bears some functionality. The relevant precursors are of the type $(R'O)_nM\text{-}X\text{-}A$, where *A* represents the functional organic group, and *X* is a chemically inert spacer linking *A* and the metal alkoxide moiety [14]. However the explanation of sol-gel process, in this case, is limited to "simple" metal alkoxydes indicated with $M(OR)_n$, (where *M*=Si, Ti, Zr, Al etc., *OR*, an alkoxy group Oc_nH_{2n+1}).

The reaction is generally divided into two steps: hydrolysis of metal alkoxides to produce hydroxyl groups, followed by polycondensation of the hydroxyl groups and the residual alkoxyl groups to form a three-dimensional network.

The polycondensation reactions develop via two competing mechanisms:

- oxolation: the formation of an oxygen bridge
- olation: the formation of a hydroxo bridge

Generally, both the hydrolysis and condensation reactions occur simultaneously once the hydrolysis reaction has been initiated. Both the hydrolysis and condensation steps generate low molecular weight byproducts such as alcohol and water. These small molecules must be removed from the system, and such removal would lead, in the limit, to tetrahedral SiO_2 network if the species were silicon. The removal of these byproducts also contribute to the high shrinkage that occurs during the classical sol-gel process.

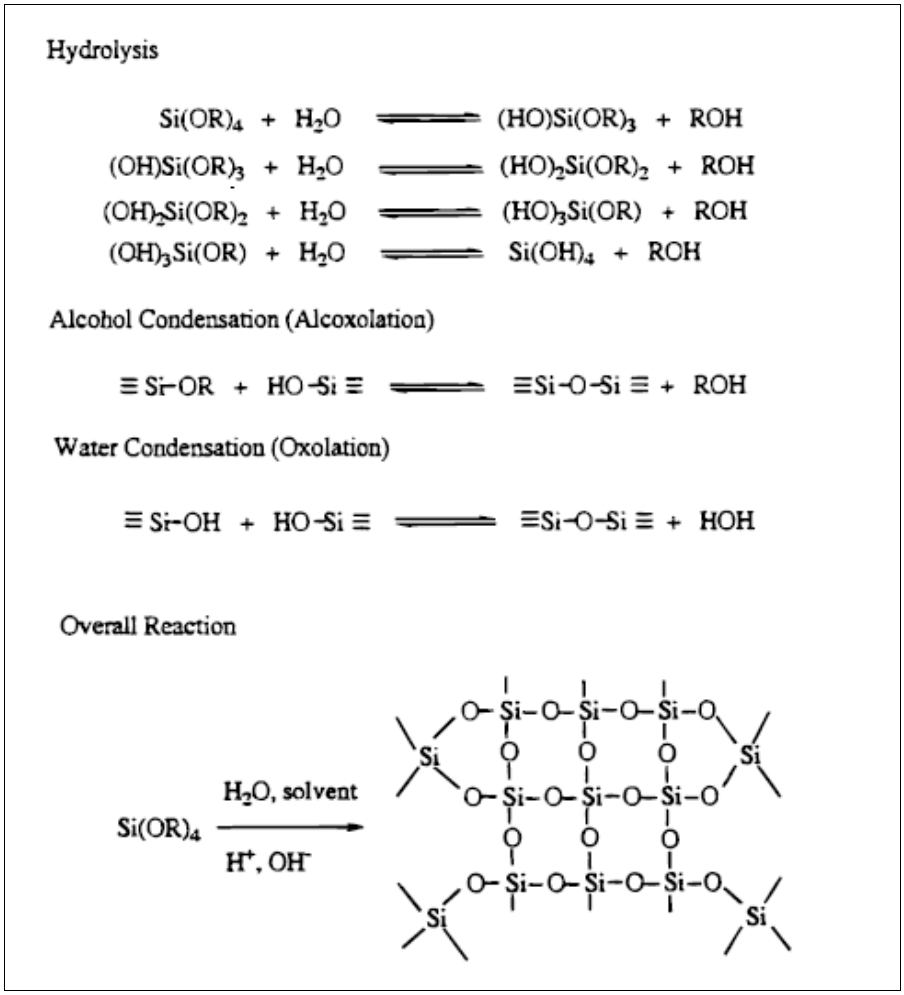

Fig. 18 General sol-gel process for an alkoxysilane.

The structure and morphology of the resulting metal-oxo macromolecular networks are dependent on the respective rates of the different reactions. Rearrangement reactions occur, leading preferentially to weakly branched polymers. When these structures reach macroscopic size, a gel in which solvent and free polymer are entrapped is obtained. The gel state is not the only possibility. Other final forms, such as colloidal solutions or precipitates, can be obtained. The formation of gels or colloidal species reflects different growing processes and different polymer-solvent interactions. Control of the nature of the intermediate species through the reaction conditions is essential to tailor the final structures. The reactivity of the metal alkoxides (nature of M and R), hydrolysis ratio (H_2O/M), solvent, reaction temperature, the use of complexing agents or catalyst are the main parameters used to achieve control over the size and morphology of the resulting materials [23].

Both hydrolysis and condensation occur by nucleophilic substitution (S_N) mechanism which

involve three steps: nucleophilic addition (A_N), proton transfer within the transition states, and removal of the protonated species as either alcohol or water. For non-silicate metal alkoxides, generally no catalyst is needed for hydrolysis and condensation because they are very reactive. In the case of silicon based metal alkoxides, the hydrolysis and condensation reactions typically proceed with either an acid or base as catalyst. In the case of the common silicon alkoxides, since the hydrolysis rate is high under an acidic environment relative to that of condensation, acid catalysis promotes the development of more linear or polymer-like molecules in the initial stages. For a pure metal alkoxide system, this will result in the formation of high-density, low fractal dimension structures. On the other hand, base catalysis results in a higher condensation rate. Therefore this environment tends to produce more a dense-cluster growth leading to dense, colloidal particulate structures [24].

The chemical reactivity of the metal alkoxide in the hydrolysis step is determined by both the nature of the metal, M, and the steric hindrance of the alkoxy groups. The major parameters appear to be the electrophilic character of the metal atom, and its ability to increase its coordination number, N. In fact, the hydrolysis and condensation reactions in the sol-gel process generally start with the nucleophilic addition of the hydroxylated groups onto the electrophilic metal atoms which results in an increase of the coordination number of the metal atom in the transition state. The degree of reactivity of a given metal or semi-metal atom of an alkoxide is not due only to the electrophilic nature but rather is more a function of degree of unsaturation. The unsaturation degree of the metal coordination can be simply expressed by the difference N-Z, where N is the coordination number usually found in the oxide, and Z is the oxidation state. The difference of reactivity between silicon alkoxides and other transition-metal alkoxides is demonstrated by the variation of the (N-Z) value.

alkoxides	χ	N	Z	$N-Z$
$Si(OPr^i)_4$	1.90	4	4	0
$Sn(OPr^i)_4$	1.96	6	4	2
$Ti(OPr^i)_4$	1.54	6	4	2
$Zr(OPr^i)_4$	1.33	7	4	3

Tab. 2 Electronegativity (χ), coordination number (N), and degree of unsaturation (N - Z) for some metals [22].

Tab. 2 lists the electronegativity and the degree of metal unsaturation for a few metal alkoxides. It is noted that silicon has a low electrophilicity and zero degree of unsaturation.

Therefore, silicon alkoxides are less reactive. The gelation therefore takes several weeks when neutral water is added and the reaction rate must be increased by using catalysts. On the other hand, non-silicate metal alkoxides, including elements such as Ti, Zr and Al with higher unsaturation, all have much higher reactivity than silicon. They are so sensitive to moisture, even in the absence of a catalyst, that precipitation of the oxide will generally occur as soon as water is present. The sequence of reactivity is expressed as follows: $Zr(OR)_4 > Ti(OR)_4 > Sn(OR)_4 >> Si(OR)_4$.

There are so many examples of sol-gel materials in the scientific and patent literature that it is impossible to discuss or even mention all different types. In this chapter only two specific chemistry paths to obtain hybrid materials are presented:

- *Inorganic particles embedded in a sol-gel matrices*. This approach involves the incorporation of inorganic nanoparticles (e.g. metal oxides NPs) into organic resins or polymers. To avoid optical scattering, the particle size should be controlled below 25 nm. Often pre-made or commercial purchased metal oxide nanoparticles have been incorporated into organic or polymeric matrices. However, the nanoparticles tend to aggregate unless surface modification is implemented to decrease the inter-particle attraction [25].
- *Sol-gel matrices with in situ generated inorganic particles or clusters*. This process is based on the hydrolysis and condensation of precursors such as metal alkoxides to prepare network-like hybrid materials. It offers a versatile design under mild conditions and low cost fabrication with domain size at nanometric scale. However, one drawback of the above in situ synthesis is that un-reacted reactants and un-removed educts might exist in the final hybrid material and influence the properties. In addition, the reaction stages and solution viscosity cannot be exactly controlled throughout the continuous sol–gel process.

In particular these two approaches for sol-gel materials preparation will be used in the experimental section to produce TiO_2 resists for NIL.

3.2. SOL-GEL MATERIALS AS RESIST FOR NANOLITHOGRAPHY

The research activity on new lithographic resist materials, alternative to widespread used polymeric systems, has known increasing development in recent years, in particular as regards

the synthesis of sol–gel resists.

The sol–gel synthesis is an economic, relatively fast and effective method for film realization. Among the most attractive features of a sol–gel processing, it is worth to mention the low process temperatures (typically <200°C), the possibility to obtain large surface coatings, and the relatively cheap experimental setups required for material synthesis and deposition.

Subsequently a few examples of specific sol-gel materials used in nanolithography are reported.

Bridged polysilsesquioxanes (BPS)-based materials

A new kind of resist for direct X-ray photolithography is a hybrid organic–inorganic sol–gel, belonging to the class of bridged polysilsesquioxanes (BPS)-based materials. BPS precursors contain a variable organic fragment attached to two (or more) trifunctional silyl groups. The resist material is based on a bis(triethoxysilyl) benzene precursor. The monomer presents a distinctive organic group, the aromatic ring, covalently attached to two alkoxysilyl groups by non-hydrolyzable carbon–silicon bonds. The peculiar feature of a hybrid BPS-based material is represented by its native porosity. When applied to lithography, the BPS-based resist presents some innovative characteristics: the possibility (1) to direct transfer patterns on sol–gel films through X-ray irradiation, avoiding time-consuming fabrication processes, (2) to produce nanostructures without the addition of a photocatalyst and (3) to exploit the porous structure to increase the potentially reactive surface area, as stated before [26].

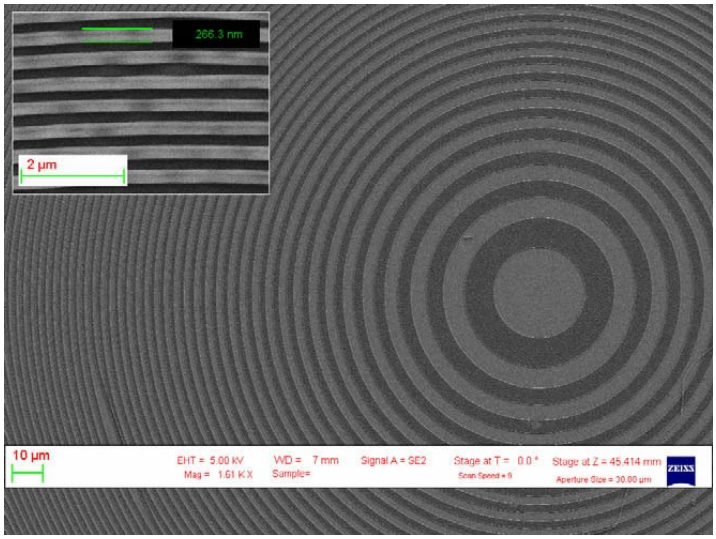

Fig. 19 SEM picture of X-ray patterned film. The inset shows a zoomed section of the nanostructures, where a 266.3nm edge is measured [26].

Fig. 19 shows the patterned film obtained with an irradiation dose of 20 J/cm^2 through a mask made of a 2μm Si_3N_4 membrane, presenting features in gold grown up to 2μm. SEM images of the final pattern show a good definition of the structure profile and a complete removal of the residual layer. The spatial resolution is well below 300nm, as it can be seen by the sharp edges of the zone plate structure.

Glycidoxypropyltrimethoxysilane based sol-gel materials

A specific organic–inorganic film based on 3-glycidoxypropyltrimethoxysilane (GPTMS) with epoxy rings acting as silica network modifier and sensitive to radiation has been developed for photonics application [27-29]. This resist has a controlled inorganic crosslinking degree and an almost total absence of organic polymerization. The film has been exposed to electron beam or X-ray synchrotron radiation. Both the interactions induce the polymerization of the organic part of the film generating its hardening after post exposure baking. The exposed material becomes insoluble determining a negative-resist like behaviour: the nanolithographic process results from the dissolution of the un-exposed areas in proper solvents. The optimized dose has been determined to be 12μC/cm^2 for electron-beam lithography [27]. Instead for X-ray lithography the optimized dose has been determined to be 6000mJ/cm^2 [27].

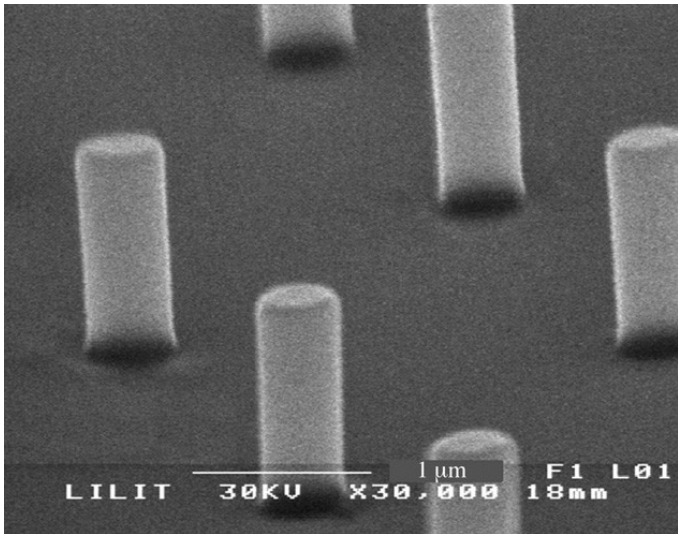

Fig. 20 Examples of hybrid sol–gel structure obtained by X-ray lithography [28].

The spatial resolution that we have obtained for the nanometric structures is below 200nm, both with EBL and XRL. Fig. 20 reports an example of the obtained structures. In the figure, pillars with an aspect ratio of 3 are shown: height is around 1.5μm and the diameter is 500nm.

TiO_2 sol-gel materials

To simplify the UV-NIL process, the UV-curable resins can be replaced with a photosensitive titanium organic compound, reducing the number of processing steps for fabricating TiO_2 nanopatterns and making the fabrication process even more cost-effective. process for the fabrication of well-ordered TiO_2 nanostructures using photosensitive titanium(IV) di-n-butoxide bis(2-ethylhexanoate). It was found that exposure to UV light resulted in the rapid breakdown of organic ligands in this photosensitive compound, allowing the photochemical conversion of a film of this compound to TiO_2 at room temperature [30].

As a result, a hybrid micro/nano-patterned TiO_2 film was achieved, as shown in Fig. 21.

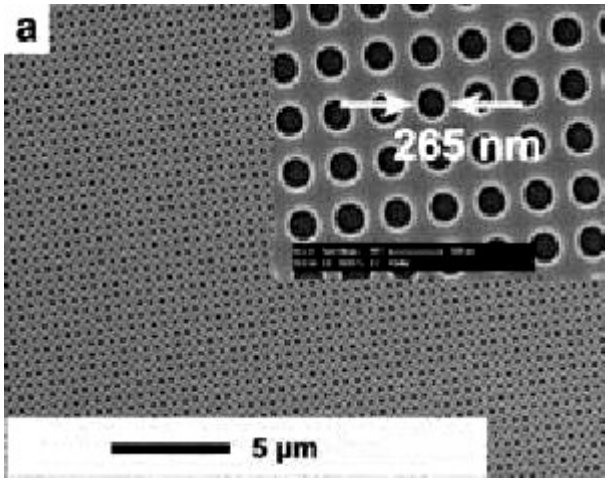

Fig. 21 SEM images of micropatterned TiO_2 using PDMS mold with hexagonal-type holes 180nm in depth and 265nm in diameter [30].

ZrO_2 sol-gel materials

Zirconium dioxide is a suitable materials to manufacture optical filters, alternative gate dielectrics in microelectronics, oxygen sensors, planar optical waveguide etc.

A systems based on MEMO (3-methacryloxypropyltrimethoxysilane) and zirconium n-propoxide precursors was studied by *Zhang et al.* [31]. The hybrid organic–inorganic coating solution is mainly based on MEMO, which has a methacrylate group that enables it to be polymerized upon UV light irradiation. MEMO-based thick hybrid coatings for integrated optics and materials protective applications. This material belongs to UV-patternable hybrid sol-gel (UVPHSG) glass materials that contain one or more photosensitive organic groups, usually with unsaturated CC bonds, which can be polymerized upon UV light irradiation. By combining the characteristics of sol-gel and polymer, the UVPHSG glass provides many advantages over pure inorganic sol-gel coatings or organic polymer coatings. (e.g. a general

problem in preparing pure inorganic sol-gel films is the cracking of thicker layers. By using hybrid sol-gel precursors, thick layers of up to several tens of microns can be coated without any cracks). Compared with organic polymer coatings, the hybrid sol-gel films also manifest advantages such as low optical propagation loss, high chemical and mechanical stability as well as good compatibility with different substrates to be coated.

Fig. 22 shows an SEM picture of ridge waveguides of 10μm width and 8μm thickness developed on a 500nm SiO_2/Si wafer make using photolithography (UV density about 25mWcm^{-2}).

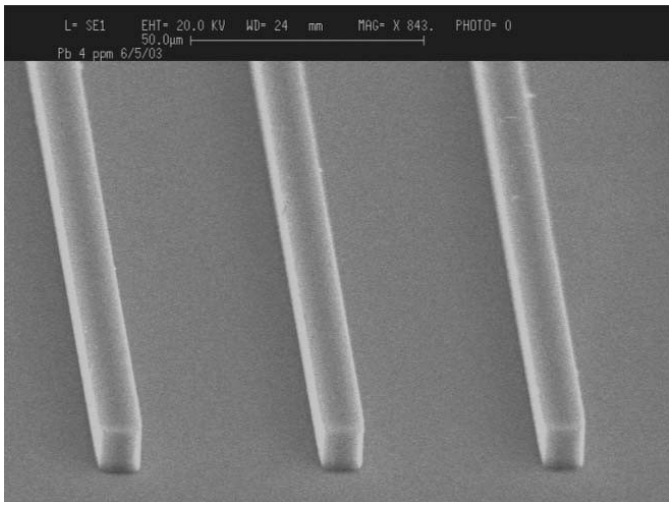

Fig. 22 SEM micrograph of a series of hybrid sol-gel strip waveguides of 10μm width and 8μm thickness [31].

But the potential for miniaturization of some devices is offset by the fact that conventional methods of patterning ZrO_2 using the lift-off technique remain unreliable. The lift-off process is almost always unsuccessful especially when complicated features are desired. To overcome this problem, an electron-beam-sensitive spin-coatable ZrO_2 resist is used [32]. This resist is capable of direct writing on a sub-10nm resolution. Spin-coatable ZrO_2 resist was prepared by reacting zirconium n-butoxide, $Zr(OBu^n)_4$, with benzoylacetone, BzAc. $Zr(OBu^n)_4$ easily undergoes hydrolysis. This is due to the presence of electronegative butoxyl groups, that makes the zirconium atom susceptible to nucleophilic attack. In order to suppress the hydrolysis and condensation reactions, $Zr(OBu^n)_4$ was stabilized by chelating agents such as BzAc. Electron beam patterning results in 9nm wide lines. Features as small as 10nm could be patterned on a 30nm pitch.

Another fine-patterning technique used to fabricate two-dimensional (2D) ZrO_2 surface-relief is the two-beam interference method [33]. Photosensitive ZrO_2 gel film was prepared from Zr-

tetrabutoxide chemically modified with benzoylacetone. The gel film was exposed to two-beam interference fringe (1.0μm period) of He-Cd laser and then rotated by 90° in its own plane, followed by an additional exposure. Leaching of the gel film with ethanol gave lattice or island types of 2D-gratings depending on the dose of laser irradiation. These gratings, especially island type, showed excellent antireflection effect in a range of wavelength longer than the period of the gratings.

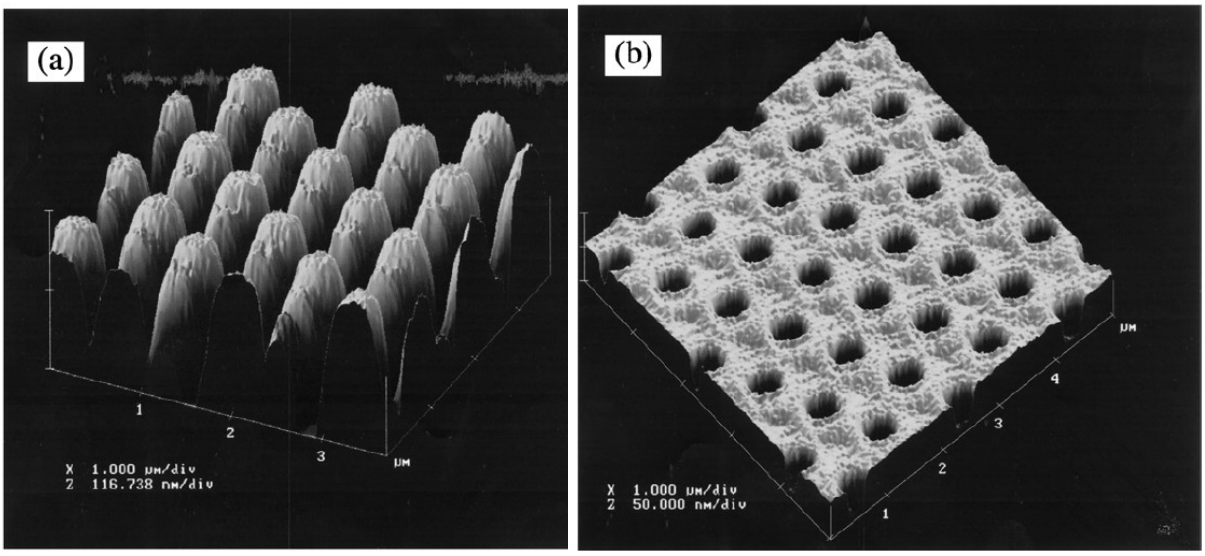

Fig. 23 AFM images of 2D-diffraction gratings formed on silica glass substrate; (a) island type and (b) lattice type [33].

Other metal oxide sol-gel materials

A wide range of metal oxides can be obtained and subsequently patterned from sol–gel precursors [34]. SnO_2, a transparent semiconductor, has recently been investigated for optoelectronics, hybrid microelectronics, and solar energy conversion applications. Many of these applications would benefit from the ability to pattern regular arrays of SnO_2 particles over a large surface area. Using a tin chloride precursor, a SnO_2 sol was obtained and used for patterning. Arrays of SnO_2 features generated from a 200nmx200nm mold by embossing are shown in Fig. 24A.

ZnO is a stable, wide-band gap semiconductor with good electrical conductivity. Various devices employ thin films of ZnO such as piezoelectric transducers, solar cells, and gas sensors. In particular, improved performance in solar cell and gas sensor applications could be achieved if highly ordered arrays of ZnO features could be fabricated. A ZnO sol was obtained using a zinc acetate precursor (Fig. 24B). Unlike the SnO_2 features, these patterns

were not sharply defined. This sol formulation contained diethanolamine (DEA), which has a boiling point that is above the drying temperature of the oven. The residual solvent may account for the deformed features observed.

Indium tin oxide (ITO) is commonly used as a transparent conductor in electronic, optoelectronic, and mechanical applications, such as window heaters, solar cells, and liquid-crystal displays. ITO features were patterned using a sol derived from indium nitrate and tin chloride precursors (Fig. 24C). In the literature there are many other examples of ITO resists patterned with room-temperature nanoimprint lithography starting from sol-gel ITO [35] as a replicated material or ITO NPs solution [36]. Sol-gel ITO material is 5% oxide and 95% solvent. The solvent consists of turpentine, ethyl acetate and butyl acetate. The oxide's concentration is 95% In_2O_3 and 5% SnO_2. ITO NP dispersed solution, containing 20wt % ITO NPs, in an isopropyl alcohol IPA.

Barium titanate is a ferroelectric ceramic that is commonly used for its dielectric, piezoelectric, and optical properties. It is used extensively as the filler component in polymer–ceramic composites. The ability to control the shape, orientation and size of dielectric heterostructures is of paramount importance to applications such as sensors, current limiters, acoustic actuators, microwave absorbers, and the fabrication of photonic band gap structures. The $BaTiO_3$ features shown in Fig. 24D were patterned from a barium acetate and titanium isopropoxide-based sol using a 200nmx200nm PFPE mold.

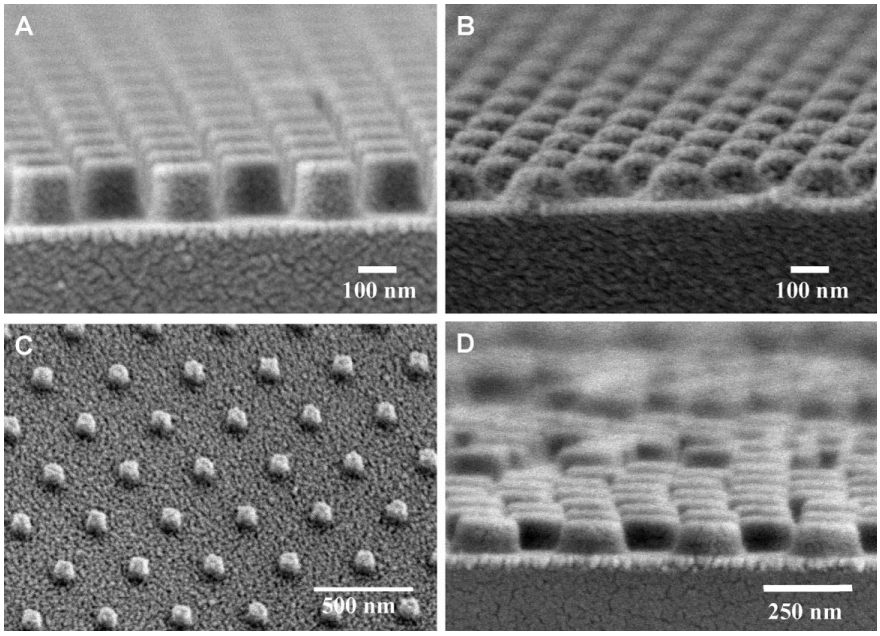

Fig. 24 SEM images of arrays of various inorganic oxide features on glass made: (A) SnO_2; (B) ZnO; (C) ITO; (D) $BaTiO_3$.

4. TITANIUM DIOXIDE

4.1. GENERAL REMARKS

Titanium dioxide, also known as titanium(IV) oxide or titania, is the naturally occurring oxide of titanium, chemical formula TiO_2. TiO_2 belongs to the family of transition metal oxides.

Titanium dioxide occurs in nature as well-known minerals rutile, anatase and brookite. The most common form is rutile, which is also the most stable form. Anatase and brookite both convert to rutile upon heating. Rutile, anatase and brookite all contain six coordinated titaniums. The three crystal structures differ by the distortion of each octahedral and by the assembly patterns of the octahedral chains. Anatase can be regarded to be built-up from octahedrals that are connected by their vertices, in rutile, the edges are connected, and in brookite, both vertices and edges are connected. Additional high-pressure forms have been synthesized starting from rutile: TiO_2(II), which has the PbO_2 structure, and TiO_2(H) with the hollandite structure [37].

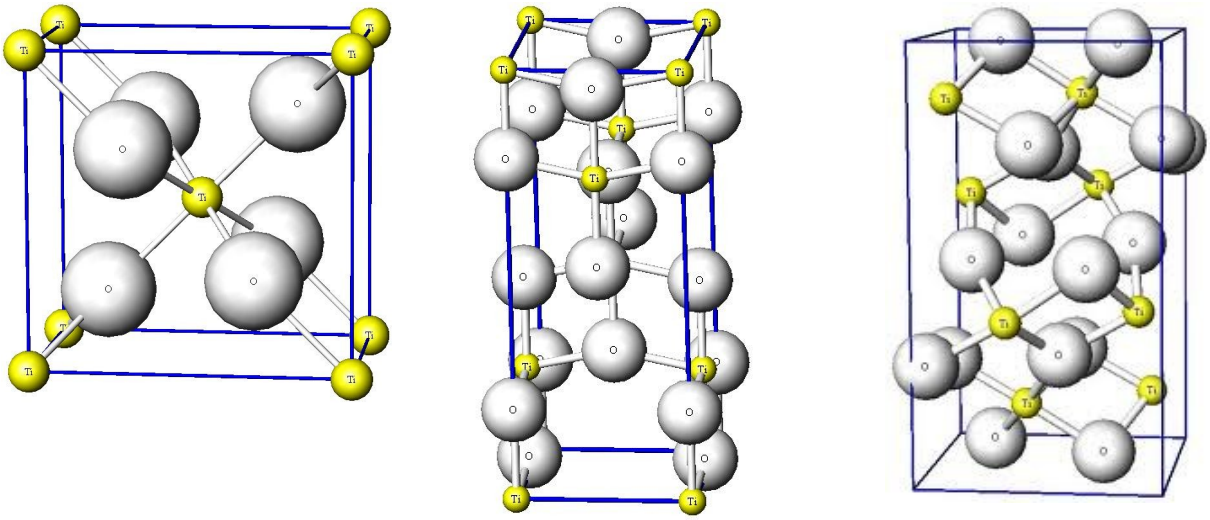

Fig. 25 Crystalline structured of TiO_2 allotropic forms: (left) rutile, (centre) anatase, (rigth) brookite. (Ti atoms are yellow and O atoms are grey).

Thanks to its remarkable optical, mechanical, electronic and photocathalitic properties, TiO_2 has attracted much attention in various fields of applications. It is used as a white pigment in paints (51% of total production), plastic (19%), and paper (17%), which represents the major end-use sectors of TiO_2. TiO_2 has received a great deal of attention due to its chemical

stability, non-toxicity, low cost, and other advantageous properties. As a result of its high refractive index, it is used as anti-reflection coating in silicon solar cells and in many thin-film optical devices. TiO_2 is successfully used as gas sensor (due to the dependence of the electric conductivity on the ambient gas composition). Due to its hemocompatibility with the human body, TiO_2 is used as a biomaterial (as bone substitute and reinforcing mechanical supports). TiO_2 is also used in catalytic reactions acting as a promoter, a carrier for metals and metal oxides, an additive, or as a catalyst. Rutile is investigated as a dielectric gate material for MOSFET devices as a result of its high dielectric constant (ε>100). In batteries, the anatase form is used as an anode material in which lithium ions can intercalate reversibly. For solar cell applications, the anatase structure is preferred over the rutile structure, as anatase exhibits a higher electron mobility, lower dielectric constant and lower density. Nanostructured TiO_2 especially is extensively studied in the field of solar cells [37].

4.2. TiO_2 SYNTHESIS: SOL-GEL METHOD

TiO_2 can be prepared in the form of powder, crystals, or thin films. Both powders and films can be built up from crystallites ranging from a few nanometers to several micrometers. The various synthesis approaches to obtain TiO_2 can be divided in two main categories: solution routes and gas-phase routes.

For some applications, especially the synthesis of thin films, liquid-phase processing is one of the most convenient and utilized methods of synthesis. This method has the advantage of control over the stoichiometry, producing homogeneous materials, allowing formation of complex shapes, and preparation of composite materials. However, there are several disadvantages among which can be: expensive precursors, long processing times, and the presence of carbon as an impurity. In this class of processes belong: precipitation(co-)methods, solvothermal methods, sol–gel methods, microemulsion methods, combustion synthesis and electrochemical synthesis [37].

For thin films, most synthesis routes are performed from the gas phase. These can be chemical or physical of nature. Most of these techniques can also synthesize powder, if a method to collect the produced particles is employed. The main techniques are: chemical vapor deposition (CVD), physical vapor deposition (PVD) and spray pyrolysis deposition.

Among all these methods, only the sol-gel methods will be dealt accurately. Sol-gel methods

are used for the synthesis of thin films, powders, and membranes. Two types are known: the non-alkoxide and the alkoxide route. Depending on the synthetic approach used, oxides with different physical and chemical properties may be obtained. The sol–gel method has many advantages over other fabrication techniques such as purity, homogeneity, felicity, and flexibility in introducing dopants in large concentrations, stoichiometry control, ease of processing, control over the composition, and the ability to coat large and complex areas. The non-alkoxide route uses inorganic salts (such as nitrates, chlorides, acetates, carbonates, acetylacetonates, etc.), which requires an additional removal of the inorganic anion, while the alkoxide route (the most employed) uses metal alkoxides as starting material. This method involves the formation of a TiO_2 sol or gel or precipitation by hydrolysis and condensation (with polymer formation) of titanium alkoxides. In order to exhibit better control over the evolution of the microstructure, it is desirable to separate and temper the steps of hydrolysis and condensation. In order to achieve this goal, several approaches were adopted. One of them is alkoxide modification by complexation with coordination agents such as carboxylates, or βdiketonates that hydrolyze slower than alkoxide ligands. Additionally, the preferred coordination mode of these ligands can be exploited to control the evolution of the structure. Acid–base catalysis can also be used to enable separation of hydrolysis and condensation steps. It has been demonstrated that acid catalysis increases hydrolysis rates and ultimately crystalline powders are formed from fully hydrolyzed precursors. Base catalysis is thought to promote condensation with the result that amorphous powders are obtained containing unhydrolyzed alkoxide ligands. On the other hand, acetic acid may be used in order to initiate hydrolysis via an esterification reaction, and alcoholic sols prepared from titanium alkoxide using amino alcohols have been shown to stabilize the sol, reducing or preventing the condensation and the precipitation of titania. These reactions are followed by a thermal treatment (450–600°C) to remove the organic part and to crystallize either anatase or rutile TiO_2. Recent variants of the sol–gel method lowered the necessary temperature to less than 100°C. The calcination process will inevitably cause a decline in surface area (due to sintering and crystal growth), loss of surface hydroxyl groups, and even induce phase transformation.

As titanium sources, Ti(*O*-E)$_4$, Ti(*i*-OP)$_4$, and Ti(O-*n*Bu)$_4$ are most commonly used. The sol–gel method has been widely studied particularly for multicomponent oxides where intimate mixing is required to form a homogeneous phase at the molecular level. Thus, different metal ions were introduced into TiO_2 powders and films by this method and the photocatalytic

activity was improved to varying extent.

For nanostructured thin films, the sols are often treated in an autoclave to allow controlled growth of the particles until they reach the desired size. Oswald ripening takes place during this process, leading to a homogeneous particle-size distribution. If a film is made using these particles, substances can be added to prevent cracking and agglomeration or increase the binding and viscosity after this ripening process. The resulting paste can be deposited on a substrate. The solvent is evaporated and the particles are interconnected by a sintering process, normally at air temperatures around 450°C. At this temperature, organic additives are also removed from the film. Slow heating and cooling is important to prevent cracking of the film. In most cases, the resulting film has a porosity of 50%. Thin films can also be made from the sol by dip or spin coating.

4.2.1. Specific examples of TiO_2 thin films

The sol–gel method is one of the most important techniques for the synthesis of various functional coatings or films, because it possesses a number of advantages over conventional film formation techniques, such as low temperature processing, easy coating of large surfaces, homogeneous multicomponent oxide films, and good control of composition and optical properties of the final material.

C.-C. Wu et al. have prepared epoxy/titania hybrid film using a diglycidyl ether of bisphenol A prepolymer with a metal alkoxide precursor and a coupling agent, 3 glycidyloxypropyltrimethoxysilane to avoid phase separation. In fact the introduction of the coupling agent results in the reinforced interfacial interaction between the epoxy resin and inorganic nanoparticles. The theoretically calculated content of TiO_2, in the hybrid resists is 10wt%. The weight percent was calculated under the assumption that all the metal alkoxide $Ti(OEt)_4$ was converted to metal oxides. The addition of inorganic nanoparticles enhance the thermal properties and etching resistibility of the epoxy resin. It can also reduce the shrinkage and improve dimensional stability [38].

Another sol–gel method was used to produce titania thin films by *Phadke et al* [39]. It consisted of a molar ratio of 1:4:40 of titanium isopropoxide (TIP) to acetic acid to alcohol. The acetic acid acts as a modifier of the TIP and initiates an esterification reaction that frees the water for hydrolysis. Different kinds of alcohols were tested for uniform coatings. 1-butanol was chosen because it produced coatings of uniform thickness with very few defects

4.3. PHOTOCATALYTIC PROPERTIES OF TiO_2

It is now well known that titanium dioxide (TiO_2) is one of the most superior material for decomposing organic materials due to its strong photocatalytic property. The photocatalytic activity can be significantly enhanced by reducing the size of the TiO_2 particle. By reducing the size of the TiO_2 particle, the surface area of TiO_2 increases leading to improvement of photoefficiency and thus photocatalytic property, because high surface area would make the surface of the particle more active to light and H_2O adsorption [40].

The physical and chemical processes occurring during the photocatalytic process of TiO_2 will be present concisely. By invoking the electronic energy band structure of TiO_2, one can describe its photocatalytic activity. TiO_2 is a semiconductor that presents two crystalline forms: anatase and rutile. Anatase has a band gap of 3,2eV and for rutile it is 3,0eV. Anatase has been found to be the most active form. The action spectrum for anatase shows a sharp decrease in activity above about 385nm. If this material is irradiated with photons of the energy >3,2eV (wavelength λ<388nm), the band gap is exceeded and an electron is promoted from the valence to the conduction band. Consequently, the primary process is the charge-carrier generation: $TiO_2 + h\nu \rightarrow h^+ + e^-$. This band picture assures a sufficiently long lifetime of e^-–h^+ pair to diffuse to the surface of the catalyst and initiate a redox reaction. The photocatalytic process includes chemical steps that produce reactive species: hydroxyl radical, hydrogen peroxide, superoxide, conduction band electron, and valence band hole [41].

4.4. TiO_2-BASED MATERIALS FOR NANOLITHOGRAPHY

TiO_2 has several attractive material properties and its nanopattern fabrication have been studied intensively because of its wide band gap and photocatalytic nature. TiO_2 nanopatterns can be made by conventional patterning techniques, consisting of deposition, photolithography or electron beam lithography, and etching processes or by nanoimprint lithography.

Conventionally, TiO_2 is patterned by sputtering it on to a prepatterned organic resist and then performing lift-off. But the lift-off process remains delicate, especially when complicated features and/or thick films of TiO_2 are desired.

To eliminate the problems associated with lift-off, *Saifullah et al.* propose a sol-gel-based

spin-coatable TiO_2 resist that is not only amenable to direct-write using an electron beam but is also capable of providing sub-10nm resolution. TiO_2 resist prepared by chemical modification of titanium *n*-butoxide, $Ti(OBu^n)_4$, with benzoylacetone, BzAc. The electron beam sensitivity of TiO_2 resist is $35mC/cm^2$ and has a contrast $\gamma=1$. Exposure to the electron beam makes spin-coatable TiO_2 resists insoluble in acetone. This property was successfully employed to produce lines that were 8nm wide. Features that are ≤ 10nm wide can be patterned with a 30nm pitch [42].

Liu et al. present a method of sub-100nm direct pattern transfer of compound semiconductor using sol-gel-derived spin-coatable TiO_2 resist as mask. They demonstrate the technique on InP compound semiconductor using inductively coupled plasma reactive ion etching (ICP-RIE). Various sub-100nm scale inductively coupled plasma etching patterns are obtained with a high-quality etching profile. The smallest feature is as small as 20nm wide with a depth of over 600nm. The optimal dose of TiO_2 resist for E-beam lithography is $220mC/cm^2$. The sample InP compound semiconductor etching selectivity to TiO_2 resist is as high as 9:1 with aspect ratio of over 30:1 [43].

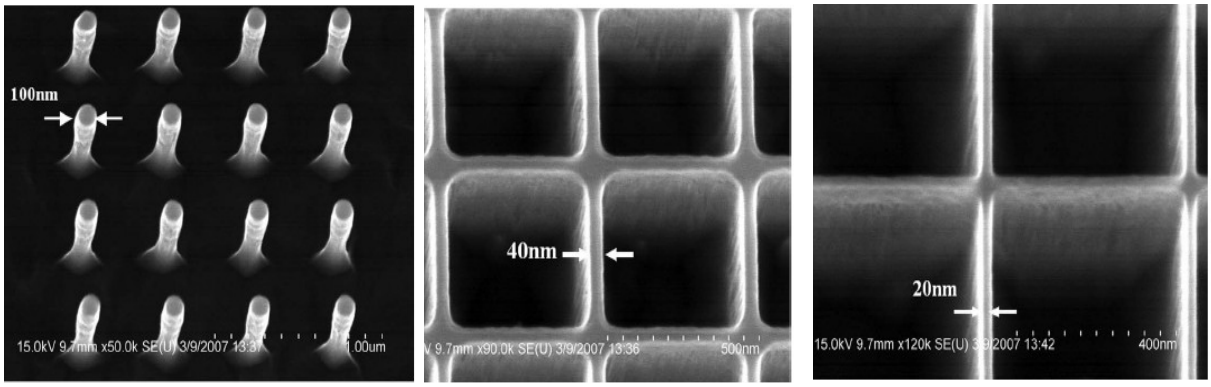

Fig. 26 ICP-RIE etching using sol-gel-derived TiO_2 resist as a mask. (left) SEM pictures of 100nm diameter pillars etched by ICP-RIE. (center) SEM pictures of 40nm wide grid etching pattern; etching depth is over 1200nm. (right) SEM pictures of grid-shaped etching patterns. The line is as small as 20nm wide and over 600nm deep [43].

Concerning the use of TiO_2 sol-gel in non conventional techniques, the literature reports various examples. *Goh et al.* demonstrate a method for embossing titania sol-gel precursor with poly(methyl methacrylate) (PMMA) molds to make thin films of titania that have dense arrays of 35-65nm diameter pores [44]. Thermal infiltration was used to fill the narrow pores with mold material. A thin layer of PMMA covered with a thick layer of PDMS was used as the mold so that the mold would be permeable, but mechanically stable and flexible. The

anodic alumina was etched to avoid damaging the mold during retrieval from the template. Finally, the mold was dissolved after embossing the semiconductor to prevent sticking. These techniques have enabled us to pattern dense arrays of deep, narrow, straight pores in titania, a semiconductor that is often used in photovoltaic and photocatalytic applications. Specifically, they nanostructure titania (TiO_2) films from sol-gel precursors to resemble the structure of an anodic alumina (AAO) template with pore diameters of 35-65nm.

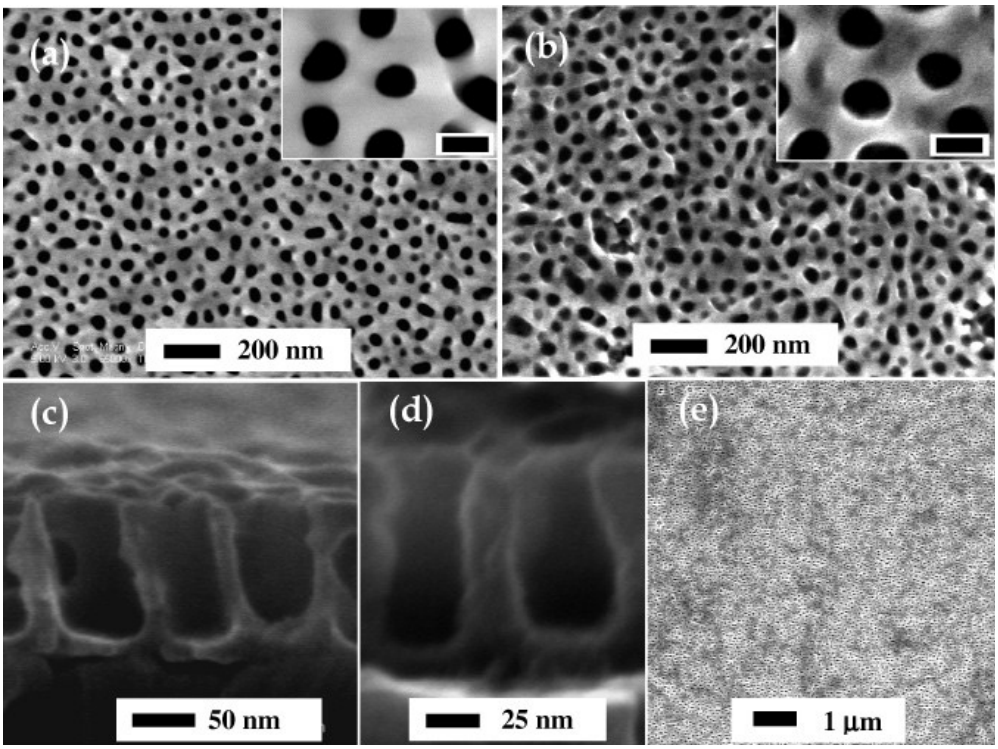

Fig. 27 SEM images of (a) typical initial AAO template, (b) typical embossed TiO_2 structures after PMMA removal with acetonitrile, the average pore diameter is 45nm, (c) embossed TiO_2 structures on FTO substrate after calcinations (cross section), the average pore diameter is larger because the initial template used has larger pore diameter, (d) smaller-diameter pores with one showing 30nm diameter, and (e) embossed TiO_2 at a larger scale showing uniformity of the replication. The insets in (a) and (b) are respectively images at a higher magnification; the scale bar corresponds to 50nm [44].

Lim et al. demonstrate two different approach to direct nanoimprint lithography of TiO_2. The first is to spin-coat sol-gel solutions onto a substrate for a short time and emboss with the mold before the solution dried. This method however trapped air between the solution and the mold interface and resulted in a final TiO_2 structure with a high density of voids. The second method involves spin-coating the sol-gel solutions onto the mold directly and then embossing on the substrate prior to solution drying. TiO_2 was imprinted using a polymerizable liquid consisting of a mixture of titanium methacrylate, ethylene glycol dimethacrylate, and azobis-

(isobutyronitrile). The resin underwent free radical polymerization when imprinted using a silicon mold at 110°C with pressures as low as 10bar. Heat-treatment of the imprinted structures resulted in the loss of organics and their subsequent shrinkage (~75%) without the loss of integrity or aspect ratio, and converted them to TiO_2 nanostructures as small as ~20nm wide [45].

Other precursors for TiO_2 sol-gel materials is used by *Yoon et al.* for fabricating nanopatterns using reverse-imprint lithography. Ethanol based TiO_2 sol was prepared using tetrabuthylorthotitanate $C_{16}H_{36}O_4Ti$ and diethanolamine $C_4H_{11}NO_2$. TiO_2 sol was then coated on the surface of the replicated polymer mold of hard-polydimethylsiloxane and polydimethylsiloxane by spin coating and transferred to the substrate by the reverse imprinting process at 200 °C. A postimprint annealing process was subsequently carried out to form the TiO_2 polycrystalline phase. A TiO_2 nanopattern, as small as 50nm, was formed [46].

A direct ultraviolet (UV)-assisted nanoimprinting procedure using photosensitive titanium di-n-butoxide bis(2-ethylhexanoate) is employed for the nanopatterning of anatase titanium dioxide (TiO_2) structure by *H.-H. Park et al.* [47].

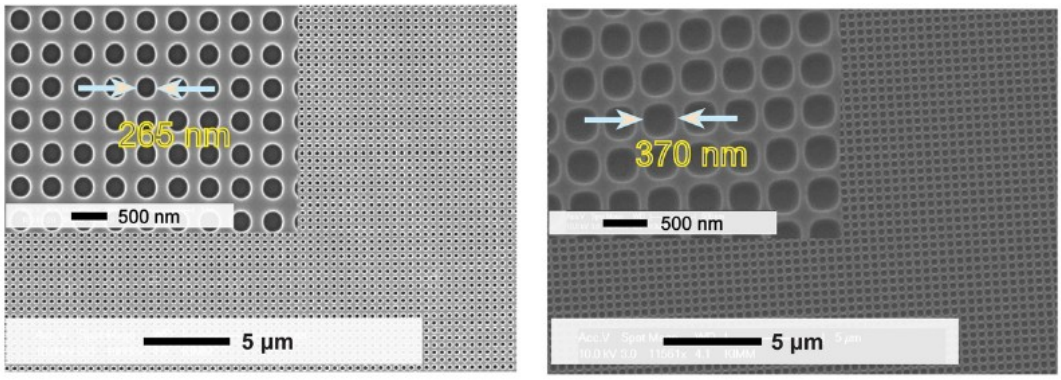

Fig. 28 (left) SEM image of imprint results of the TiO_2 nanostructure with dot arrays of a 265nm diameter mold and (right) SEM image of the imprinted TiO_2 nanostructure annealed at 400°C for 1h [47].

The ultraviolet-assisted nanoimprint lithography process consists a polyurethane acrylate mold pressed against the film at a pressure of 2bar at room temperature for 3min. The film was then exposed to UV light with a dose of approximately 52 mW/cm^2 with a major wavelength peak of 365nm to induce a photochemical reaction. After annealing process, the hole-diameter of the TiO_2 nanostructure increases instead the height decreases. Despite the shrinkage, macroscopically uniform and crack-free patterned structures were obtained (Fig. 28).

5. APPLICATIONS

5.1. APPLICATIONS OF NANOIMPRINT LITHOGRAPHY

The high resolution and high throughput capability of nanoimprinting lithography (NIL) makes it a very useful technique in many electrical, optical and magnetic device applications that require precision patterning of large areas of nanoscale structures. For electronic devices, NIL has been used to fabricate MOSFET, high resolution OLED pixels and organic TFTs. For optics and photonics, intensive study has been conducted in fabrication of subwavelength resonant grating filter, waveguide polarizers, anti-reflective structures, integrated photonics circuit and plasmonic devices. Another area where nanoimprinting-based technology may play an important role is in micro- and nanofluidic devices for biological and lab-on-a-chip applications [12,14].

For clarity, the application of nanoimprint can be divided into two main categories: patter-transfer applications and directly patterned devices. In the first category, pattern-transfer applications, the nanoimprinted resist structure is used as a temporary masking layer for a subsequent pattern-transfer step. In the second category, material devices, the imprinted pattern adds functionality to the film, which is the end product.

In many pattern-transfer applications, the main issue is high throughput with nanoscale resolution. Disregarding this issue, it is of minor importance whether the resist film is patterned by means of electromagnetic radiation, electrons or by mechanical deformation. Only few steps in the process flow are different. The advantages of NIL come into play if high resolution is needed over a large area. In addition to its high resolution, the NIL technique also offers the capability for 3D or multilevel imprinting, when the stamp is structured of different heights. Nanoscale patterned films find specific and wide range of applications within optics, electronics and nano-biotechnology.

As an example of optical applications, *Moujoud et al.* [48] demonstrate an efficient, tunable Long Period Waveguide Grating (LPWG) filter based on a new hybrid sol-gel material. LPG has many applications, such as band-rejection filters, optical sensors, and wavelength selective polarizing elements. Up to now, most LPWGs have been realized in polymer materials, while LPWG devices based on sol-gel materials remains relatively unexplored. Two LPWG structures were fabricated by soft lithography: the standard structure where the

gratings are fabricated on the top of the ridge waveguide and a new structure with gratings integrated on the top and on the bottom of the same sol-gel ridge waveguide. The devices were operated at communication wavelengths of 1550 and 1310nm, respectively. The integration of two filters on the same structure can drastically reduce the size and cost of the device.

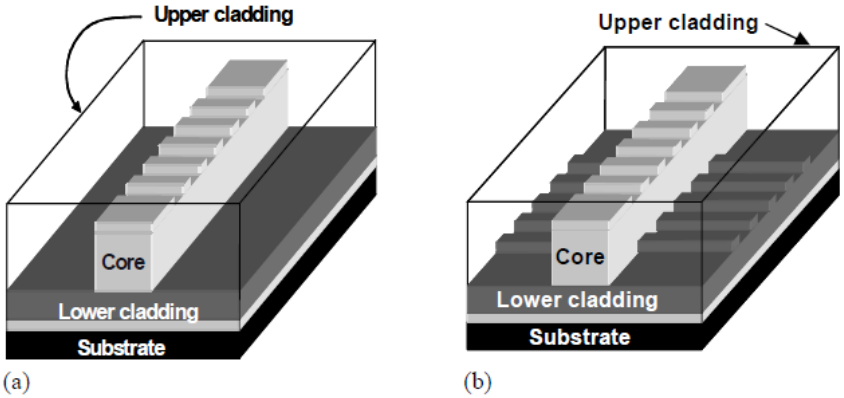

Fig. 29 Two possible configurations for physically patterned LPWG in optical waveguides: (a) Grating patterned on the top of the core, (b) Grating patterned both in top and bottom of the core [48].

Another new field in which the nanolithographic processes are taking place is the production of solar cells. For example the study of a photovoltaic cell made with poly(3-hexyl thiophene) infiltrated into mesoporous titania (*McGehee*) [49] showed that aligning polymer chains in straight pores enhances the charge-carrier mobility to a point that is thought to be adequate to remove charge from solar cells at the same rate as it is generated by the sun. This inspired the researchers to make semiconductor films with straight smooth-walled pores having diameters in the range of 10-20nm, lengths of 200nm or more, and an orientation perpendicular to the substrate using nanoimprinting.

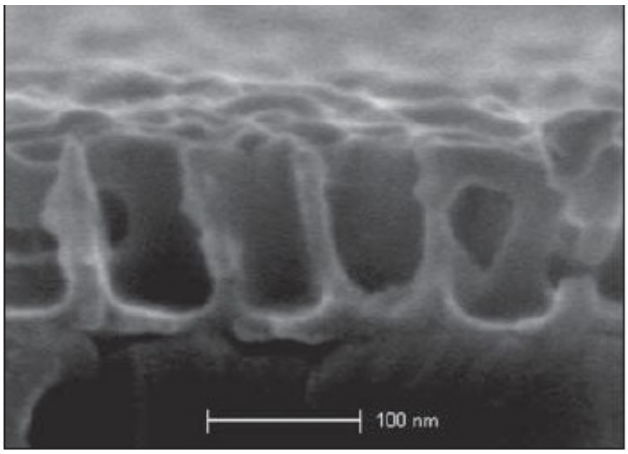

Fig. 30 SEM image of embossed TiO_2 structures on fluorine-doped tin oxide substrate after calcination [49].

The pores of an anodic alumina film were filled with poly(methyl methacrylate) (PMMA) to make a mold for nanoimprinting titania. Then the PMMA mold was pressed into a film of titania sol–gel precursor. Once the titania was solidified, toluene was used to dissolve the PMMA, leaving the desired nanoporous film. A scanning electron microscopy image of a film with 40-nm-diameter pores is shown in Fig. 30.

5.2. APPLICATIONS OF TiO_2-BASED MATERIALS

The excellent properties of titania makes it the material of choice in many applications. In fact TiO_2 thin films has been extensively investigated for its potential application in solar cells, optical waveguides, photonic crystals, anti-reflective coatings and gas sensors. One or more examples concerning the principal applications of TiO_2 are reported.

Anti-reflective coatings.

Glasses and plastics suffer from reflection losses at the substrate-air interface. AR-coatings are applied for solar cells, displays, eye glasses, computer screens and lenses in optical equipments to reduce the reflectance and increase the efficiency of the optical devices [50].

Nowadays AR-coatings were used, for example, in LCD monitor. When the external light is strong, the surface glass of a LCD monitor screen appearing glare and reducing the quality of the display. The best way to overcome this problem is to use surface treatments. The preparation of antireflection coated film has become a necessity. There are tradeoffs, to be considered, enhancing the antireflection properties of the materials will also affect their refractive index. In order to synthesize the front panel of monitor with a high refractive index optical film *W.-M. Chiu et al.* uses titanium dioxide nanoparticles mixed with methyl methacrylate (MMA), 2-hydroxyethyl methacrylate (2-HEMA), and tri(ethyleneglycol) dimethacrylate (TEGDMA) as crosslinking agent. It can be noted that with the addition of a crosslinking agent, the refractive index has a slight upward trend; the transparency rate of thin film is still close to 90%, which conforms to the demand for optical elements with high refractive index [51].

Photonic crystals

Dielectric thin films with periodic nanopatterns, known as photonic crystals (PhC), can

exhibit many interesting optical properties such as photonic band gap, i.e., the frequency range where an electromagnetic wave cannot propagate through the films. Thus, PhC are expected to be useful in the implementation of new functional optical devices and optical properties, such as bent waveguides, superprism phenomenon, self-collimated beam propagation, form birefringence, and so on. A photonic crystal is composed of periodic arrangements of dielectrics material. If the periodicity and the symmetry of the crystal and the dielectric constants of the materials used are chosen appropriately, the photonic crystal will selectively couple to particular wavelengths and exclude others. In particular, titanium dioxide (TiO_2) is attracting wide attentions for applications in photonic crystals (PhC). First of all, TiO_2 has a fairly large refractive index among the transparent metal oxides (>2.5 at anatase phase, and >2.7 at rutile phase), which is large enough to form a photonic band gap in PhC structures. Secondly, the optical absorption loss of TiO_2 is about 10 times lower than that of silicon at the optical communication wavelength of 1.5μm. Thirdly, its thermal expansion coefficient is very small ($7\sim9\times10^{-6}K^{-1}$ over a wide range from room temperature to 1000°C). Considering all these advantages, TiO_2 should be considered as an important candidate for PhC engineering [52].

UV patternable high refractive index inorganic–organic hybrid materials prepared by sol–gel process are nanoimprinted in order to get photonic crystal nanopatterns by *W.S. Kim et al.*. Non-hydrolytic sol–gel process can make a UVcurable and relatively high refractive index hybrid material, which can be cured without a significant shrinkage for nanoimprinting. This hybrimer has low absorption loss and is very well polycondensed. Holes having 105nm diameter, 408nm pitch, and 127nm depth were obtained [53].

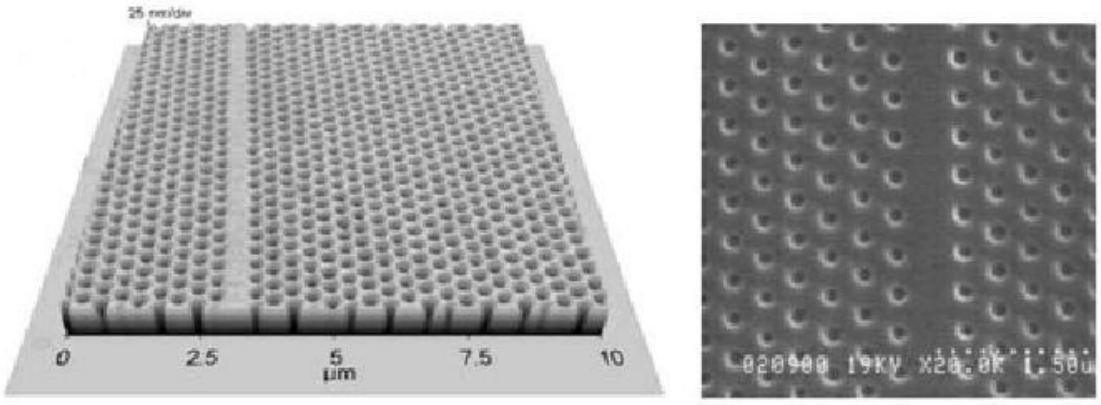

Fig. 31 AFM and SEM images of imprinted hole nanostructures with 105nm diameter and 127nm depth by UV-based nanoimprint technique.

B. Saekow et al. fabricated a photonic crystal biosensor device that consists of SOG (Silicon On Glass) material and titanium dioxide (TiO_2) thin films as low and high refractive indexes dielectrics layers, respectively [54]. NIL process was used to duplicate periodic line as gratings structure from Ni-master mold onto SOG/glass. The fabricated device was provided as an array of sensors aligned and attached to bottomless of well ordered array of PDMS. The sub-wavelength grating structure of the low-k material were fabricated using 700nm period line-pair optical interference grating patterned on Ni as master mold. Then this Ni-master mold was used to duplicate grating pattern on spun-SOG/glass through nano-lithography process. The patterned SOG film with 200nm grating depth was used as low-k layer and then 150nm thick of TiO_2 as high-k layer was evaporated onto its surface. A PDMS sheet with 30-well arrays are attached onto the surface of photonic device after RF plasma treatment surfaces to provide liquid containment.

Optical waveguides

The basic components of communication networks are passive components like star couplers, multiplexers and power splitters made from **Y** junctions and couplers. Waveguides are the cornerstones of their operation. Channel waveguides in particular are basic components of integrated optics, and the development of fabrication technology for them is hence essential to the realization of high-performance devices of that kind.

Optical waveguide thin films have been prepared by *Que and Kam* from composites of TiO_2 and organically modified silane at low temperature by sol-gel technique. Channel waveguides can easily be fabricated by embossing. The period of the embossed grating was measured as 1,1μm while the embossed depth of the grating is 57nm [55].

Other studies of titania/organically modified silane hybrid optical waveguides are reported by *Que et al.* and *Li et al.*. *Que et al.* prepared a single layer optical waveguide thin film with thickness of more than 1,30μm by sol-gel spin-coating technique. The patterns were fabricated from by wet etching in HF solution at different etching time [56]. In another article the same research group processed a $SiO_2/TiO_2/\gamma$-glycidoxypropyltrimethoxysilane composite materials for optical waveguide applications [57]. Waveguide films with thickness more than 1.7μm were prepared on a silicon substrate by a single-coating process and low-temperature heat treatment. About 1.3dB/cm propagation loss of the planar waveguide film with low titanium content (0,2M) has been obtained.

Instead *Li et al.* prepared a sol-gel material patterned with gratings of 300nm pitch and 80nm linewidth and waveguide gratings with varying periods imprinted in a single step and with excellent uniformity into the gel films coated on a quarter of 4in. wafers. Waveguide gratings showed smooth profiles with root mean square roughness less than 6 nm. The smoothness and hydrophilic surface property of the patterned silica film make it potentially useful for providing spatial confinement for micro- and nanofluidic applications [58].

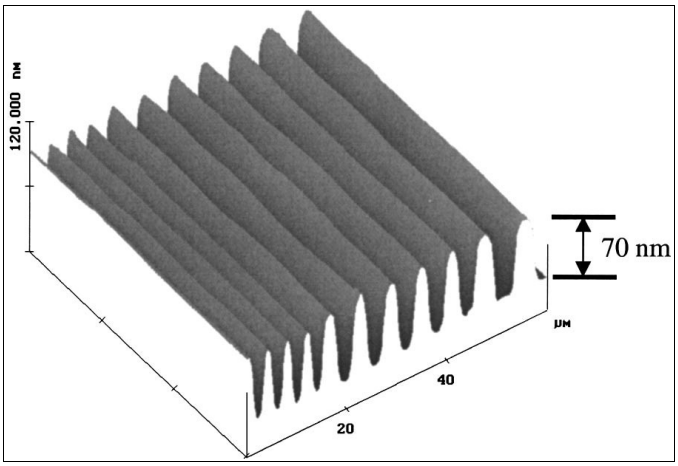

Fig. 32 Directly imprinted 70nm deep SiO2–TiO2 waveguide gratings (after heat treatment) were inspected by AFM. From the left- to right-hand side, the grating period varies from 4 to 10mm [58].

Gas sensors

Sensors with optical waveguides are usually characterized by high sensitivity, fast response times and low costs. Much effort has been devoted to ammonia and pH sensing using sol–gel-derived material. These sensors are usually based on pH-dependent changes in absorbance or luminescence of indicators entrapped in the silica/titania matrices. Bromothymol blue (BTB) is one of the indicators which changes its color with pH. Specifically molecules of BTB were entrapped in SiO_2-TiO_2 films prepared by *Łukowiak et al.* [59]. This film can be used as an optical planar waveguide sensor for ammonia because it reacts also to gaseous ammonia. The necessary requirement is that the structure without the photoresist should be applied to permit interactions of the entrapped molecules with the environment. The indicator molecules entrapped in the silica–titania film would absorb the light coupled in the planar waveguide. Coupling out the laser light would allow monitoring of changes with a detector. The grating couplers with a period of 640nm have been obtained.

Another type of gas sensor was fabricated by *Zuruzi et al.*. They produced a gas-sensor arrays with 20μm nanostructured titania (ns-titania) pads as sensing elements [60]. Fig. 33 is an

optical microscopy image of a sensor array fabricated using two-mask process. After annealing the ns-titania pad array, the circuit was completed by deposition and development of a photoresist layer, followed by metal lift-off.

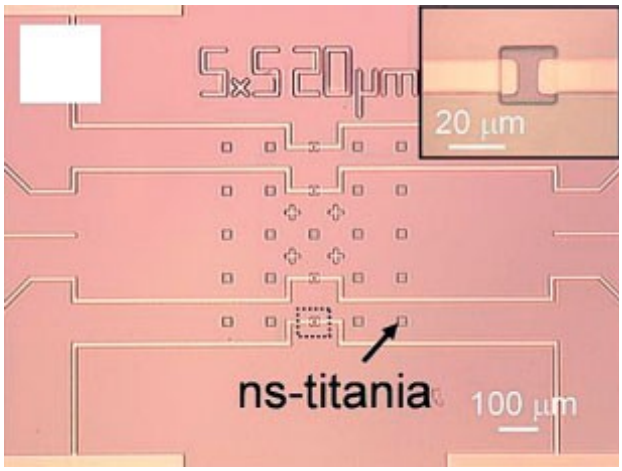

Fig. 33 A circuit with an integrated ns-titania 20μm pad array as resistive components in devices.

The work function of semiconducting titania is sensitive to surface states created by gas adsorption, and this property has been utilized for gas-sensing applications. By functionalizing the structures with appropriate chemical moieties, it may also be possible to use this fabricated ns-titania array as biomolecular sensors. Integration of ns-titania into Ti-based devices fabricated using bulk Ti micromachining technologies for biomedical applications is possible.

Solar cells

The dye sensitized solar cells (DYSC) provides a technically and economically credible alternative concept to present day p-n junction photovoltaic devices. In contrast to the conventional systems where the semiconductor assumes both the task of light absorption and charge carrier transport the two functions are separated here. Light is absorbed by a sensitizer which is anchored to the surface of a wide band gap semiconductor. Charge separation takes place at the interface via photo-induced electron injection from the dye into the conduction band of the solid. Carriers are transported in the conduction band of the semiconductor to the charge collector. The use of transition metal complexes having a broad absorption band in conjunction with oxide films of noncrystalline morphology permits to harvest a large fraction of sunlight. Nearly quantitative conversion of incident photons into electric current is achieved over a large spectral range extending over the whole visible region. *Grätzel* has

chosen as favored material titanium dioxide, TiO_2. It has many advantages for sensitized photochemistry and photoelectrochemistry as a low cost, widely available and non-toxic materials. The nanoporous structure permits the specific surface concentration of the sensitizing dye to be sufficiently high for total absorption of the incident light, necessary for efficient solar energy conversion. The nanoporous TiO_2 is obtained by an hydrothermal synthesis. A specific advantage of the procedure is the ease of control of the particular size, and hence of the nanostructure and porosity of the resultant semiconductor substrate [61].

Another type of solar cells fabrication is based on conjugated polymers. Conjugated polymers are promising photovoltaic materials because they are strong light absorbers and solution processable and can be deposited onto flexible substrates at low cost. One of the most efficient polymeric solar cell utilizes a disordered bulk heterojunction in which the conjugated polymer is mixed with an electron acceptor. However it was discovered that ordered bulk heterojunctions made by filling inorganic nanostructures with organic semiconductors have distinct advantages over their disordered counterparts because the morphology can be precisely controlled. Metal oxide (TiO_2, ZnO, etc.) templates can be fabricated with continuous pathways or pores on the scale of the exciton diffusion length in the organic semiconductor. Consequently, the device possesses the ideal morphology for maximizing charge collection efficiency regardless of the polymer used.

Williams et al. fabricated an ordered bulk heterojunction photovoltaic cells using a perfluoropolyether (PFPE) elastomeric mold to control the donor-acceptor interfacial morphology within devices. Anatase titania nanostructures with postlike features ranging from 30 to 100nm in height and 30 to 65nm in spacing were fabricated using the Pattern Replication In Nonwetting Templates (PRINT) process [62].

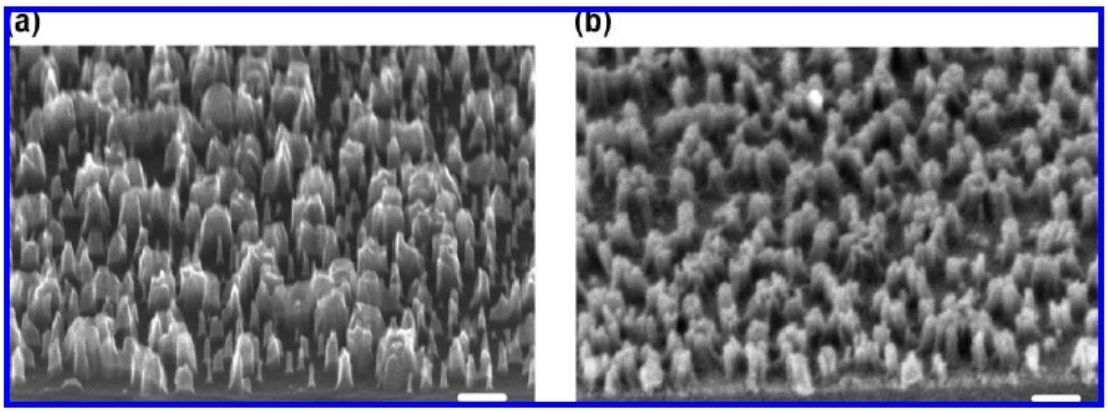

Fig. 34 SEM image of (a) NSL silicon master template with 3-min RIE and (b) anatase titania nanostructure replicated using PRINT from the silicon master. Scale bars are 100nm.

6. EXPERIMENTAL DETAILS

In this study hybrid organic-inorganic sol-gel materials based on TiO_2 were prepared, characterized and tested using thermal and micro and nanoimprinting lithography (T-NIL). Fabrication process, material properties and radiation interaction were analysed with various techniques.

6.1. MATERIALS

In this study two different titania preparation approaches were considered. The first approach was to prepare TiO_2 hybrid materials is incorporating TiO_2 nanoparticles into organic resins or polymers (TiO_2 ex-situ). The second approach is producing TiO_2 domains into organic resin or polymer matrices using the sol-gel method (TiO_2 in-situ). This process is based on the hydrolysis and condensation of precursors such as metal alkoxides to prepare network-like hybrid materials.

To prepare TiO_2 ex-situ, 3-glycidoxypropyltrimethoxysilane (GPTMS) was used as organic matrice where a solution of TiO_2 anatase nanoparticles (20wt%, 15nm-diameter) in 2-propanol (TiO_2 NPs) was dispersed. 2-methoxyethanol (MetOEtOH) was employed as solvent, bidistilled water for hydrolysis, sodium hydroxide (1M) as catalyst and a small amount of titanium isopropoxide (Tiiso) as further TiO_2 precursor. They are all purchased from Aldrich (except TiO_2 NPs) and use without further purification.

For TiO_2 in-situ, the same materials mentioned earlier were used for synthesis, except the TiO_2 NPs were substituted with another TiO_2 precursor: titanium isopropoxide. The Fig. 35 shows chemical structures of principal compounds used for synthesis of both solutions.

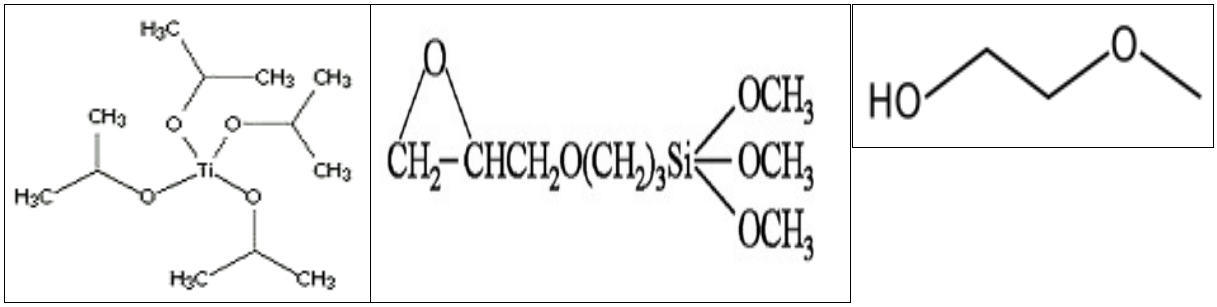

Fig. 35 Structures of principal compound used for synthesis of TiO_2 ex-situ and TiO_2 in-situ. (left) titanium isopropoxide, (centre)3-glycidoxypropyltrimethoxysilane, (right) 2-methoxyethanol.

6.2. SYNTHESIS OF HYBRID SOL-GEL MATERIALS

The synthesis reported below are referred to the final optimised recipes for ex-situ and in-situ TiO_2 materials although different recipes and titania contents were studied and modified during the study. The final recipes are the result of adjustments and changes arising from the experimental resist performance observations.

TiO_2 ex-situ

The sol consists of a volume ratio of 1:2:4=GB^+ : TiO_2 NPs : MetOEtOH. GB^+ indicates a basic sol-gel solution of GPTMS acidified with concentrated HCl 37%. The synthesis of GB^+ involves GPTMS hydrolysis at 80°C for 1h with H_2O and NaOH (GPTMS:H_2O: NaOH=1:3:0,003). The concentration of GB^+ results to be 220g/L.

Two different solutions were prepared. In the first one, GB^+ was mixed with TiO_2 dispersion and MetOEtOH (volume ratio GB^+:TiO_2 NPs:MetOEtOH=1:2:2). Whereas in the second solution, Tiiso was mixed with MetOEtOH. The amount of titanium was about 10% respect the moles of GPTMS contained inside the considered volume of GB^+. Both solutions were left to stir for 10min at room temperature, followed by another 10min of sonication. Then the solution containing titanium isopropoxide was poured into the GB^+-TiO_2 NPs solution and agitated for 10min at 70°C. The resulting solution had a volume ratio of GB^+:TiO_2 NPs:MetOEtOH=1:2:4. It was evaporated to remove solvents. The evaporated solution was diluted again with 2-butanone. The weight ratio is SiO_2:TiO_2=65:35 (assuming that all titanium isopropoxide is transformed into TiO_2) while the concentration is 90g/L.

Finally the solution was centrifuged at 5000rpm for 7min and then spin-coated. The final solution was viscous, dull and whitish. It remains stable for 24h.

TiO_2 in-situ

The sol was prepared in two different steps. In the first one, GPTMS was mixed with water (molar ratio H_2O:GPTMS=3:1) and the solution was stirred at room temperature for one night. This pre-hydrolysis step is necessary to compensate the higher reactivity of titanium alkoxides, with respect to that of silicon alkoxides. In the second step, MetOEtOh and NaOH (0,3%M in GPTMS) were added in this order. Separately, Tiiso was added to MetOEtOH at a

1:1 volume ratio, and the solution was stirred for about 10min. 2-metoxyethanol plays two different roles, acting as solvent as well as stabilizer of titanium alkoxide toward the hydrolysis reaction. It has the ability to coordinate Tiiso, decreasing its hydrolysis rate. The two solutions were then mixed and a fluorinated monomer bisphenol F diglycidyl ether (BFDGE) (10% respect TiO_2 moles) was added to solution in order to decrease the hardness of the film due to high TiO_2 content.

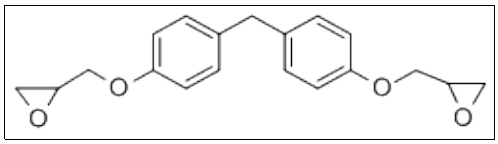

Fig. 36 Chemical structure of bisphenol F diglycidyl ether.

The final solution reached a concentration of 150g/L (related to SiO_2 and TiO_2 content) and a molar ratio of approximately SiO_2:TiO_2=90:10. Further MetOEtOH was added to reach a sol concentration of 100g/L. Finally the sol was sonicated for 30min and left to react under stirring for 1h at room temperature and for 2h at 80°C.

The sol was filtered with a microporous membrane (0,2μm Millipore) before use. The final solution appeared clear and slightly yellow until gelation occurred, which took approximately 2 weeks.

6.2.1. History of the recipes

TiO_2 ex-situ

In TiO_2 ex-situ synthesis, the first tests were carried out simply by mixing at room temperature TiO_2 NPs and GB with the following volume ratio: GB:TiO_2 NPs=1:1/1:2/2:1. The solutions were then spin-coated onto clean silicon chips at 3000rpm for 30s and UV irradiated for 10min (dose 94,1J/cm^2) in order to decompose the organic components present inside the films and obtain a completely inorganic network. A Hamamatsu LC5 UV mercury-xenon lamp with a maximum emission intensity of 3500mW/cm^2 at 365nm has been used as irradiation sources. The distance between lamp and sample was 3cm. The Fourier transmission infrared spectroscopy spectra showed that the peaks associated with the organic groups present in the precursors did not disappear after irradiation. The simplest explanation may be the high film thickness. In fact, if the film is thick it may happen that only a

superficial layer is subject to photocatalysis and the rest of material thickness remains organic. To produce thinner films, a solvent was added, specifically methoxyethanol (T_{eb}=124°C). But also this change did not yield the expected results. Therefore a small amount of titanium isopropoxide was added to the sol with the aim to create a network that traps the TiO_2 NPs avoiding agglomeration. Inside the sol-gel GB^+ solution, the molecules of GPTMS are bonded together through Si-O-Si bonds, the long chains containing the epoxy ring are not polymerized. Task of titanium isopropooxide is to catalyse the epoxy rings polymerization, building a structure that embody the NPs. Titanium isopropoxide acts as catalyst but its function is inhibited in a basic environment. Hence GB solution is acidified with some drops of chloridric acid.

During TiO_2 ex-situ synthesis it is necessary to consider also the following parameters:

Order of mixing. It is not possible mix all the ingredients together because the solution gelify. The insertion of titanium isopropoxide gives different effects if it is immediately added to GB^+ and NPs or is added later after being left to react with the solvent for a short time. In the second case the photocatalitic effect is more rapid.

Stirring temperature. Too high temperature (T>80°C) and long mixing times (t>15min) determine the solution gelification.

Solvent. Changing the solvent e.g. tetrahydrofuran (T_{eb}=66°C) instead of methoxyethanol entails higher doses for degradation of organic compound after UV irradiation and also the surface of the film becomes dull. Furthermore the ratio between solvent and TiO_2 NPs must be kept constant (1:1) even if increasing NPs amounts leads to problems of segregation. This sets a limit of TiO_2 NPs content.

TiO_2 NPs concentration. If the concentration of TiO_2 NPs is increased from GB^+:TiO_2 NPs:MetOEtOH=1:2:4 to GB^+:TiO_2 NPs:MetOEtOH=1:3:4 without increase of solvent content. The films become thicker and inhomogeneous at the same spin-coating rate and FTIR spectra (Fig. 37) present strong peaks related to organic surfactant present in TiO_2 dispersion that are more difficult to remove with UV radiation.

Different TiO_2 NPs dispersion. TiO_2 NPs dispersed in different solvent e.g. 2-isopropanol, etylacetate, butylacetate, acetone, ethanol gives unhomogeneous and dull films full of comets.

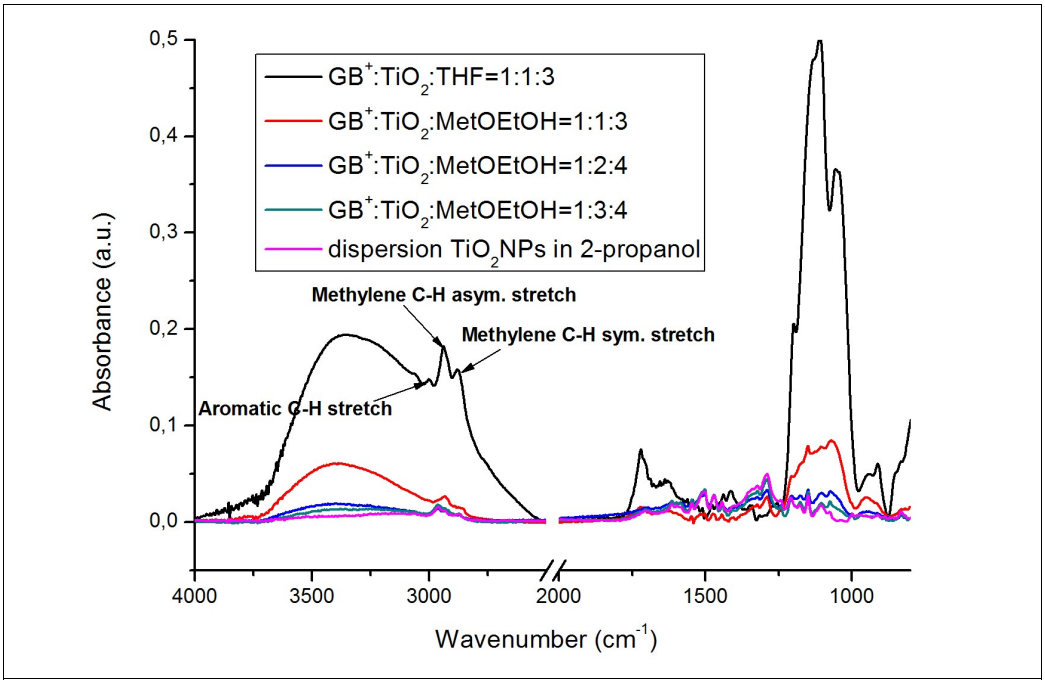

Fig. 37 FTIR curves of TiO_2 ex-situ at different solvent and NPs concentrations. Spining rate:5000rpm, UV dose:94,1J/cm^2.

The evaporation step was introduced in order to obtain thick, bright and homogeneous film without cracks. It is difficult to control the evaporation rate, however, it seems that 25min are sufficient to evaporate most of the solvents. The choice of the most suitable solvent in which disperse the evaporated extract, derived from tests with different solvents: toluene, ethyl acetate, butyl acetate, butanone. Only butanone did not give problems of mixture.

TiO_2 in-situ

The synthesis of TiO_2 in-situ is based on the recipe previuosly developed in Padova University lab. The titania content was increased up to a molar ratio of almost SiO_2:TiO_2=90:10, changing the synthesis conditions. In addition a fluorinated monomer was added to solution in order to decrease the hardeness of films (due to the high TiO_2 content) and to avoid adhesion between film and stamp in demolding step of thermal imprinting. For this purpose different monomer were tested: glycerol diglycidyl ether (GDE), glycidyl hexadecafluorononyl ether (GD16), bisphenol F diglycidyl ether (BFDGE) and Zonyl® FSN 100. The monomer that gives better imprinting results and more stable solution was bisphenol F diglycidyl ether (BFDGE).

6.3. FILMS DEPOSITION

Both TiO_2 in-situ and ex-situ films were deposited by spin coating technique on silicon substrate. The Si substrates had not to be cleaned with solvents, oxygen plasma or treated with adhesion promoter (e.g. hexamethyldisilazane) in order to avoid adhesion problem. In fact the TiO_2 solutions do not adhere to substrate if it is contaminated. A controlled film thickness was achieved by varying the spinning rate.

TiO_2 ex-situ

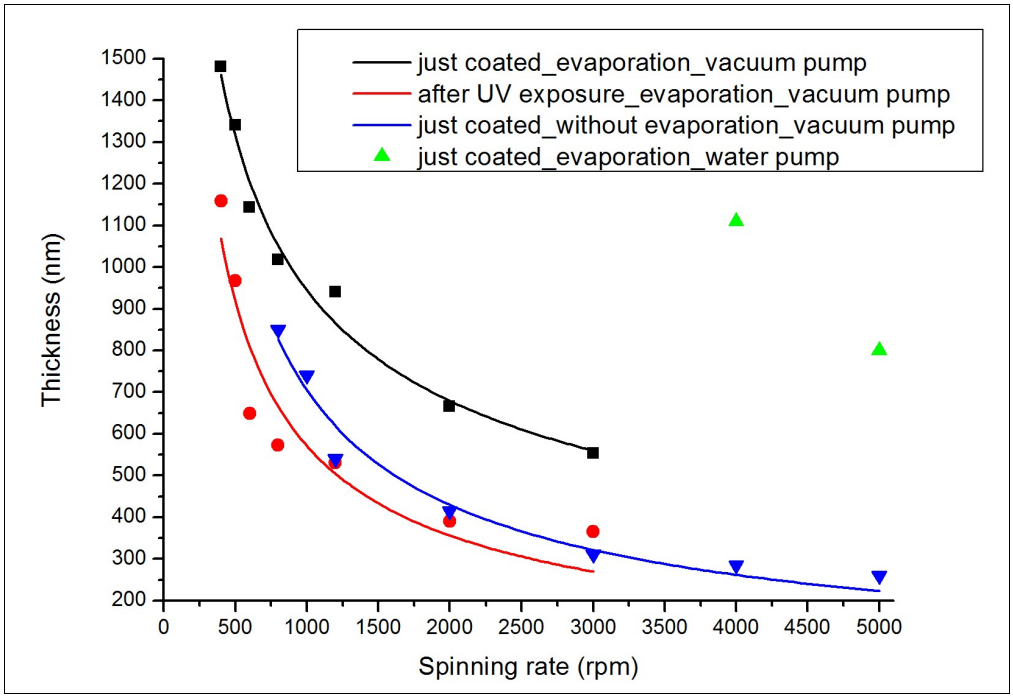

Fig. 38 Spin-curves of TiO_2 ex-situ in different situations. (black) TiO_2 ex-situ solution prepared with evaporation step using vacuum pump. (red) TiO_2 ex-situ solution prepared with evaporation step using vacuum pump after 117,6J/cm^2 UV dose. (green) TiO_2 ex-situ solution prepared with evaporation step using water pump. (blue) TiO_2 ex-situ solution prepared without evaporation step.

The coating TiO_2 in-situ solution was spin-coated at various spin-coating rate in order to achieve high thickness. The maximum thickness obtained is nearly 1,5µm. During deposition, the solvent present inside the solution evaporates. At low spinning rate, cracking, disomogeneities and edges effects are common problems. Fig. 38 shows the spin-curves of

ex-situ solution in different conditions. As it can see the step of evaporation is a critical step because varying method of evaporation, the thickness that can be obtained changes. Using a water pump to remove the solvent, evaporation is more effective and reached thicknesses higher even at high rate. Obviously solutions prepared without evaporation have lower thickness at same rate compared evaporated sol. The shrinkage after UV irradiation (117,6J/cm^2 dose) is approximately 42% for thin film prepared with evaporation step.

With the evaporation techniques used in this study, it is not possible to have a good control of final concentration. In fact, the films thickness is difficulty reproducible, therefore for each new preparation it is necessary to check the film thickness before imprinting. With best control of evaporation technique this problem can be surely solved.

After deposition TiO_2 in-situ films received a post-application bake (PAB) of 80°C for 2min.

TiO_2 in-situ

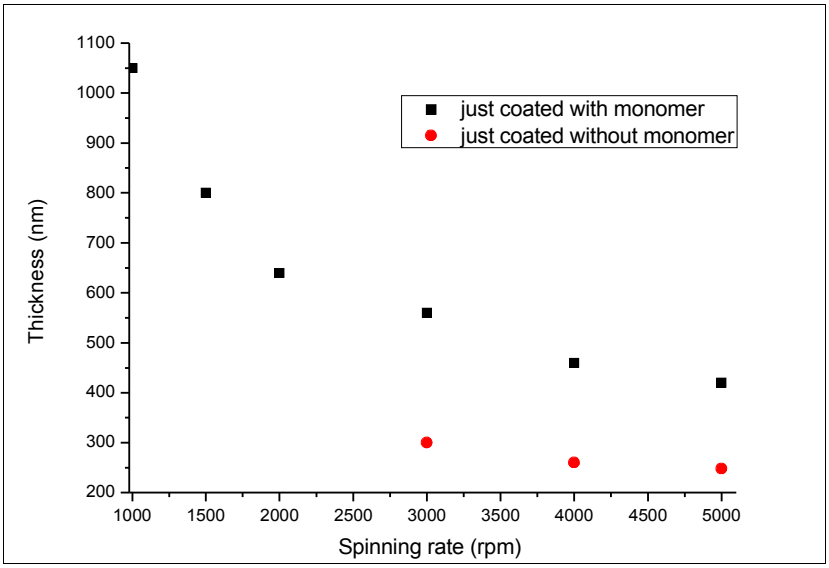

Fig. 39 Spin-curves of TiO_2 ex-situ just coated with or without BFDGE monomer.

TiO_2 in-situ thin films were deposited by spin coating technique on untreated silicon substrate. A controlled film thickness ranging from 400nm to 1µm was achieved by varying the spinning rate between 1000 and 5000rpm. The use of momomer increases films thickness because the solution becomes more viscous.

6.4. FILMS CHARACTERIZATION

A number of analysis techniques was applied to determine the properties of prepared sol-gel resists and final titania films:

- The rheological study of the solutions was conducted using AR2000ex rheometer to measure the viscosity of the solutions.
- The film microstructure and the response at UV irradiation have been analysed by infrared absorption spectra in the range 4000-800cm^{-1}, recorded by Fourier transform infrared spectroscope (Jasco FT-IR-620 and Nicolet Magna IR-560) with a resolution of ±1cm^{-1}. Ultraviolet-visible (UV-vis) absorption spectra from films deposited on quartz slides were measured in the range of 200-800nm by a spectrophotometer (Jasco V-570), with the accuracy of ±0,3nm.
- The cristallinity of TiO_2 layers were confirmed by X-ray diffraction (Philips PW1710). Refractive index and the thickness of the coatings on silicon substrates was measured by ellipsometry (Sopra GES 5E spectroscopic ellipsometer).
- The film thickness has been examined also with a Tencor Alpha-Step 500, surface profiler. SEM micrographs of patterned films were obtained using Zeiss LEO 1550 scanning electron microscope.
- Morphology of imprinted structures was analysed with Nanosurf EasyScan AFM system was used.

6.5. THERMAL IMPRINT LITHOGRAPHY

Printing processes were performed on 1x1cm silicon chips in an ESCO EHN-3250 nanoimprinter. At the pressure set to 0.3MPa on the machine and the plates area is 150x150mm, the force applied results in 6750N. The pressure applied on a pattern depend on the area of the protrusion present on a stamp. In case of stamp having micrometer-scale patterns, about 50% of the stamp area was covered with protrusions. For example, if the stamp was 1x1cm=1cm^2, the printing area was half of it, 0,5cm^2. The printing force was 13500N that makes a pressure of 135MPa. In case of sub-μm scale stamp with about 1mm^2 of printing area, so the pressure has to be scaled by a factor 100.

The imprinting processes consists of these steps: (1) the TiO_2 sol solutions were spin-coated

onto an oxidized Si wafer substrate. (2) After spin-coating, the mold was placed on the substrate. A specific pressure and temperature were applied for a given time. During the imprinting, the TiO_2 sol filled the cavity of the mold completely, and the organic solvent of TiO_2 sol was removed by temperature. Consequently, a TiO_2 sol was converted to a TiO_2 gel during imprinting and nano-sized patterns of a TiO_2 gel were produced after detaching (3) the mold. In order to transform the TiO_2 gel to pure inorganic TiO_2, the substrate with TiO_2 gel patterns was irradiated with UV light.

6.5.1. Fabrication of original silicon master mold

The Si master mold was made by electron-beam lithography (EBL) and plasma etching. The fist step was the deposition of an intermediate SiO_2 hard mask onto a Si wafer. Then an electron-beam sensitive resist (ZEP 520A) was spin-coated. E-beam patterning of various shapes (mainly lines and dots) with sizes from 50 nm to 3μm was performed in a dose range of 300-1075μC/cm^2. The photoresist was developed in anyl-acetate and rinsed in MIBK:IPA solution. After the development the underlying SiO_2 and Si were etched using fluorine and chlorine plasmas, respectively. After the Si etching process, SiO_2 was removed using a buffered oxide etch solution.

The μm- and subμm-stamps were fabricated by copying the original silicon mold with Ormostamp.

6.5.2. Replica mold by Ormostamp®

Since NIL is based on the mechanical molding of polymer materials, it presents some problems such as the requirement of an expensive master mold, which is often deformed and contaminated by the imprinting process. As a result of the relatively long processing times and repeated use in low-pressure and room-temperature imprinting, pattern collapse has been observed when the imprinted features were fine and dense with a high aspect ratio. There is therefore a need for cheap replica molds with high resolution and reliable mechanical properties.

In literature different processes for stamp copy are reported. The materials used for copying sweep from poly-(dimethylsiloxane), polyurethane-based UV-curable polymers, photocurable fluoropolymers and organic-inorganic hybrid material [63-64]. The principal technique

employed for copying is UV-NIL [65].

In this study the UV-curable Ormostamp material from micro resist technology was used as a material for working stamps. The master nanoimprint templates were fabricated by electron beam lithography as described above. The replica molds were fabricated with glass backplanes. The transparent glass substrates were accurately cleaned with surfactant and 2-propanol. Afterwards the substrates were oxidized with oxygen plasma for 2min (p=0,6mbar, P=100W). The glass substrates have to be free of impurities in order to achieve optimum adhesion of the primer layer (Ormoprime08). Inappropriate processing can lead to unsatisfying quality and noticeable surface roughness of the Ormoprime films. The substrates were then spin-coated with a thin film of Ormoprime08 at 4000rpm for 60s, followed by baking on a hotplate at 150°C for 5min.

A defined amount of UV-curable material (Ormostamp) was placed on the silicon template. The glass substrate was carefully pressed onto the drop. The drop expands under the weight of the glass. Therefore it is necessary to wait until the material fills the structures to be copied. The whole set-up was UV cured (770mJ/cm^2) before separating the master and the copy. The separation phase must be done carefully with sharp tweezers and applying gentle pressure.

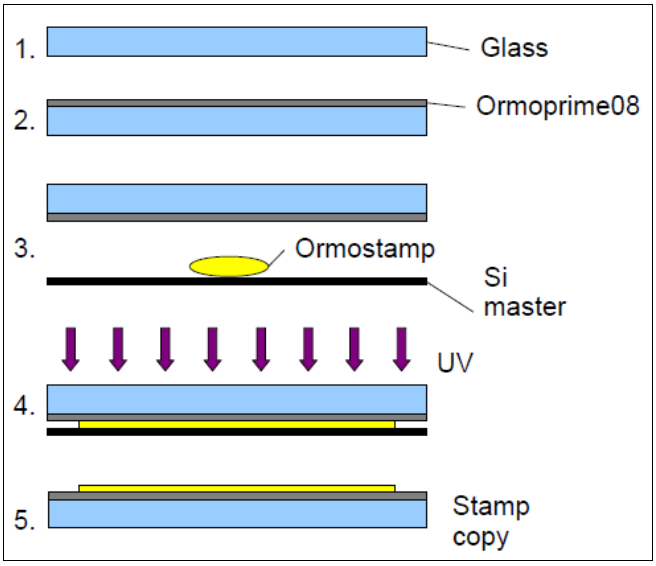

Fig. 40 Process flow of stamp copying.

One of the key issue of nanoimprinting lithography is the sticking between the resist and the mold. The high-density nanoscale features on the mold increase the surface area contacting the polymer. This leads to increased adhesion between the mold and polymer, which can be so strong that the imprinted layer may be torn away from the substrate during demolding.

Therefore, a non sticking interface between the polymer and the stamp is needed for successful demolding. Teflon-like anti-adhesion layers can be used to lower the surface energy of the stamp to aid the demolding. Self-assembled monolayers such as fluorocarbon-based silane can also be adopted as an anti-adhesive layer to increase the lifetime of the stamp mold [66-67]. In this work, the stamp copies were treated with trichloro(1H,1H,2H,2H-perfluorooctyl)silane by vapour deposition. The silanization process forms a hydrophobic surface that avoid sticking problems between mold and sample.

To copy silicon master with subµm-structures the procedure is the same. In the fabrication of deeper molds it is necessary to wait longer time before to photopolimerization so that Ormostamp can completely fill the structures.

The cleaning and rinsing procedure in acetone and isopropanol were used for the working stamps followed by a flow of nitrogen for drying. Additional ultrasonic treatment should be avoided as higher aspect ratio features start to break off.

Name	Depth of original Si template (nm)	Depth of stamp copy (nm)
S180m (µm-stamp)	250	180
S160 (subµm-stamps)	200	160
S620 (subµm-stamps)	670	620
S700 (subµm-stamps)	730	700

Tab. 3 Name and depth of stamp copies.

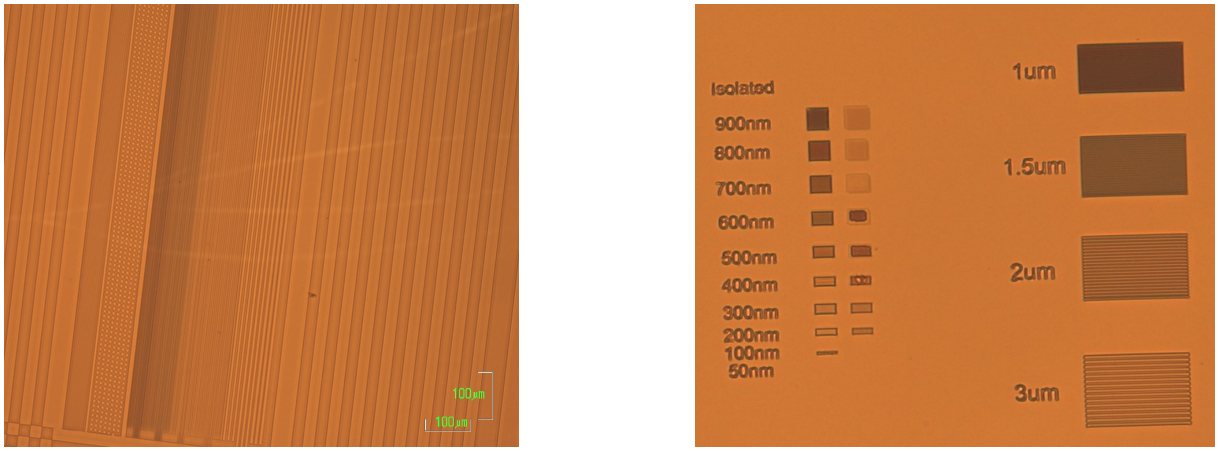

Fig. 41 Optical microscope images of stamp-copies made by Ormostamp. (left) µm-stamp, (right) subµm-stamp.

7. SOLUTIONS AND FILMS CHARACTERIZATION

7.1. VISCOSITY MEASUREMENTS

Before showing the TiO_2 in-situ and ex-situ rheology results, it is necessary a short introduction about the difference between thermoplastic and thermosetting behaviour. Thermoplastic (polymeric) materials are processed in the molten viscoelastic state, their final shape and internal structure established by cooling, and they can be softened and reshaped by reapplication of heat and pressure. Also, their polymeric chains, whether linear or branched, are not cross-linked after molding. Thermoset polymers usually go through three stages. In the A-stage, the resin is still soluble and fusible. In the B stage, a prepolymer is formed, but are still thermoplastic. They can, however, spend only a relatively short time in the molten state because the temperatures that promote flow also cause the material to crosslink. The crosslinking reaction is accomplished in the final stages of polymerization (the C-stage) during molding of the product under the controlled influence of heat and pressure over time. Thus, thermosets build their final structure during processing, forming a three-dimensional internal structural network of highly crosslinked polymer chains. And the final product is insoluble and not thermally reformable. TiO_2 in-situ and ex-situ hybrid sol-gel materials can be assimilated to thermosetting polymers. Therefore the characteristics of these materials will be detailed here [68].

Developing the proper cure level is perhaps the most critical step for a thermoset polymer. The most effective and economical way to do this is to design a thermoset cure cycle derived from measurements of the curing resin's dynamic viscosity profile as a function of temperature and time. From a series of measurements, it is possible to obtain the minimum viscosity. The minimum viscosity represents the time period and temperature range over which resistance to flow is lowest.

A rheometer is the device used to measure the rheology of a fluid. There are two distinctively different types of rheometers. Rheometers that control the applied shear stress or shear strain are called rotational or shear rheometers, whereas rheometers that apply extensional stress or extensional strain are extensional rheometers. In this case a shear rheomether was used.

Fig. 42 shows viscosity curves of TiO_2 in-situ and ex-situ materials. The measurements were performed at constant strain: 10% at 1Hz for in-situ and 3% for ex-situ in a temperature range

from 20°C to 160°C (temperature ramp: 6°C/min). Titania ex-situ shows higher viscosity values than titania in-situ due to the presence of nanoparticles already formed in the sol. In-situ presents a plateau of minimum viscosity for a wide range of temperatures.

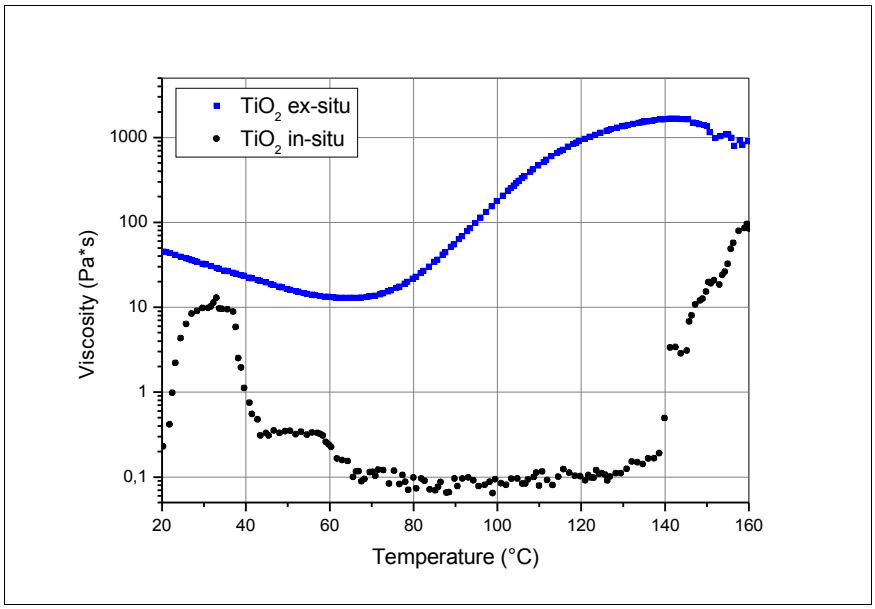

Fig. 42 Viscosity curves at constant strain for TiO_2 in-situ and ex-situ.

7.2. UV-VIS TRANSMISSION PROPERTIES

UV–visible transmission and absorption spectra were measured for a wavelength range of 200–600 nm (Fig. 43) for a sol–gel films of TiO_2 ex-situ and in-situ deposited on quartz slide. Both hybrid sol–gels show a high absorbance in the UV region below 300-335nm, especially TiO_2 in-situ. In fact low titanium content precursor (as in ex-situ solution SiO_2:TiO_2=65:35) is expected produce more transparent films than those prepared from higher titanium content precursors (as in in-situ solution SiO_2:TiO_2=90:10). This information was used to calculate UV dose (an amount of radiation received) for films irradiation. Depending on wavelength at which the material absorbs and on distance from UV source, the doses vary. The greater the distance from the light guide output end to the target surface, the more the maximum UV intensity drops and the more the light beam expands (Fig. 45).

Transmittance studies were performed in the UV–vis–NIR wavelength range on TiO_2 in-situ films deposited on glass substrates. TiO_2 films exhibit high transparency ~92% at 640nm for as deposited in-situ and at 690nm for ex-situ. All films showed good transmittance in the visible and NIR wavelength regions, while there is a strong absorption from 250 to 330nm. It

can be observed from Fig. 44 that the transmittance in the range 350-400nm decrease with increasing UV dose. This can be due to the elimination of the organic species with the increase of dose. Moreover sharp UV absorption edge shift from near 320 to 350 nm as UV dose increase. A possible cause can be the formation of larger titania clusters or the scattering of light caused by pores that are formed after the decomposition of organic compounds.

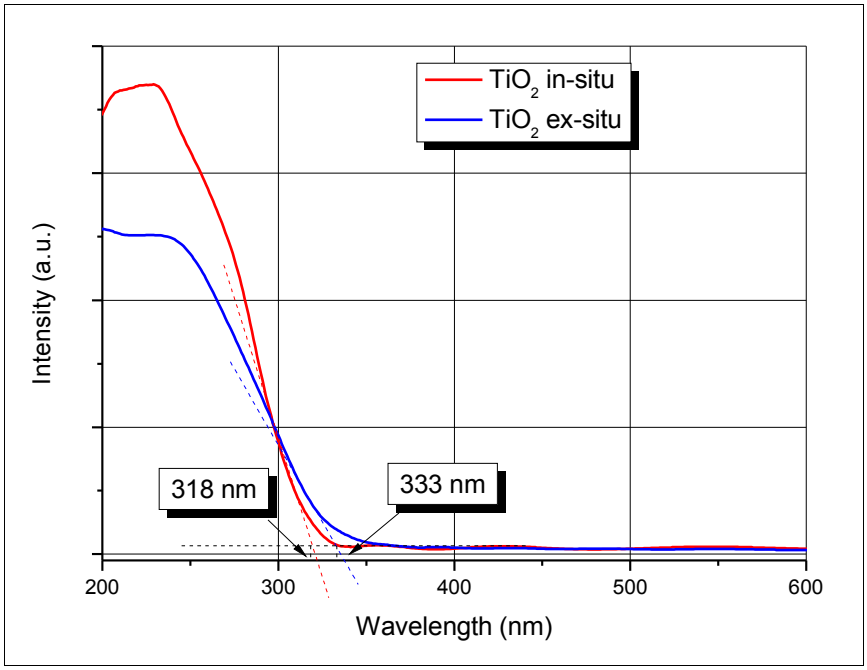

Fig. 43 UV-visible absorption spectra of TiO_2 in-situ and ex-situ film spin-coated at 4000rpm for 30s on quartz slides.

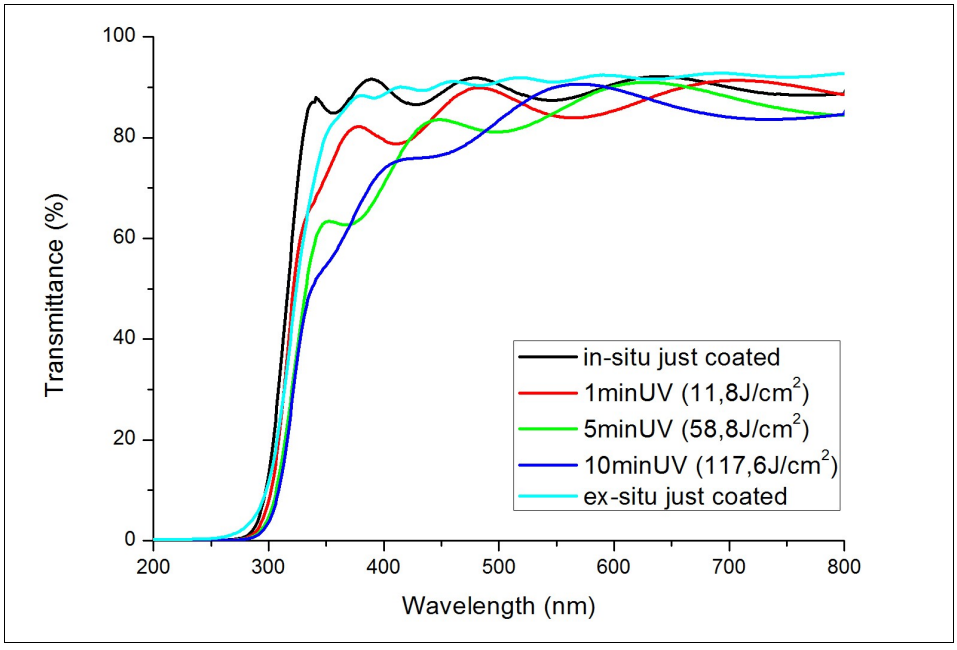

Fig. 44 Optical transmittance spectra of TiO_2 in-situ films irradiated with different doses. 640nm deposited.

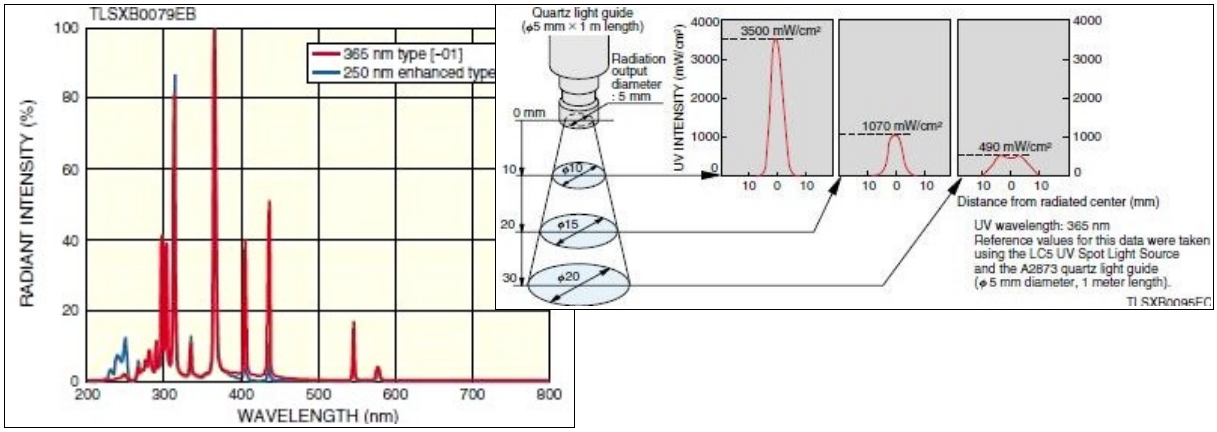

Fig. 45 (left) Radiant spectral distribution of Hamamatsu LC5 UV mercury-xenon lamp "-01" type (red). (right) UV intensity distribution vs. distance from the light guide output end to the target surface.

7.3. FOURIER TRANSMISSION INFRARED SPECTROSCOPY (FTIR)

In infrared spectroscopy, IR radiation (i.e. electromagnetic radiation with a wavelength longer than that of visible light, starting from the nominal edge of visible red light at 0.7μm, and extending conventionally to 300μm) is passed through a sample. Some of the infrared radiation is absorbed by the sample and some of it is passed through (transmitted). An infrared spectrum represents a fingerprint of a sample with absorption peaks which correspond to the frequencies of vibrations between the bonds of the atoms making up the material. Because each different material is a unique combination of atoms, no two compounds produce the exact same infrared spectrum. Therefore, infrared spectroscopy can result in a qualitative analysis of every different kind of material.

The film microstructure is been investigated by infrared absorption spectra, in the range of 800-4000cm^{-1} recorded by Fourier transform infrared spectroscope (Jasco FT-IR-620).

TiO_2 ex-situ

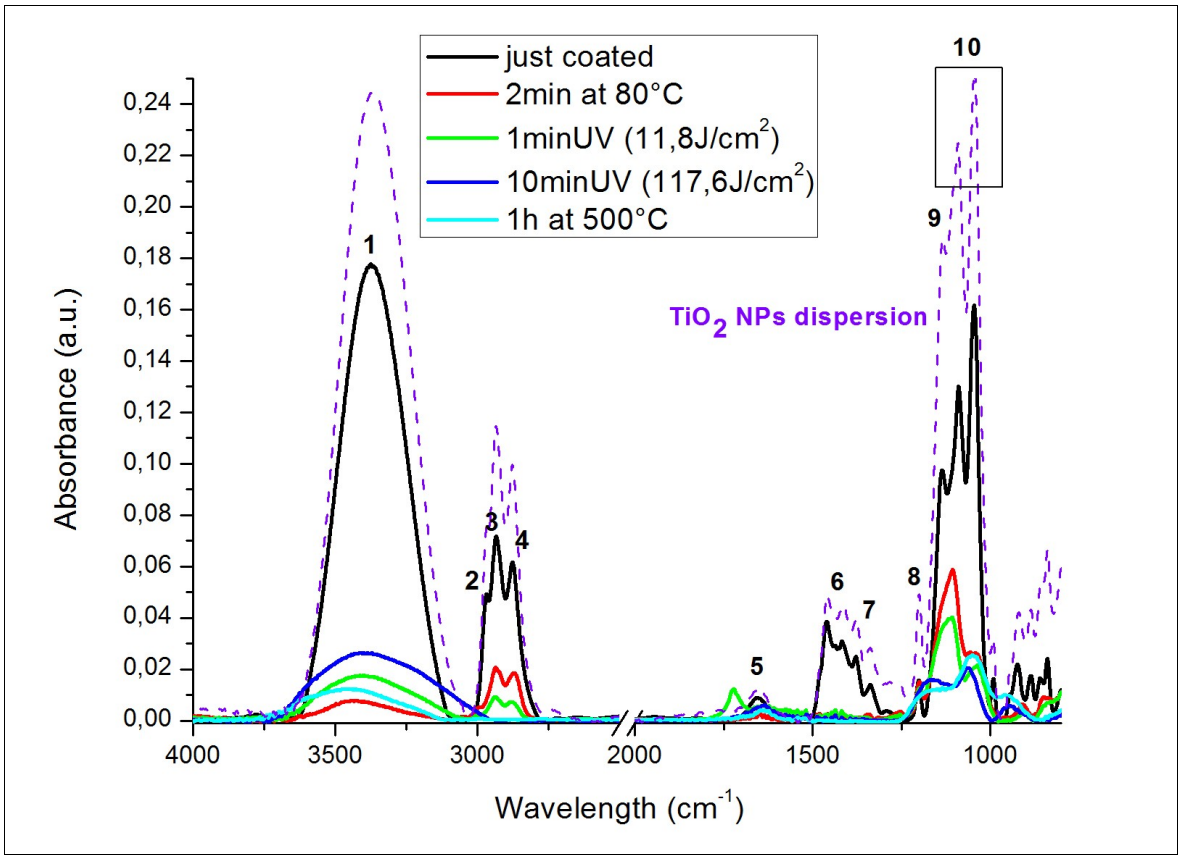

Fig. 46 FTIR spectra of TiO2 ex-situ (spinning rate: 4000rpm_30s).

	Group frequency wavenumber (cm^{-1})	Assignment
1	3370	Hydroxy group, O-H stretch
2	2970	Methylene C-H sym. stretch
3	2935	Methylene C-H asym. stretch
4	2875	Methyl C-H sym. stretch
5	1655	C=O stretch
6	1460-1420	Methylene C-H bend
7	1380-1340	Aliphatic nitro compound
8	1200	SiO_2 out-of-phase asym. stretch
9	1135	Organic siloxane (Si-O-C)
10	1090-1045	SiO_2 stretch (Si-O-Si)

Tab. 4 FTIR peaks assignment for TiO_2 ex-situ films.

The decreasing of the epoxy vibration absorption (linked to methylene C-H stretch at 2970cm^{-1}) indicates the almost complete opening reaction when the film is exposed to 117,6J/cm^2 of

irradiation. At the same time a damage of the structure is observed, as indicated by a decrease of the absorbing bands around (2935 and 2875 cm^{-1}, methylene and methyl C-H absorption, respectively). The opening of the epoxy ring is associated with the formation of C=O bonds, having typical IR absorption in the region between 1640 and 1780cm^{-1}. This might derive from the degradation of more labile organic species such as the C–O–C bonds of the etheric group in the propylic chain.

The band at a frequency of ~1100 cm^{-1} is assigned to Si−O−CH_3 stretching vibrations of methoxy groups bonded to silicon. This band decreases in intensity with increasing UV dose and temperature, and there is a corresponding growth of the band at 1058 cm^{-1}, which is indicative of a formation of the silicon-oxide skeleton. The shoulder at ≈ 1200 cm^{-1} (for the films heated at 500°C or irradiated with 117,6J/cm^2 UV dose) is attributed to the transverse optical mode of the out-of-phase mode of the asymmetric stretching vibration as due to the longitudinal optical component of the high-frequency vibration of SiO_2 [57]. In the 1000-800cm^{-1} range, the main vibrational mode of different silica species overlaps and a structural evolution in this interval is evident. This is probably originates by a rearrangement in the silicate species present in the inorganic network. Furthermore, a broad band between 3700cm^{-1} and 3000cm^{-1}, observed in all the samples is attributed to O−H stretching and decrease with UV dose or temperature. This shows that the films contain a large amount of hydroxyl or water molecules and a rise in the UV dose (which results in a heating of irradiated material) or a thermal treatment leads to a decrease of hydroxyl and even vanish. The series of peaks between 1460 and 1340cm^{-1}, present only in the just coated sample, could be attributed to surfactants used in the TiO_2 NPs dispersion. These peaks disappears after heat treatment or UV irradiation. Since the type of surfactants used are unknown, the attribution of these peaks can not be unique. Probably the surfactants used are similar to cetyltrimethylammonium bromide (CTAB), which is one of the most common surfactants [69]. In fact some of peaks can be attributed to nitro compound.

TiO_2 in-situ

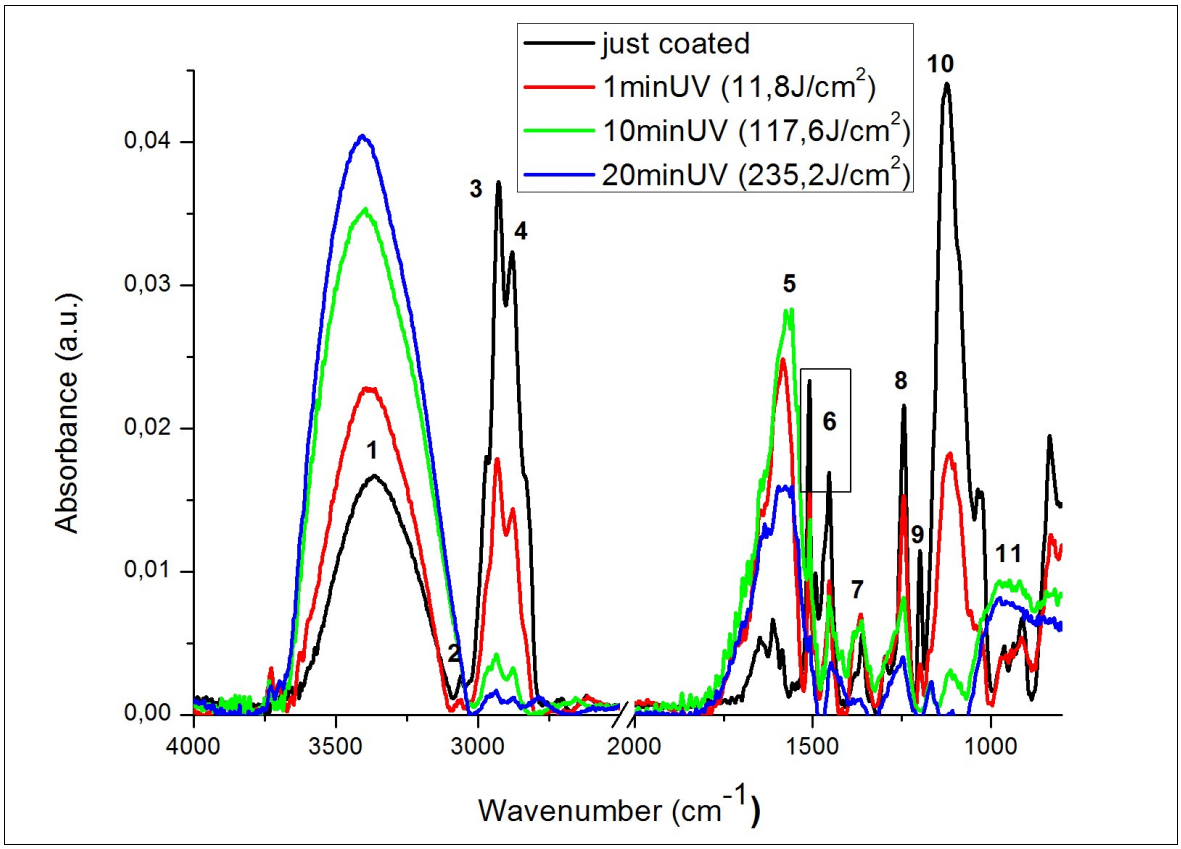

Fig. 47 FTIR spectra of TiO_2 in-situ (spinning rate: 4000rpm_30s).

	Group frequency wavenumber (cm^{-1})	Assignment
1	3360	Hydroxy group, O-H stretch
2	3060	Aromatic C-H stretch
3	2920	Methylene C-H asym. stretch
4	2870	Methylene C-H sym. stretch
5	1570	Molecular water, bending O-H
6	1510-1455	Aromatic ring stretch
7	1360	Primary or secondary, O-H in plane bend
8	1240	Primary or secondary, O-H in plane bend
9	1200	SiO_2 out-of-phase asym. stretch
10	1125	Organic siloxane (Si-O-C)
11	950-960	Overlapping of different vibrations

Tab. 5 FTIR peaks assignment for TiO_2 in-situ films.

The FTIR spectra of TiO_2 in-situ film spinned at 4000rpm for 30s before and after UV exposure are reported in Fig. 47. The FTIR spectra of all samples show two representative frequency ranges.

In the first range between 3500 and 3000cm^{-1} there are the large and broad absorption band of water (at 3360cm^{-1}) and the two peaks at 2920cm^{-1} and 2870cm^{-1} relative to the C-H asymmetric and symmetric stretching. This latter peak is related to epoxy ring in GPTMS. The other characteristic vibrational mode of epoxy ring in GPTMS are at 1260-1240cm^{-1} (ring breathing) and 910cm^{-1} (antisymmetric ring stretching), but they are often overlapped with other bands. Therefore the two sharp bands at 2920cm^{-1} and 2870cm^{-1} can be used to control the organic chain evolution under UV treatment. It can be clearly seen that the propylic chain becomes progressively weaker for longer UV exposure times. The second representative region in the 1700-800cm^{-1} contains an interesting peak at 1200cm^{-1} related to epoxy rings. The broad peak visible after 10min of UV exposure and centred at 950-960cm^{-1} is probably the result of overlapping of the Si-O-Ti, Si-OH and Si-O- groups' stretching vibration. It can be seen from the FTIR spectra that there is no observable absorption band of Ti-O-Ti, which infers that the formation of TiO_2 phase is not detectable here. Peaks at 1360cm^{-1} and 1240cm^{-1} should be attributed to organic solvents. With UV irradiation these peaks become quite weak.

The band at 1570cm^{-1} is relating to bending vibrations of water molecules. This peak increases with UV exposure and then start to decrease strongly at high doses due to evaporation.

Other specific peaks are at 3060cm^{-1} and 1510-1455cm^{-1}. These peaks are associated at aromatic stretching vibrations of bisphenol F diglycidyl ether (BFDGE) and they decrease with UV irradiation.

7.4. X-RAY DIFFRACTION (XRD)

X-ray diffraction (XRD) is a versatile, non-destructive technique that reveals detailed information about the chemical composition and crystallographic structure of materials. Diffraction occurs as waves interact with a regular structure whose repeat distance is about the same as the wavelength. X-rays have wavelengths on the order of a few angstroms, the same as typical interatomic distances in crystalline solids. This means that X-rays can be diffracted from materials, which are crystalline and have regularly repeating atomic

structures. Atoms scatter X-ray waves, primarily through the atoms' electrons. An X-ray striking an electron produces secondary spherical waves emanating from the electron. This phenomenon is known as elastic scattering. A regular array of scatterers produces a regular array of spherical waves. Although these waves cancel one another out in most directions through destructive interference, they add constructively in a few specific directions, determined by Bragg's law: $2 \cdot d \cdot \sin\theta = n \cdot \lambda$. Here *d* is the spacing between diffracting planes, θ is the incident angle, *n* is any integer related to the order of diffraction, and λ is the wavelength of the beam. Hence, a diffracted beam may be described as a beam composed of a large number of scattered rays mutually reinforcing one another. The orientation and interplanar spacings of the planes inside the crystal are defined by three integers <h, k, l> called indices.

TiO_2 ex-situ

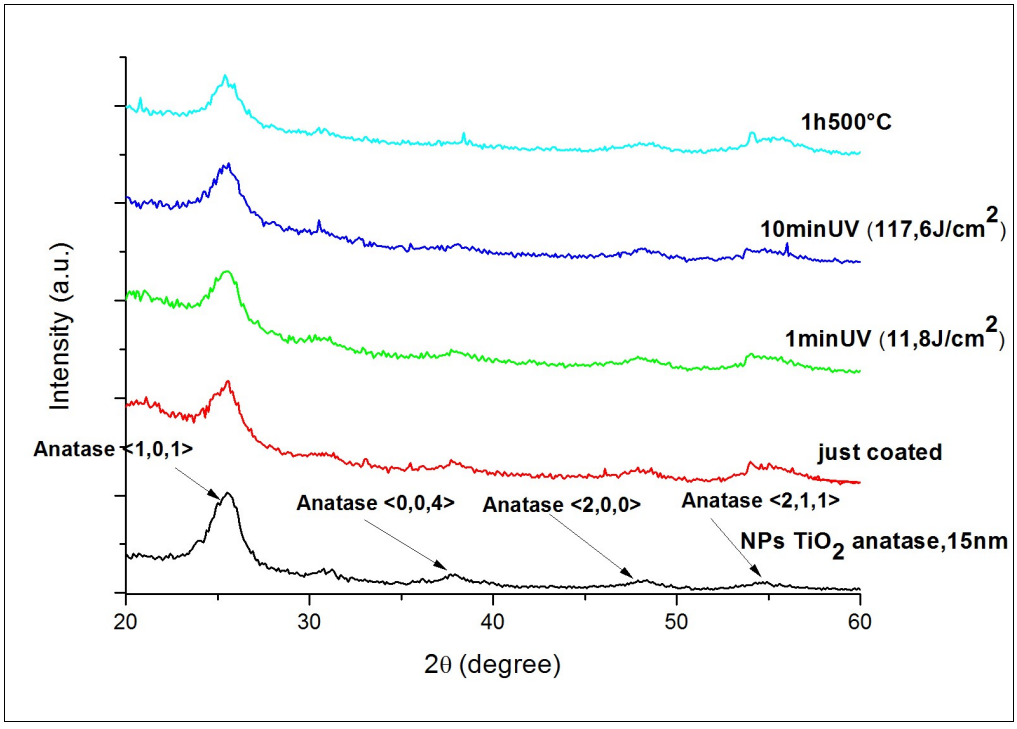

Fig. 48 XRD spectra of UV irradiated TiO_2 ex-situ films and film annealed at 500°C.

The XRD patterns of films irradiated with different doses and thermal treated are shown in Fig. 48. It can be observed that all the films present anatase phase (2θ=25,5°/48,1°/54,1°), this confirms that the TiO_2 NPs put into solution consisting really of anatase NPs.

The average crystallite size is calculated from the XRD line broadening using the Scherrer equation: $B = k \cdot \lambda / (L \cdot \cos\theta)$ where *k* is the Scherrer constant (*k*=0,9 assuming that the crystallites

are spherical), λ is the wavelength of the incident X-rays (k=1,54178Å), L is the full width at half maximum of the <1,0,1> diffraction and θ is the angle of diffraction. The average crystallite size of titania dispersion is 11,3nm, comparable with the size declared (15nm). Obviously the NPs size remains constant after thermal annealing and UV irradiation because the TiO_2 NPs were insert ex-situ into solution.

TiO_2 in-situ

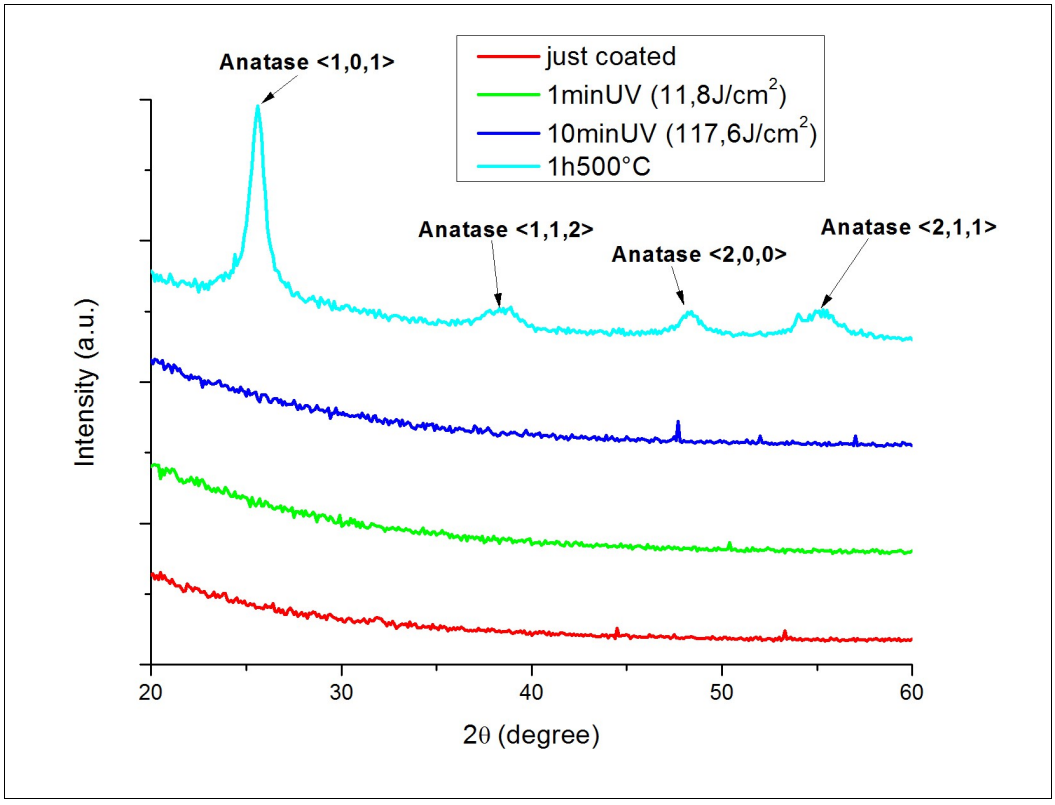

Fig. 49 XRD spectra of UV irradiated TiO_2 in-situ films and film annealed at 500°C.

Concerning in-situ TiO_2, the anatase phase can be obtained only by heat-treating the film at 500°C for 1h as suggested by X-ray diffraction studies. In fact the same film at room temperature doesn't show the presence of a crystalline phase. The crystallite size is estimated from Scherrer equation and the crystalline phase calculated from XRD peak <1,0,1> with 2θ=25,6° at an annealing temperature of 500°C is found to be 21,2nm. The film irradiated with a dose of 117,6J/cm^2 presents some small peaks at 2θ=47,7°, 52° and 57°. These peaks could be associated to brookite. Brookite is an allotropic form of TiO_2, and hence identical with rutile and anatase in composition, but crystallizing in the orthorhombic system. Moreover brookite exhibits less photocatalytic activity. As in-situ films at room temperature

show a minimum of photocatalytic activity, it is possible that they are crystalline but crystals are too small to be detectable by XRD. For this reason, the organic part could not be completely degraded after 10min of UV (as can be seen from FTIR spectra that show the persistence of small organic peaks even after 10min of irradiation). Probably longer exposure time are required.

7.5. ELLIPSOMETRY

Ellipsometry is a versatile and powerful optical technique for the investigation of the dielectric properties of thin films. Ellipsometry measures the change of polarization upon reflection or transmission. Typically, ellipsometry is done only in the reflection configuration. The exact nature of the polarization change is determined by the sample's properties (thickness or complex refractive index). Although optical techniques are inherently diffraction limited, ellipsometry exploits phase information and the polarization state of light, and can achieve angstrom resolution.

After reflection on a sample surface, a linearly polarized light beam is generally elliptically polarized. The reflected light has phase changes that are different for electric field components polarized parallel (*p*) and perpendicular (*s*) to the plane of incidence. Ellipsometry measures this state of polarization or more precisely by the complex ratio ρ written as: $\rho=r_p/r_s=\tan\Psi\cdot\exp(i\Delta)$ where Ψ and Δ are the amplitude ratio and phase shift, respectively, of the *p* and *s* components.

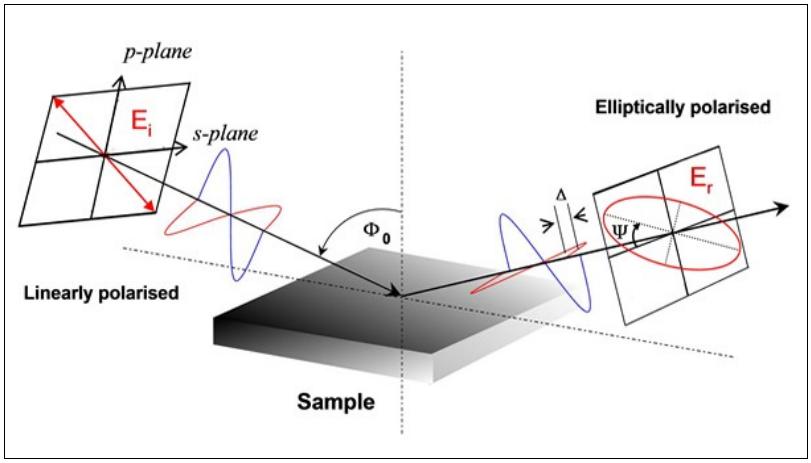

Fig. 50 Schematic of the geometry of an ellipsometry experiment.

In general the measured Ψ and Δ cannot be converted directly into the optical constants of the

sample. Normally, a model analysis must be performed. A layer model must be established. It considers the optical constants and thickness parameters of all individual layers of the sample including the correct layer sequence. Using an iterative procedure unknown optical constants and/or thickness parameters are varied, and Ψ and Δ values are calculated using the Fresnel equations. The calculated Ψ and Δ values which match the experimental data best provide the optical constants and thickness parameters of the sample [70].

TiO_2 in-situ

The optical constant, which is measured in terms of refractive index, is considered to be a gauge of the film quality. Fig. 51 shows refractive index *n* as a function of wavelength for TiO_2 in-situ material before and after UV exposure. UV irradiation was performed with OmniCure S2000 standard lamp with an intensity of 986,66mW/cm^2 at a distance of 3cm from the sample. This lamp is more powerful than lamp (Hamamatsu LC5 UV mercury-xenon lamp) used previously, so even with the same irradiation time, doses will be higher.

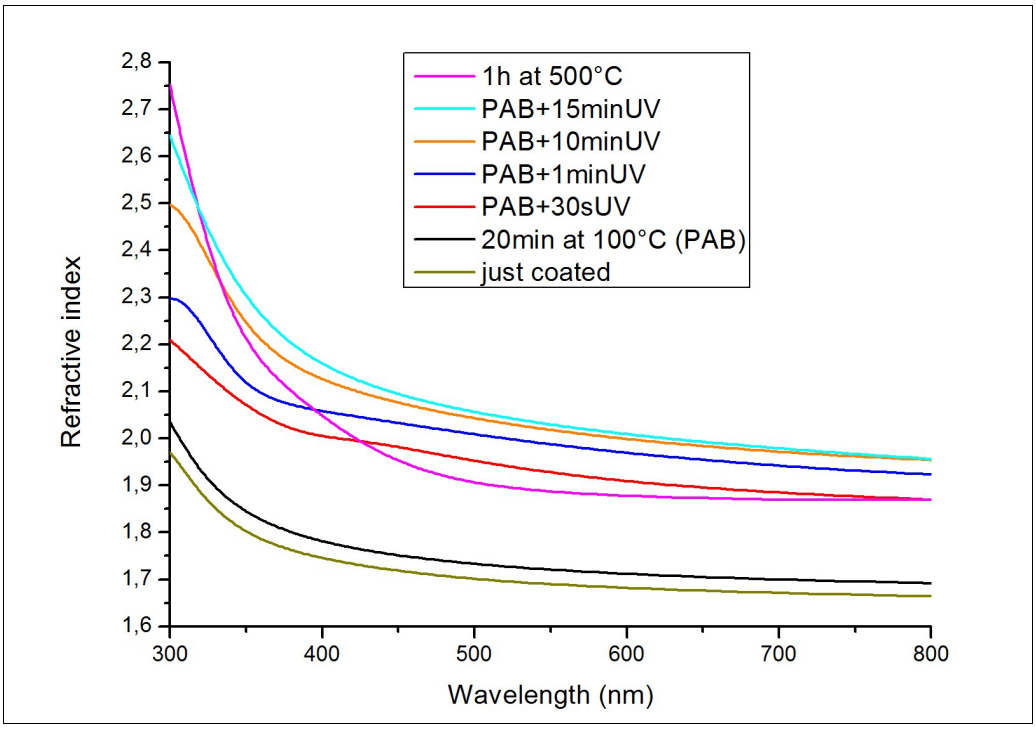

Fig. 51 Dispersion characteristics of TiO_2 in-situ films as estimated by ellipsometric method.

Refractive index increases with increasing doses, according to film densification. The rise of the refractive index with increasing UV exposure is fast at low doses and then it stabilizes after 4-6min (dose>286,8J/cm^2) of irradiation (Fig. 52).

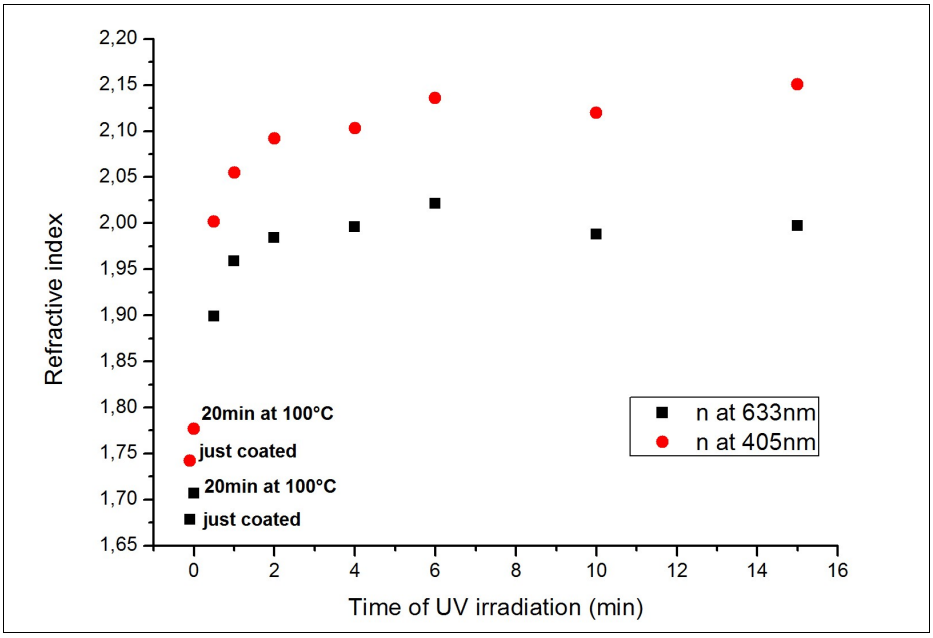

Fig. 52 Variation of refractive index at 633nm and 405nm with UV expo$_s$ure time.

In order to verify shrinkage variation of TiO_2 films during UV irradiation and annealing treatment, the thickness of various UV-irradiated was measured using spectroscopic ellipsometry as shown in Fig. 53.

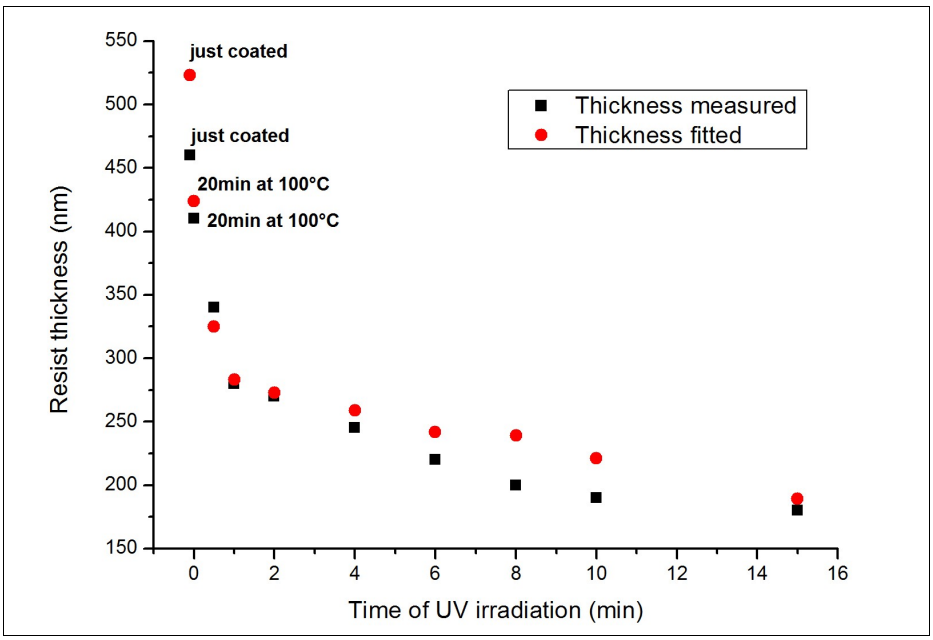

Fig. 53 Variation of films thickness (fitted with ellipsometric method and measured with profilometer) with UV exposure time.

The film thickness decrease and the refractive index increases for increasing UV exposure

time, according to the organic decomposition. Concerning the trend of n vs. UV exposure time, it can be noted that refractive index for TiO_2 in-situ irradiated 15min at 550nm (n=2,03) is different from the value of 2,52 at 550nm reported for a crystalline TiO_2 material. This lower value is fundamentally attributed to the packing density of the films, which could be related to the decomposition of the precursor and the loss of organic groups in the film upon UV irradiation. UV-irradiated TiO_2 films could have a lower packing density due to a residual micropores inside the film as well as other impurities such as carbon. The porosity of the films was calculated using: porosity=1-((n-1)/(n_d-1); where n_d is the refractive index of pore free anatase TiO_2 which is having a refractive index of 2,52 at 550nm. It can be observed from Fig. 54 that the porosity decreases abruptly with increase in UV exposure and then stabilize at around 42% after 4min (286,8J/cm^2) of irradiation.

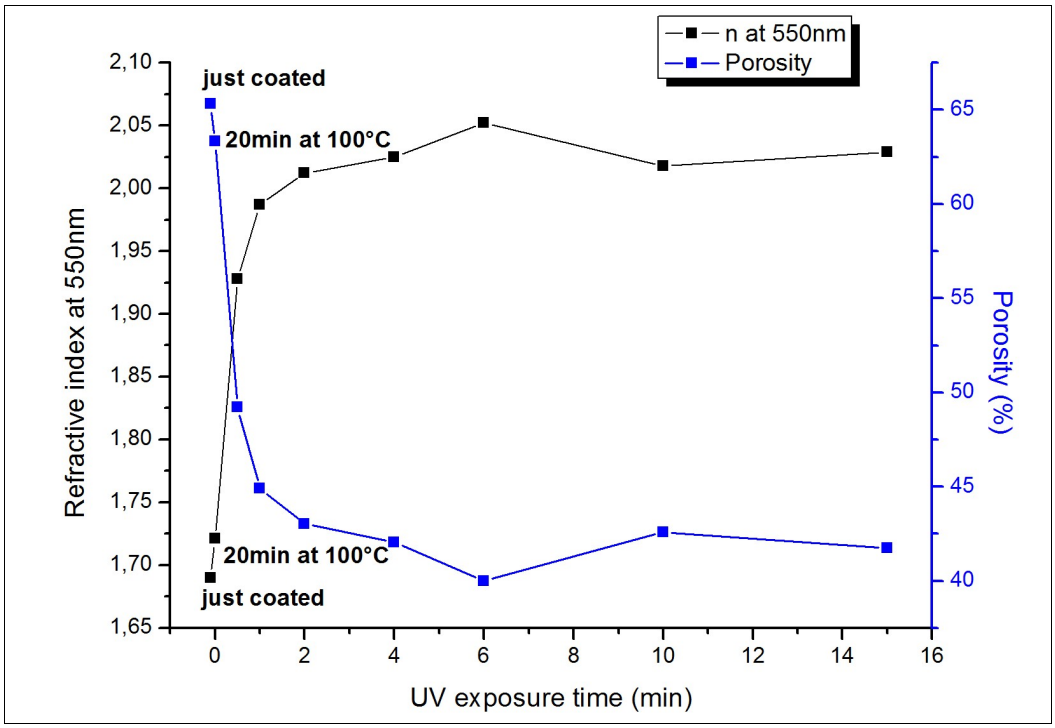

Fig. 54 Plot of the variation of refractive index and porosity of TiO2 in-situ films against UV exposure time. The values correspond to the data obtained at the wavelength of 550nm.

8. THERMAL IMPRINTING RESULTS

Nanoimprint lithography of TiO_2 ex-situ and in-situ resin was carried out in two steps. Firstly, at room temperature (25°C), a pressure of 0,3MPa (pressure set up on the imprinter machine; actual pressure is 135MPa for µm-stamps and 6750MPa for sub-µm-stamps) was applied for 3min. This was to ensure a complete filling of the mold with the resin. Secondly, while holding the pressure constant, the coated substrate and mold were heated to high temperature (80°C for ex-situ and 100°C for in-situ) for 20min or more in order to induce free radical polymerization of TiO_2 resin. After imprinting, the system was cooled down to 50°C before releasing the pressure and this was followed by a demolding.

8.1. THERMAL IMPRINTING WITH MICROMETRIC MOLDS

The Ormostamp copies of µm-mold used for imprinting had various pattern: lines, dots, squares and other arbitrary 180nm deep structures. Stamp copies are placed on 1x1cm glass slides covered with Ormostamp layer (commercial ORMOCER® hybrid polymer system for nano and micro stamp fabrication). Molds were treated with trichloro(1H,1H,2H,2H-perfluorooctyl)silane for 1h to reduce their surface energy in order to facilitate a clean demolding after imprinting.

TiO_2 ex-situ

The TiO_2 ex-situ solution was spin-coated at 5000rpm for 60s on silicon substrate. The films were baked in air on hotplate at 80°C for 2min. The final film thickness was about 700nm. The coating speed determined the residual layer thickness, but it was not optimized in these experiments. The surface presented inhomogeneity (waves due to solvents evaporation during spin-coating) of about 60nm.

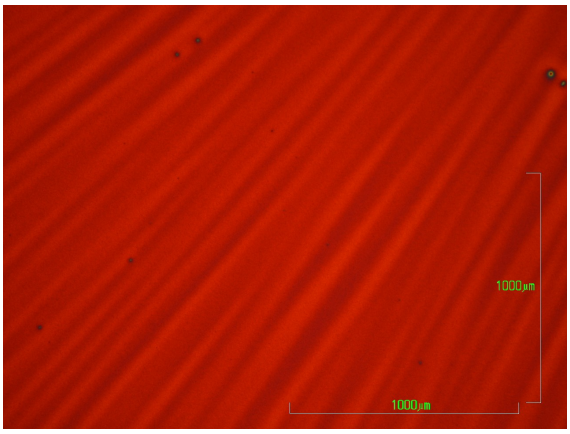

Fig. 55 Optical micrograph of TiO_2 ex-situ film surface spin-coated at 5000rpm for 60s on silicon substrate.

In order to measure patterned structures depth, a surface profilometer was used.

With the aim of achieving the optimal parameters, the nanoimprint parameters were optimized. In the tables below, the pressure, the temperatures and the time used in the imprinting tests are reported.

Pressure (MPa)	Temperature (°C)	Time (min)	Remarks
0,4	80	5	Film imprinted.
0,4	80	20	Film imprinted. Pattern depth: 45nm
0,4	110	20	Film imprinted. Pattern depth: 30nm

Tab. 6 Imprinting parameters for TiO_2 ex-situ material with initial film thickness of 700nm.

Since the thickness of TiO_2 ex-situ evaporated films was pretty high for imprinting with 180nm-stamp, the TiO_2 ex-situ solution without evaporation step was tested. Without evaporation step the solution is less viscous and films thickness decreases (~400nm).

Pressure (MPa)	Temperature (°C)	Time (min)	Remarks
0,4	RT	20	Film not imprinted.
0,4	80	20	Film weakly imprinted.
0,4	100	20	Film weakly imprinted.

Tab. 7 Imprinting parameters for TiO_2 ex-situ material with non-evaporated solution.

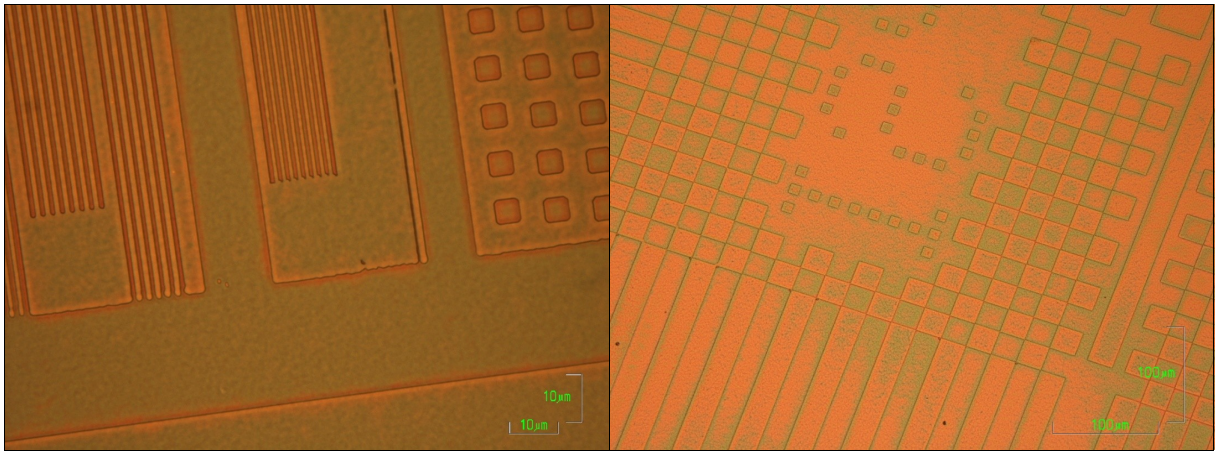

Fig. 56 Optical micrographs of TiO_2 ex-situ patterns after (right) pre-bake of 2min at 80°C and imprinting pressure of 0,4MPa at 80°C for 20min (left) pre-bake of 2min at 80°C and imprinting pressure of 0,2MPa at 100°C for 20min.

It can be observed from Fig. 56 that the patterned films appear grainy probably because of the TiO_2 nanoparticles, but structures are well defined. The maximum depth of 140nm is reached with P=0,4MPa, T=80°C and t=20min as imprinting conditions. Probably the structures are not fully printed because high solution viscosity and, perhaps, the agglomeration of the nanoparticles impede the material flow. But it can be noted that after NIL, comets or surface waviness are no longer present on films surface because of their flattened due to applied pressure.

TiO_2 in-situ

TiO_2 in-situ sol without monomer was spun coated at 5000rpm for 30s, and about 320nm thick film was left on silicon chips due to solvent evaporation during spinning. The films surface presented waves or comets of ~50nm deep.

In order to improve the surface quality of this resist, a primer (Ormoprime08) was deposited under resist. The primer was spin-coated at 6100rpm for 1min on Si substrate cleaned with oxygen plasma. The thickness was 50nm. The presence of primer decreases the comets height until 10nm. With the presence of Ormoprime08, which acts as soft layer, TiO_2 in-situ films without monomer become patternable, but they cracked (Fig. 57 right).

Pressure (MPa)	Temperature (°C)	Time (min)	Remarks
0,3	80	5	Film cracks but weakly imprinted.
0,4	RT	10	Film cracks but imprinted.

Tab. 8 Imprinting parameters for TiO_2 in-situ material with Ormoprime as primer layer and films thickness of 320nm.

The primer deposition was checked to study if it had cracked before imprinting. However, the primer did not exhibit any cracks during spin-coating process and heating. Also TiO_2 in-situ films deposition on the primer did not cause any breaks (sometimes films cracking come from different thermal expansion coefficient between film material and substrate) proving that the cracks formed really during imprinting process. Since the primer itself is patternable, the cracks origin is not related to primer patternability. The rate of increasing and decreasing temperature was slowed down in order to avoid thermal shocks and high differences in thermal gradients. The temperature was increased from room temperature to 80°C at 0,3-0.5°C s^{-1} and then it was decreased to 50°C with rate of 0.1-0.2°C·s^{-1}. Despite that the cracks remain. Another primer, GPTMS, was tested (Fig. 57 left). Theoretically it should be more compatible with the resist because it has the same composition of one resist precursor. GPTMS 100g/L was deposited at 6100rpm for 30s and baked for 5min at 80°C. Anyway cracking problems remained and therefore the primer use was not used.

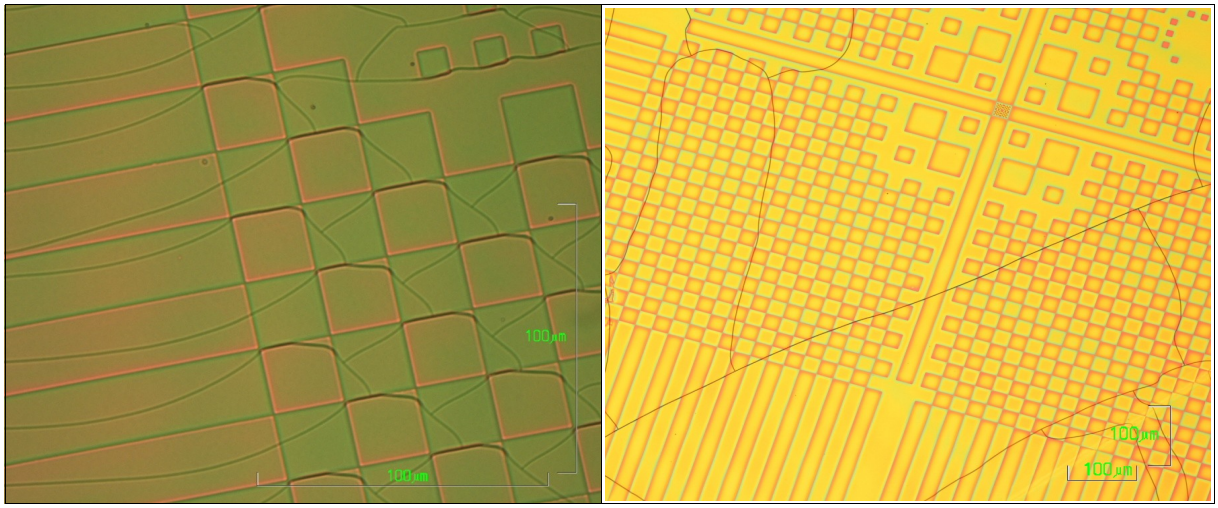

Fig. 57 Optical micrographs of TiO_2 in-situ patterns with (left) a basic solution of GPTMS as primer. Imprinting consitions: pressure of 0,4MPa at 80°C for 10min (right) Ormoprime08 as primer. Imprinting conditions: pressure of 0,2MPa at 80°C for 10min.

With the aim to be able to imprint TiO_2 in-situ material without primer-layers, the process time and the temperature were modified (as reported below), but the results were not satisfying.

In order to achieve better printing quality, a modified process was tested. The resist without the solvent was used. Evaporated drop of the resist was directly place on a stamp and covered with a silicon substrate. This method should ease the pattern filling, because the resist is a liquid phase.

Pressure (MPa)	Temperature (°C)	Time (min)	Remarks
0,4	80//100	10//10	Two temperature steps. Film weakly imprinted. Sticking problem.
0,4	100//120	10//10	Two temperature steps. Film weakly imprinted. Sticking problem.
Pressure (MPa)	Temperature (°C)	Time (min)	Remarks
0,2	RT	1 night	Drop. Film remain attached to Si substrate.
0,2	80	10	Drop. Imprinting but part of resists remains attached to the stamp.

Tab. 9 Imprinting parameters for TiO_2 in-situ material with two temperature steps or with “drop” method.

In addition to the problems listed in the table above, the TiO_2 in-situ imprinted with the "drop" method involves the gelation of the material during demolding. The material, being still in the liquid phase reacts almost instantaneously with moisture and gelifies.

In order to decrease the hardness of the film (due to high TiO_2 content) and eliminate sticking problem between the stamps and the films, a fluorinated monomer was introduced during solution preparation. The first monomer used was glycidyl hexadecafluorononyl ether (10% respect GPTMS moles). The amount of fluoro-monomer was increased to 10% respect SiO_2 and TiO_2 in moles. This high quantity of monomer added to in-situ solution made it less stable down to few days. The subsequent NIL process details are presented in the Tab. 10.

Pressure (MPa)	Temperature (°C)	Time (min)	Remarks
0,2	X	30	Film not imprinted.
0,3	80	20	Film weakly imprinted. Depth: 65nm
0,3	100	20	Film weakly imprinted. Depth: 80nm
0,2	60//100	20	Two temperature steps. Film weakly imprinted.
0,2	80//100	20	Two temperature steps. Film weakly imprinted.
0,2	100//120	20	Two temperature steps. Film weakly imprinted.

Tab. 10 Different imprinting parameters for TiO_2 in-situ material with fluorinated monomer.

An analysis of the behavior of TiO_2 in-situ solution after the addition of different monomers, with the same purpose mentioned above, was carried out. The monomer content in all solutions was 10% of TiO_2 moles.

The monomers tested were:

- glycerol diglycidyl ether (GDE)

- glycidyl hexadecafluorononyl ether (GD16)
- bisphenol F diglycidyl ether (BFDGE)
- zonyl® FSN 100

All solutions were spin-coated at 5000rpm for 30s and imprinting parameters were: P=0,3MPa, T=100°C, t=20min. The monomer that gave the "best" results in terms of imprinting depth was BFDGE. Also the GD16-solution gave good imprinting results, but the solution is not stable. GDE-film did not imprint, while Zonyl-film presented phase separation.

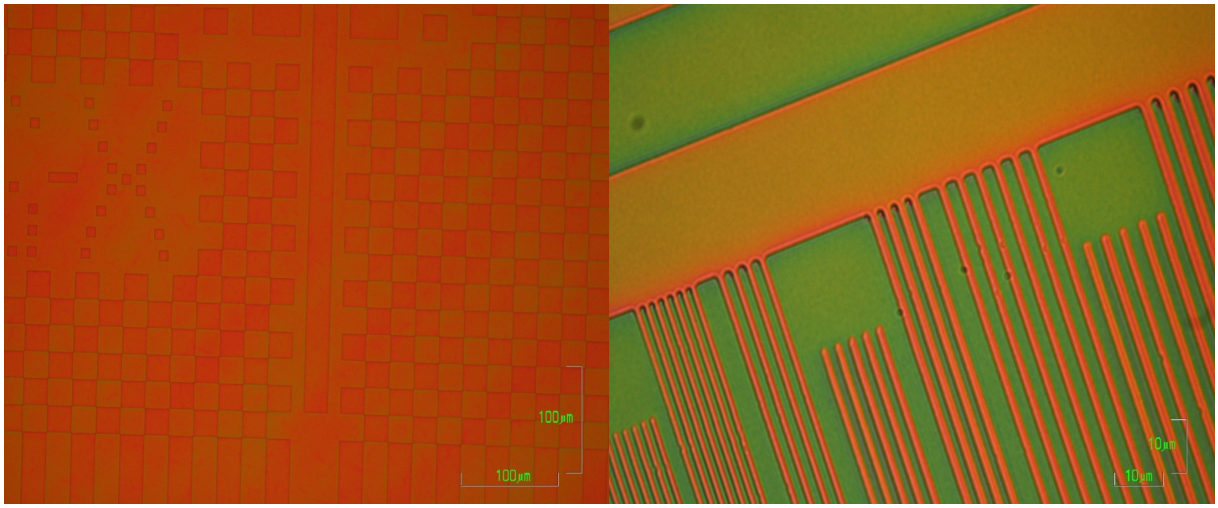

Fig. 58 Optical micrographs of TiO_2 in-situ containig (left) GD16 (10%SiO_2) or (right) BFDGE (10%TiO_2) and patterned with a pressure of 0,3MPa for 10min at 100°C.

Other tests on TiO_2 in-situ with BFDGE as soft monomer, were carried out. The imprinting conditions are listed in Tab. 11.

Pressure (MPa)	Temperature (°C)	Time (min)	Remarks
0,3	80//100	5//20	Film imprinted.
0,3	80	45	Film imprinted.
0,3	100	45	Film imprinted.

Tab. 11 Imprinting parameters for TiO_2 in-situ material containing bisphenol F diglycidyl ether (BFDGE).

Nevertheless it must be pointed out that the maximum depth achievable with all the tests is never more than 80nm and the full pattern filling was never reached. After the imprint profile

measurements using a profilometer, it can be observed a dual peaks filling morphology of the imprinted structures. Dual peak deformation mode occurs when a cavity half width W is greater than film thickness h_i (in this case W=1,5µm and h_i=320nm). Dual peak deformation is formed when the vertical and lateral velocities have the same trends. Before the flow front contact to the roof of cavity, all lateral velocities at the flow front have the same flow trends for any time step, in which the lateral velocity increases with increasing distance from the cavity center until it reaches the maximum value near the cavity sidewall. On the other hand, before the flow front contact to the roof of cavity, there are two different flow trends of the vertical velocity. One is that the vertical velocity at the flow front increases with decreasing distance from the cavity center, while the other is that the vertical velocity increases with increasing distance from the cavity center until it reaches the maximum value near the cavity sidewall. Once the vertical and lateral velocities have the same flow trend, their maximum values occur near the sidewall, which can deposit more polymers around the sidewall.

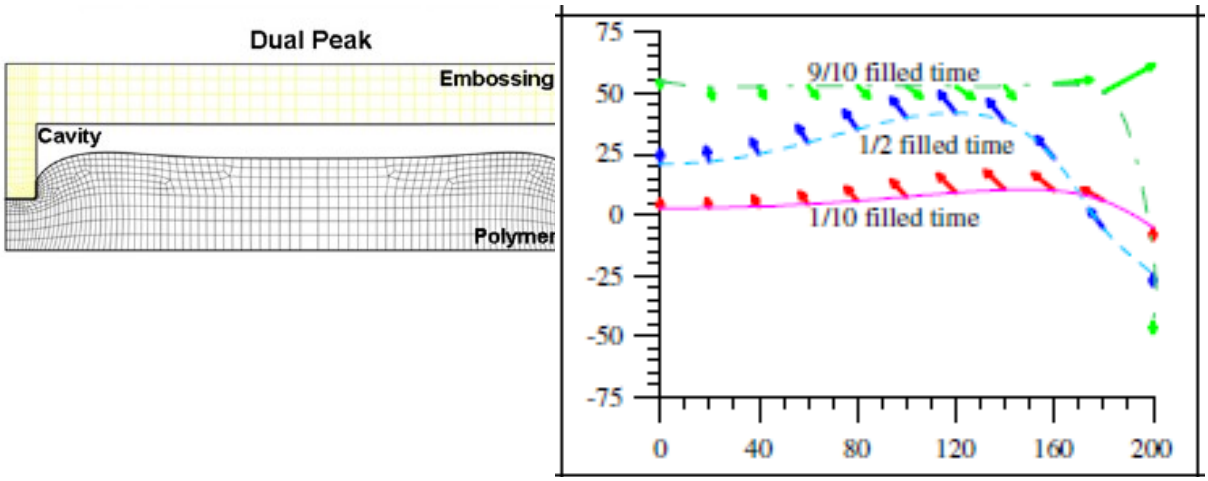

Fig. 59 (left) Nanoimprint lithography dual peak deformation mode. (right) The velocity vector at the flow front with various time steps when half convexity width, half cavity width and resist thickness are 200nm, 200nm and 100nm, respectively.

During demolding, very often that a very thin resist layer remains attached to the stamp. It forms a thin-film that is impossible to remove. To remove this thin layer from the stamp different methods were used without success: solvents (IPA and acetone) and sonication. Therefore different types of mold and different passivation treatments of stamps surface were investigated. The imprinting conditions were kept constant (0.2MPa, 80°C, 5min). The tested stamps were:

- silicon stamp silanized with trichloro(1H,1H,2H,2H-perfluorooctyl)silane in vapor phase
- silicon stamp covered with Teflon monolayer (about 10nm). The Teflon deposition was made with AMS200 etching and deposition system.
- PDMS stamp silanized with trichloro(1H,1H,2H,2H-perfluorooctyl)silane in vapor phase

The best result was obtained with Si stamp covered with Teflon. PDMS stamp did not produce any patterned surface.

Furthermore often the films of both TiO_2 sols, stamp or PDMS used as soft layer were broken. One way to solve this problem is by decreasing the imprint pressure to 0,2 or 0,3MPa, not desirable due to the shallow printing results. The use of multiple layer of paper or thick foam as soft materials is tested. They did not give satisfying results due to not practical handling of multiple layers and melting of the foam at the temperatures used during imprinting. The cracking can also be attribuited to the problems of press misalignment as well as the presence of particles on working environment.

8.2. THERMAL IMPRINTING WITH SUB-MICROMETRIC MOLDS

Three types of sub-micrometer molds were used for nanoimprinting. The patterns were composed of lines and dots with different period from 3μm to 50nm. The structure depths were: 160, 620 and 700nm. The mold with depth of 160nm will be referred to as S160, while the other two type of stamps will be called S620 and S700.

TiO_2 ex-situ

TiO_2 ex-situ sol without evaporation step was directly deposited by spin-coating onto silicon chips at 4000rpm for 30s. After deposition, coatings have been cured at 80°C for 2min. The film thickness was ~700nm. It is noted that the thicknesses reported may not coincide with thicknesses inferred from spin-curves because the preparation of TiO_2 ex-situ solution is also affected by the quality of reagents that may change over time.
Fig. 60 and Fig. 61 shows a set of micrographs of TiO_2 ex-situ imprinted with the same stamp

(S160) but with different imprinting conditions followed by 10min of UV exposure (dose: 592J/cm^2) with OmniCure S2000 standard lamp.

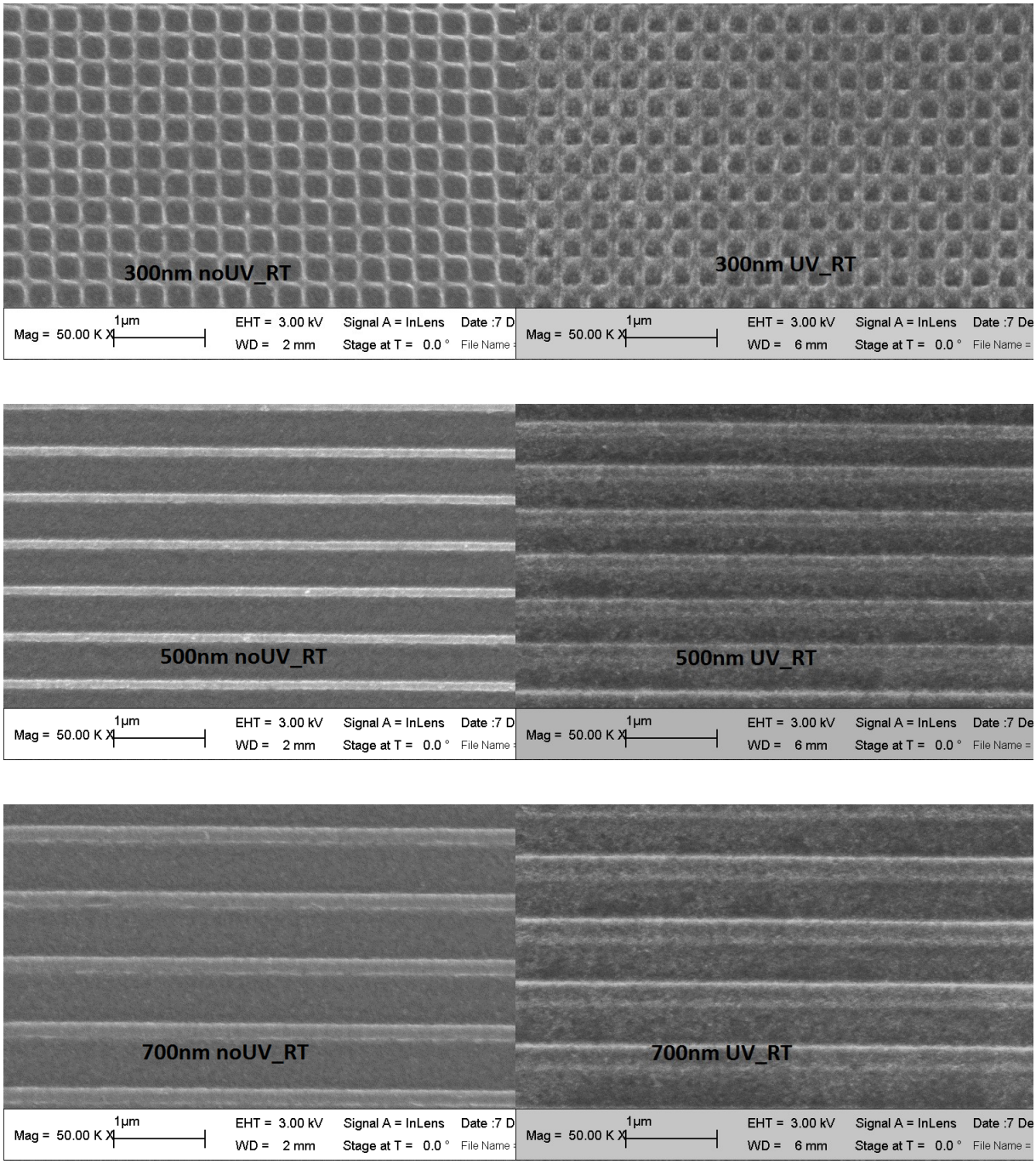

Fig. 60 SEM micrographs of 300nm, 500nm and 700nm period dots and lines before and after UV exposure, imprinted at room temperature for 20h with S160.

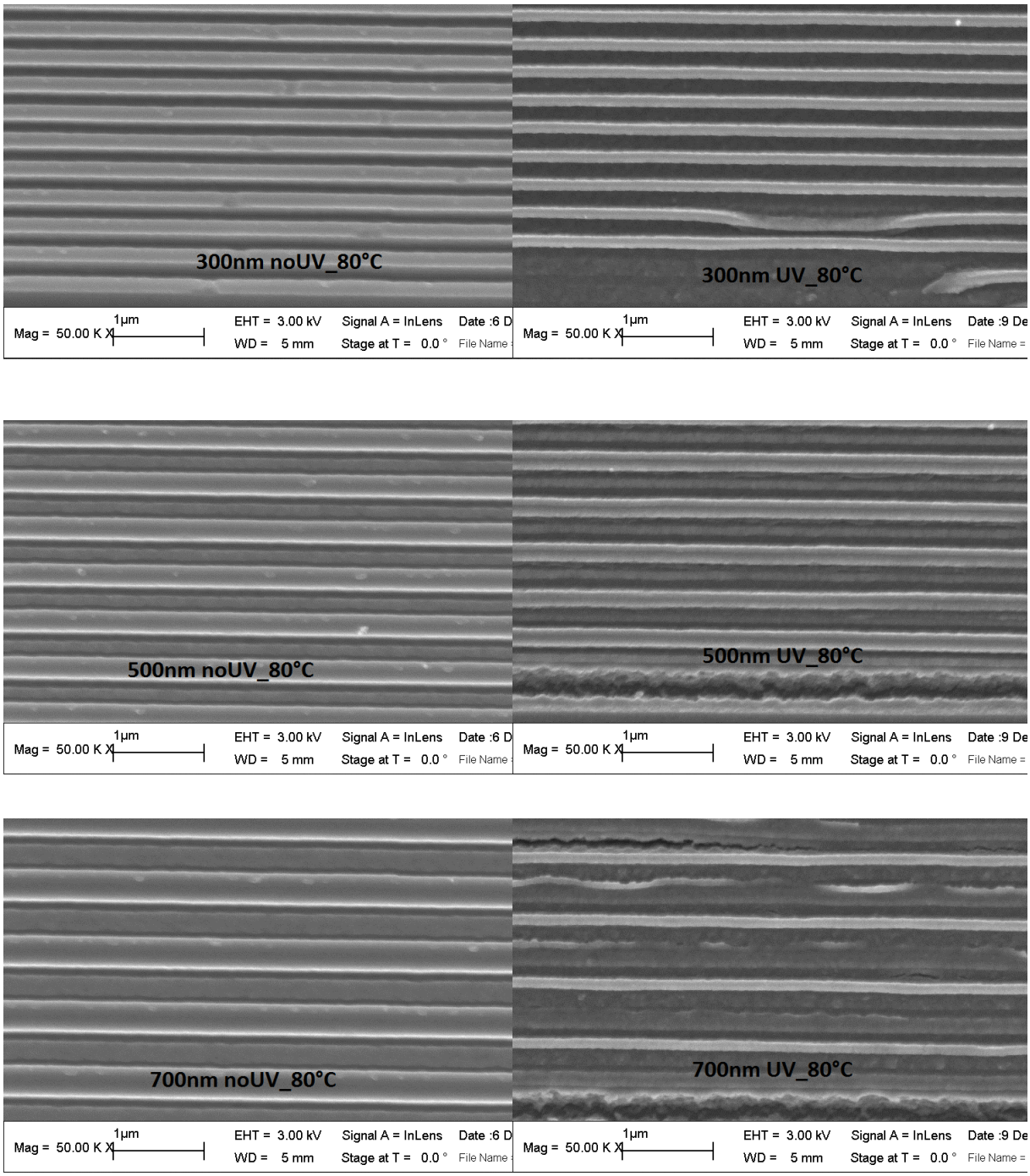

Fig. 61 SEM micrographs of 300nm, 500nm and 700nm period lines before and after UV exposure, imprinted at 80°C for 10min with S160.

The conditions that give best results in terms of imprinting sharpness before UV irradiation are: 10min at 80°C. Nevertheless darker areas on lines edges denote a non-uniform filling of the structures, which are more filled along the edges than in the central part. In addition, after UV irradiation, the structures collapse and break due to the high shrinkage. On the contrary

films patterned at room temperature presents structures (lines and dots) well defined and uniformly filled that do not break nor collapse after UV exposure. Only flaw is the apparent grainy texture of the material. Probably long imprinting time allow TiO_2 ex-situ to flow better within structures and fix them so that the subsequent exposure to UV radiation does not cause breakage or deformation.

TiO_2 ex-situ films were imprinted also with deeper stamps (S700) as shows in Fig. 62. In this case films were spin-coated at 2000rpm for 30s and baked for 2min at 80°C. The final films thickness was approximately 1μm.

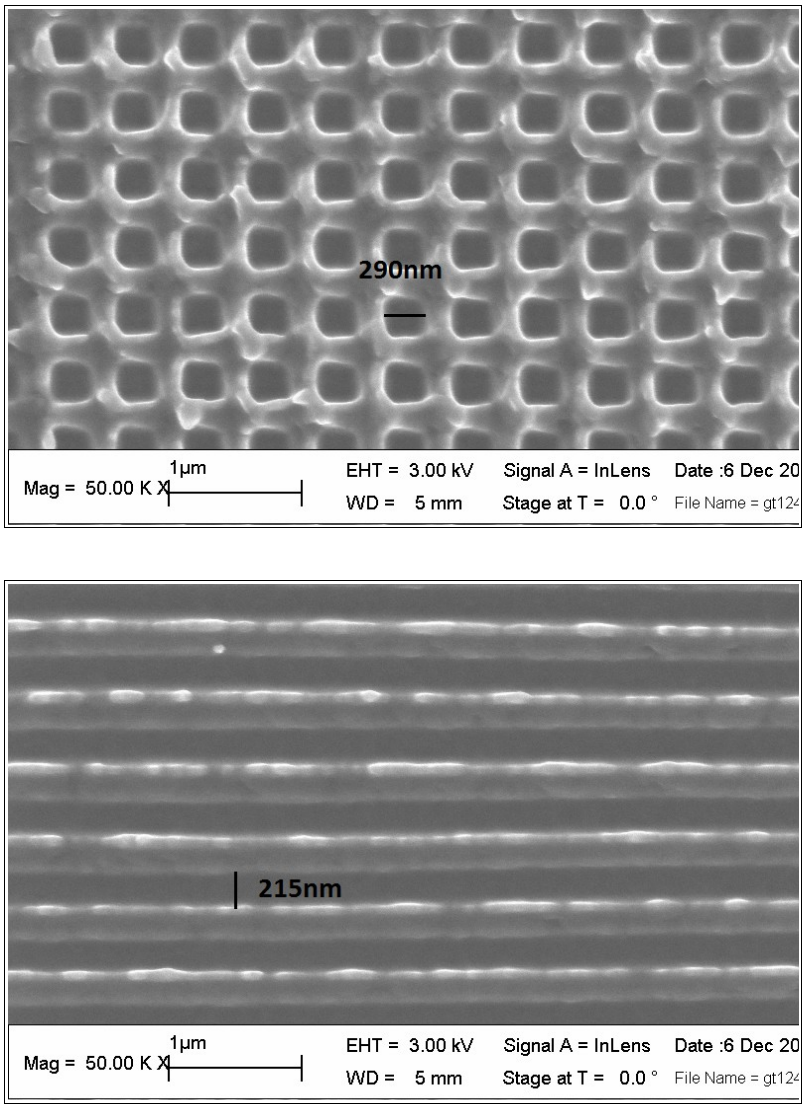

Fig. 62 SEM images of 500nm period lines and dots imprinted at room temperature for 20h with S700.

The minimum feature size of TiO_2 ex-situ with deep stamp (S700) is 500nm. Structures with smaller periods are not possible to replicate because they collapse or break. Instead, with

S160 the resolution up to 300nm was reached, and probably smaller period structures could be imprinted, however, there is a limitation due the minimum feature size on the mold. The lighter areas, that can be seen in the structures (lines and dots) with 500nm period, represent pieces of material torn away (or parts of Ormoprime which remain glued) during demolding. This means that the problem of sticking between mold and film persists.

TiO_2 in-situ

One layer of TiO_2 in-situ sol-gel film with bisphenol F diglycidyl ether (BFDGE) was spun onto silicon substrate at 2500rpm for 30s. The film thickness was about 650nm. Five identical samples were prepared with the previously described conditions of deposition. Afterwards these films were imprinted with the same pressure and for the same time but with different temperatures in order to determine the best imprinting conditions and compare them with the resist viscosity change over the time. Low values of viscosity allow better filling of the structures and therefore greater depth of imprinting. In Fig. 63 are shown the imprinting depth vs. imprinting temperature with superimposed AFM images of imprinted structures (lines of 2µm period).

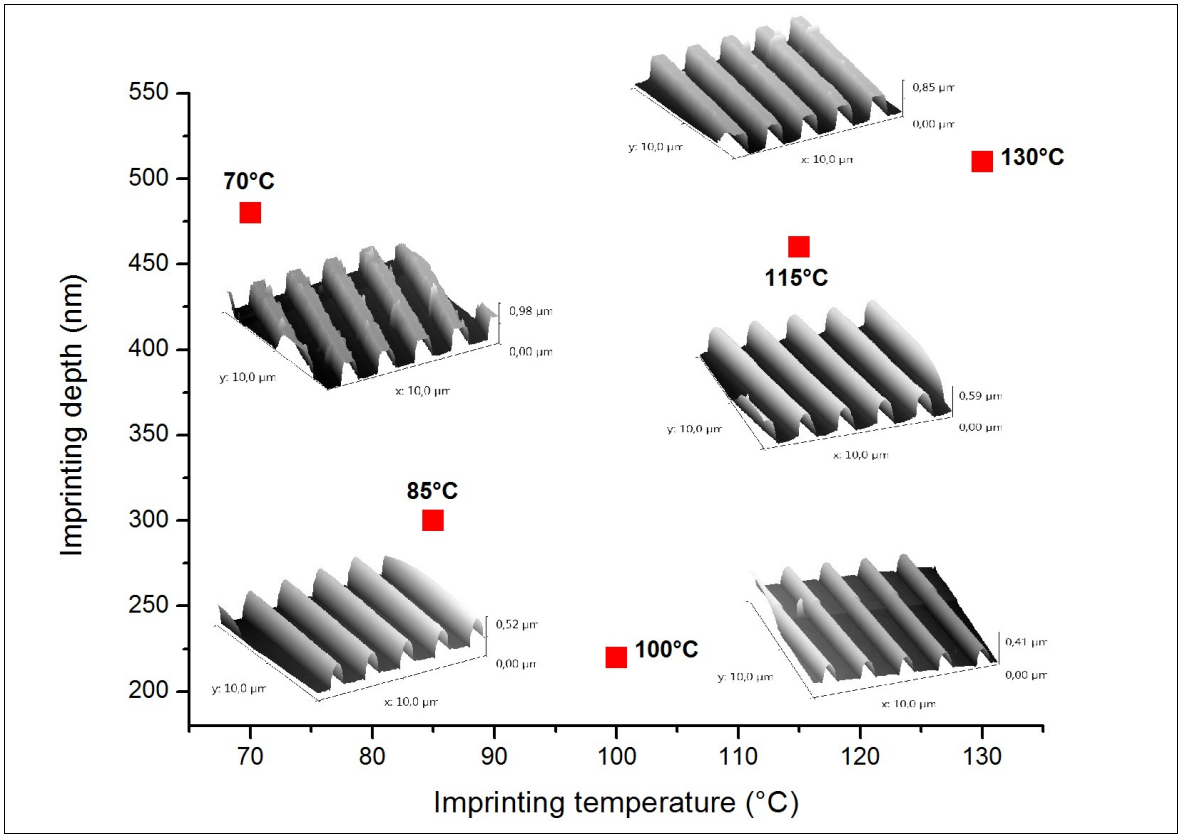

Fig. 63 Imprinting depth vs. imprinting temperature with superimposed AFM images of imprinted structures

(period:2μm).

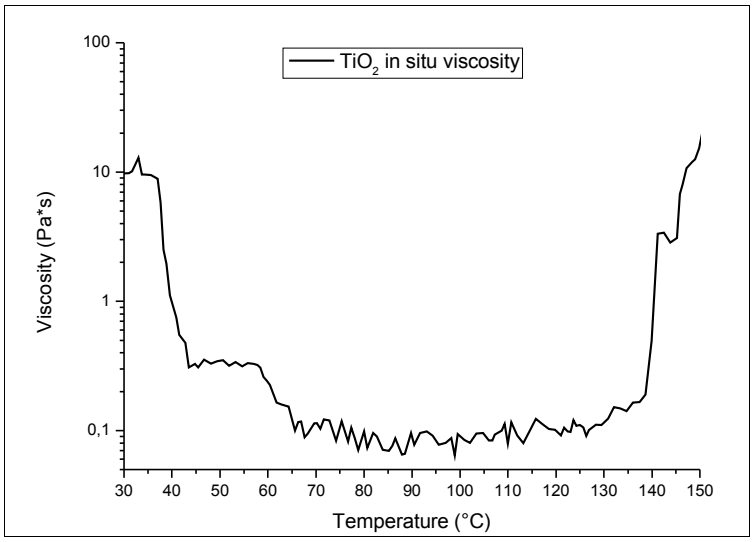

Fig. 64 Viscosity curve of TiO_2 in-situ in the range from 30°C to 150°C.

Imprinting depth measured by AFM shows a performance opposite to what one would expect. As in the range of temperatures between 70°C and 130°C, the viscosity values has a trend comparable to a convex curve, consequently the values of imprinting depth should follow a concave curve. On the contrary the values of imprinting depth present a convex trend. This different trend may be due to the fact that (i) the rheological curve was obtained by testing the material in liquid phase while during the imprinting, the material is in gel phase, (ii) stress that the material is subjected during a viscosity test (shear stress) are different from the compressive forces that acts during imprinting and (iii) viscosity measurements are performed with a thickness of liquid different from thickness of patterned films. However, the increase of viscosity at around 120-130°C can explain the highest imprinting depth, because at this temperature the film starts to crosslink, allowing the maintenance of the depth after pressure removal.

The maximum imprinting depth reached is 510nm at 130°C. The sample imprinted at 130°C also shows the best pattern filling. In fact AFM profile of this sample is rectangular instead of curved like other samples. Curved profiles mean incomplete pattern filling. The corners of lines are not completely filled of material. Generally TiO_2 in-situ material need a higher temperature of imprinting as its T_g will be higher than that of TiO_2 ex-situ because the amount of titania is higher (harder material) and there is the presence of bulky and rigid side groups due to momomer.

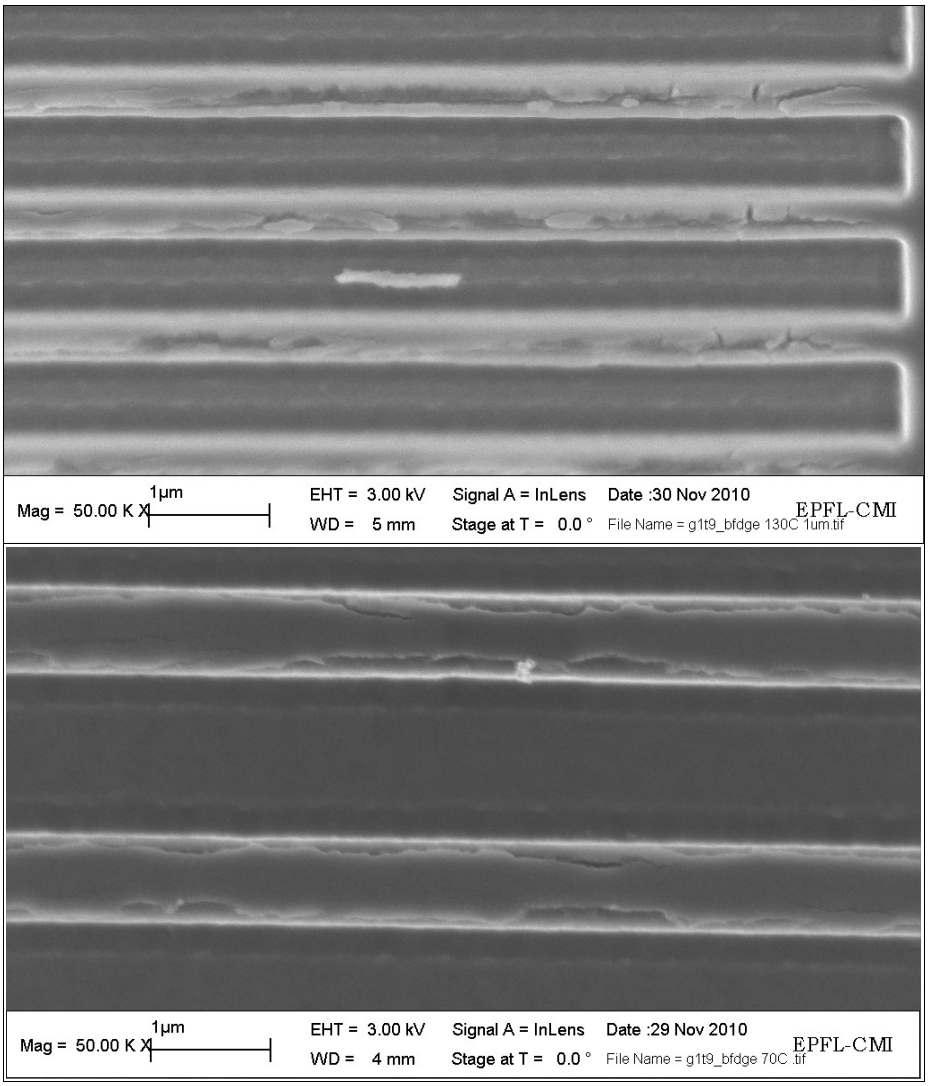

Fig. 65 SEM images of TiO_2 in-situ imprinting results at (top) 130°C and (bottom) 70°C. Both patterns represent 1µm period lines.

The sample imprinted at high temperatures (130°C) shows cracks in the film between patterned structures, probably caused by greater shrinkage than sample patterned at low temperature (70°C). Both samples exhibit darker edge lines due to inhomogeneous filling (one peak configuration).

The smallest period that it is possible to print with S700 and S620 is 500nm (as shown in Fig. 66). The average dots diameter is 430nm, while the average linewidth is 105nm.

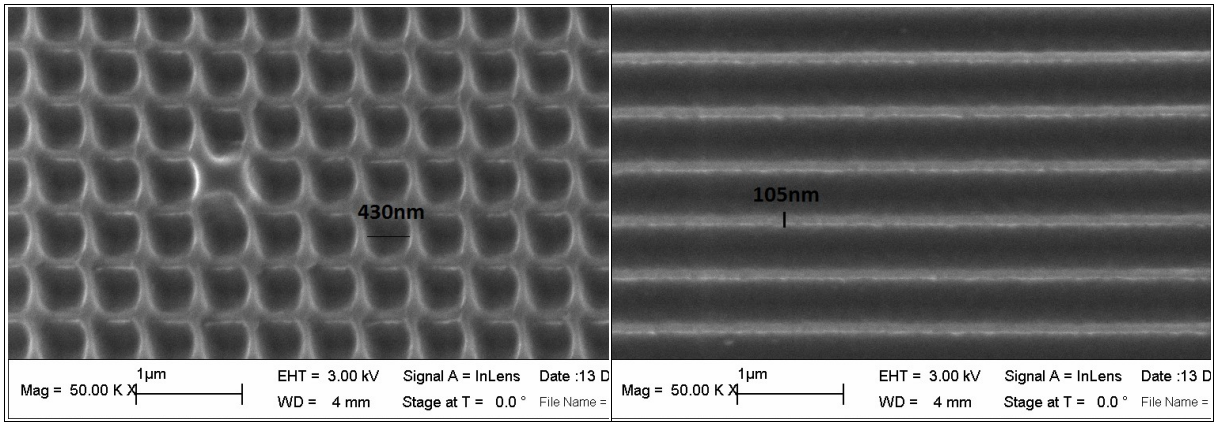

Fig. 66 SEM micrographs of TiO_2 in-situ 500nm period dots and lines, imprinted with S700 (P=0,4MPa, T=100°C, t=20min).

Instead with S160, gratings up to 200nm pitch and isolated lines are clearly visible. In this case films were spin-coated at 4000rpm for 30s. The final films thickness was approximately 400nm.

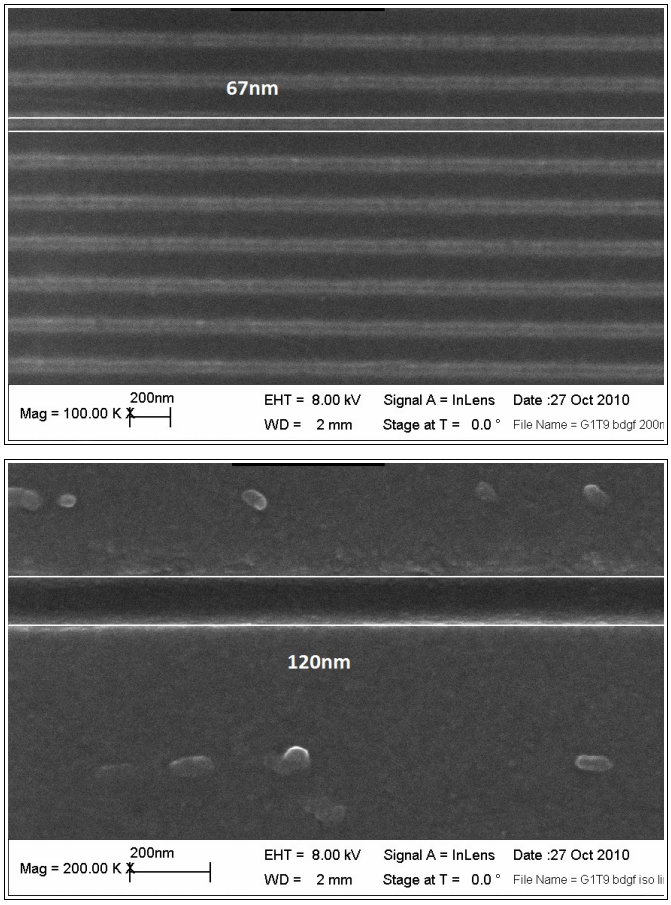

Fig. 67 SEM micrographs of TiO_2 in-situ (up) gratings with 200nm pitch and (bottom) isolated lines, imprinted with S160(P=0,4MPa, T=100°C, t=20min).

CONCLUSIONS

Sol-gel derived TiO_2 ex-situ and in-situ materials from basic catalyzed solutions of 3-glycidoxypropyltrimethoxysilane mixed with anatase nanoparticles and titanium isopropoxide, respectively, have been studied. The titanium dioxide content of both materials is very high: more than 50wt%. Single-layer films with a thickness of more than 1μm has been prepared on solid silicon substrate by single spin coating. A detailed study of the structural and optical properties of the films using various experimental tools provided an insight into the effect of UV exposure on the physical properties. The major observations of this study can be summarized as follows.

The almost total decomposition of organic compounds in a TiO_2 ex-situ and in-situ materials is complete after 20min of exposure to UV light (235J/cm^2 dose). The photochemical conversion of the photosensitive titanium organic compound to TiO_2 is confirmed by FTIR. The deposited TiO_2 ex-situ and in-situ thin films have high transparency in the visible range (350-800nm), while there is a strong absorption from 200 to 300nm..

XRD results show the TiO_2 in-situ film exhibiting nano-crystalline (anatase) phase at 500°C with crystallite size of 21,2nm and confirm that TiO_2 NPs put into ex-situ solution consisting really of anatase NPs.

The refractive index of the TiO_2 in-situ irradiated film (592J/cm^2 dose) at the wavelength of 550nm was 2,03. The refractive index increases with increasing UV doses according to film densification. However it is noted lower packing density due to a residual micropores inside the film as well as other impurities such as carbon.

Nano-patterned TiO_2-based materials is obtained using a direct patterning method, based on thermal nanoimprint lithography. The TiO_2 ex-situ and in-situ sols are used instead of an imprint resin, and the TiO_2 gels patterns are obtained after imprinting. TiO_2 ex-situ and in-situ gel patterns are converted to inorganic TiO_2 patterns by UV exposure. Patterned films are studied by different techniques including optical microscopy, AFM and SEM. Using mold copies made by Ormostamp®, lines and dots as small as 100nm can be patterned up to 300nm pitch. Specifically the resolution of TiO_2-based materials depends on the depth of the mold used. With 160nm-deep stamp, the minimum feature size for TiO_2 ex-situ material is 214,3nm linewidth and 300nm pitch while for TiO_2 in-situ material, 67nm wide grating with 200nm period was fabricated. With 700nm-deep stamp, lines as small as 215nm and with 500nm period were achieved for, TiO_2 ex-situ material, instead TiO_2 in-situ material reach a resolution of 105nm linewidth and 500nm pitch.

The direct writing of these hybrid sol-gel TiO_2-based materials using nanoimprint lithography offers an easy way to pattern micro and nanostructures for various applications such as hard optical coatings thanks to their high refractive index and high titania content.

REFERENCES

[1] A. E. Grigorescu and C. W. Hagen, “Resists for sub-20-nm electron beam lithography with a focus oh HSQ: state of the art”, *Nanotechnology* 20 (**2009**)

[2] J. Choi et al., “Status of UV imprint lithography for nanoscale manufacturing”, *Elsevier* **2010**

[3] C. W. Gwyn et al., “Extreme ultraviolet lithography”, *J. Vac. Sci. Technol. B* 16, 3142 (**1998**)

[4] A. Heuberger, “X-ray lithography”, *Microelectronic Engineering*, Vol.5, December **1986**, Pag. 3-38

[5] “Handbook of microlithography, micromachining and microfabrication” Volume 1, P. Rai-Choudhury, Editor

[6] “Polymer-based photonic crystals fabricated with single-step electron beam lithography”, *Advanced Materials*, 19, 3052 (2007)

[7] H. Mohseni and R. Gelfand, “Squeezing light for single-molecule spectroscopy”, *SPIE Newsroom*, 26 May **2009**

[8] E. A. Costner et al., “Nanoimprint lithography. Materials development for semiconductor device fabrication”, *Annu. Rev. Mater. Res.* **2009,** 155-180.

[9] J. E. ten Elshof et al., “Micrometer and nanometer-scale: parallel patterning of ceramic and organi-inorganic hybrid materials”, *Journal of the European Ceramic Society* 30 (**2010**) 1555-1577.

[10] Y. Chen and A. Pépin, “Nanofabrication: conventional and nonconventional methods”, *Electrophoresis* **2001**, 22, 187-207.

[11] H. Schift, “Nanoimprint lithography: an old story in modern times? A review”, *J. Vac. Sci. Technol. B*, Vol.26, No. 2, Mar/Apr **2008**.

[12] B. Bhushan, “Handbook of Nano-technology”, *Springer* **2007**.

[13] L. J. Guo, “Nanoimprint lithography: methods an material requirements”, *Adv. Mater.* **2007**, 19, 495-513.

[14] L. J. Guo, “Recent progress in nanoimprint technology and its applications”, *J. Phys. D:*

Appl. Phys. 27 (**2004**) R123-R141

[15] C.-H. Li et al., "ORMOSILS as matrices in inorganic-organic nanocomposites for various optical applications", Proc. *SPIE* 1758, 410 (**1992**);

[16] M. Mühlberger et al., "UV-NIL with working stamps made from Ormostamp", *Microelectronic Engineering* 86 (**2009**) 691–693

[17] H. Schift and L. J. Heyderman, "Alternative lithography. Unleashing the potentials of nanotechnology", edited by C. M. Sotomayor Torres, **2003** *Kluwer Academic/Plenum Publisher*, New York. **16**

[18] Y. Hirai et al., "Study of the resist deformation in nanoimprint lithography", *J. Vac. Sci. Technol. B*, **2001**, 19, 2811.

[19] H. D. Rowland et al., "Impact of polymer film thickness and cavity size on polymer flow during embossing: toward process design rules for nanoimprint lithography", *J. Micromech. Microeng.* 15 (**2005**) 2414-2425.

[20] C. H. Lin and R. Chen, "Effects of mold geometries and imprinted polymer resist thickness on ultrasonic nanoimprint lithography", *J. Micromech. Microeng.*17 (**2007**) 1220-1231.

[21] J. Zhu et al., "Optimum design of processing condition and experimental investigation of grating fabrication with hot embossing lithography", *Acta Mechanica Solida Sinica*, Vol.22, No.6, **2009**.

[22] J. Wen and G. L. Wilkes, "Organic/inorganic hybrid network materials by the sol-gel approach", *Chem. Mater.*, Vol.8, No.8, **1996 22**

[23] U. Schubert et al., "Hybrid inorganic-organic materials by sol-gel processing of organofunctional metal alkoxydes", *Chem. Mater.*, Vol.7, No.11, **1995**

[24] Judeinstein and C. Sanchez, "Hybrid organic-inorganic materials: a land of multidisciplinarity", *J. Mater. Chem.*, **1996**, 6(4), 511-525

[25] C. Chang et al., "Preparation and characterization of TiO_2 hybrid sol for UV-curable high-refractive-index organic–inorganic hybrid thin films", *J. Sol-Gel Sci. Technol.* (**2010**) 55:199–206

[26] L. Brigo et al., "New hybrid organic–inorganic sol–gel positive resist", *Microelectronic Engineering* (**2009**)

[27] G. Brusatin et al., “Design of hybrid sol–gel films for direct x-ray and electron beam nanopatterning”, *Nanotechnology* 19 (**2008**)

[28] G. Della Giustina et al., “Direct nanopattern of hybrid sol–gel films”, *Materials Science and Engineering* C 27, (**2007**), 1382–1385

[29] G. Della Giustina, “Electron beam lithography of hybrid sol–gel negative resist”, *Microelectronic Engineering* (**2009**)

[30] H.-H. Park, “Photo-induced hybrid nanopatterning of titanium dioxide via direct imprint lithography”, *J. Mater. Chem.*, **2010**, 20, 1921–1926

[31] X. Zhang et al., “Thick UV-patternable hybrid sol-gel films prepared by spin coating”, *J. Mater. Chem.*, **2004**, 14, 357-361

[32] K. R. V. Subramaniam et al., “Direct writing of ZrO_2 on a sub-10nm scale using an electron beam”, *Nanotechnology* 15, **2004**, 158-162

[33] N. Tohge et al., “Fabrication of Two-Dimensional Gratings Using Photosensitive Gel Films and Their Characterization”, *Journal of Sol-Gel Science and Technology* 26, 903–907, **2003**

[34] M. J. Hampton, “The patterning of sub-500 nm inorganic oxide structures”, *Adv. Mater.* **2008**, 20, 2667–2673

[35] Y. Kang et al., “UV irradiation effect on sol-gel indium tin oxide nanopatterns replicated by room-temperature nanoimprint”, *J. Vac. Sci. Technol. B* 27*,* **2009**

[36] Ki-Yeon Yang et al. “Direct indium tin oxide patterning using thermal nanoimprint lithography for highly efficient optoelectronic devices”, *J. Vac. Sci. Technol. B 27*, **2009**

[37] O. Carp et al., “Photoinduced reactivity of titanium dioxide”, *Progress in Solid State Chemistry* 32 (**2004**) 33-117

[38] C.-C. Wu and S. L.-C. Hsu, “Preparation of epoxy/silica and epoxy/titania hybrid resists via a sol-gel process for nanoimprint lithography”, *J. Phys. Chem. C*, Vol.114, No.5, **2010**

[39] S. Phadke, “Broad band optical characterization of sol–gel TiO_2 thin film microstructure evolution with temperature”, *Thin Solid Films* 518 (**2010**), 5467–5470

[40] S. Banerjee et al, “Physics and chemistry of photocatalytic titanium dioxide: visualization of bactericidal activity using atomic force microscopy ”, *Current Science*, Vol.90, No.10, **2006**

[41] A. Fujishima et al., “Titanium dioxide photocatalysis”, *Journal of Photochemistry and Photobiology C: Photochemistry Reviews 1* (**2000**) 1-21

[42] M. S. M. Saifullah et al., “Sub-10nm electron beam nanolithography using spin-coatable

TiO_2 resists", *Nano Lett.*, Vol. 3, No. 11, **2003**

[43] B. Liu et al., "Sub-100nm nanolithography and pattern transfer on compound semiconductor using sol-gel-derived TiO_2 resist", *Journal of The Electrochemical Society*, P57-P60, **2008**

[44] C. Goh et al., "Nanostructuring titania by embossing with polymer molds made from anodic alumina templates", *Nano Lett.*, Vol.5, No.8, **2005**

[45] S. H. Lim et al., "Direct imprinting of high resolution TiO_2 nanostructures", *Nanotechnology* 21, (**2010**)

[46] K. Yoon et al., "Formation of TiO_2 nanopattern using reverse imprinting and sol-gel method", *J. Vac. Sci. Technol. B*, 27, Nov/Dec **2009**

[47] H.-H. Park et al., "Optical characterization of anatase TiO_2 films patterned by direct ultraviolet-assisted nanoimprint lithography", *Microelectronic Engineering*, (**2010**)

[48] A. Moujoud et al., "Double component long period waveguide grating filter in sol-gel material", *Optics Express 15149*, Vol.15, No.23, November **2007**

[49] M. D. McGehee, "Nanostructured organic–inorganic hybrid solar cells", *MRS Bulletin*, Vol.34, Febrary **2009**

[50] P.W. Oliveira et al., "Generation of wet-chemical AR-coatings on plastic substrates by use of polymerizable nanoparticles", *SPIE*, Vol.3136, **1997**

[51] W.-M. Chiu, "Synthesis and characterization of titanium dioxide optical films by sol–gel processes", *Journal of Applied Polymer Science*, Vol.103, 2271–2280 (**2007**)

[52] X. Wang et al., "Photonic crystal structures in titanium dioxide (TiO_2) and their optimal design", *Optics Express* 14867, Vol.13, No.5, March **2005**

[53] W.-S.Kim et al. "Nanopatterning of photonic crystals with a photocurable silica–titania organic–inorganic hybrid material by a UV-based nanoimprint technique", *J. Mater. Chem.*, **2005**, 15, 4535–4539

[54] B. Saekow et al., "High refractive index dielectric prepared by electron beam evaporation for photonic crystal optical biosensor application", *Avanced Materials Research* Vols. 93-94 (**2010**) pp545-548

[55] W. Que and C. H. Kam, "Sol-gel fabrication and properties of optical waveguides and gratings made from composites of titania and organically modified silane", *Optical Engineering*, Vol.41, No.7, July **2002**

[56] W. Que et al., "Sol-gel fabrication of low temperature organic-inorganic hybrid film patterns for photonic applications", *Advanced Materials Research* Vol. 31 (**2008**) pp14-16

[57] W. Que et al., "Preparation and characterizations of $SiO_2/TiO_2/\gamma$-glycidoxypropyltrimethoxysilane composite materials for optical waveguides", *Appl. Phys. A* 73, 171–176 (**2001**)

[58] M. Li et al., "Large area direct nanoimprinting of SiO2–TiO2 gel gratings for optical applications", J. Vac. Sci. Technol. B 21(2), Mar/Apr **2003**

[59] Anna Łukowiak et al., "Optical properties of SiO_2–TiO_2 thin film waveguides obtained by the sol-gel method and their applications for sensing purposes", *Optical Materials* 27 (**2005**) 1501-1505

[60] A. S. Zuruzi and N. C. MacDonald, "Facile fabrication and integration of patterned nanostructured TiO_2 for microsystems applications", *Adv. Funct. Mater.*, **2005**, 15, No.3

[61] M. Grätzel, "Sol-gel processed TiO_2 films for photovoltaic applications", *Journal of Sol-Gel Science and Technology* 22, 7–13, **2001**

[62] S. S. Williams et al., "Nanostructured titania-polymer photovoltaic devices made using PFPE-based nanomolding techniques", *Chem. Mater.,* **2008**, *20,* 5229–5234

[63] B. K. Lee et al., "Replica mold for nanoimprint lithography from a novel hybrid resin", *Langmuir* **2009**, 25(19), 11768–11776

[64] J. Kim, "Low-cost fabrication of transparent hard replica molds for imprinting lithography", *Adv. Mater.* **2009**, 21, 4050–4053

[65] J. Wan et al., "Duplication of nanoimprint templates by a novel SU-8/SiO_2/PMMA trilayer technique", *J. Vac. Sci. Technol. B* 27, Jan/Feb **2009**

[66] Z. W. Zhong et al., "Investigation of antiadhesive coatings for nanoimprinting lithography", *Materials and Manufacturing Processes*, 25: 658-664, **2010**

[67] N. Y. Lee and Y. S. Kim, "A poly(dimethylsiloxane)-coated flexible mold for nanoimprint lithography", *Nanotechnology* 18, (**2007**)

[68] "Understanding rheology of thermosets", revised by A.J. Franck, TA Instruments

[69] S. Dai et al., "Preparation of highly crystalline TiO_2 nanostructures by acid-assisted hydrothermal treatment of hexagonal-structured nanocrystalline titania/ cetyltrimethyammonium bromide nanoskeleton", *Nanoscale Res. Lett.* (**2010**) 5:1829–1835

[70] R. M. A. Azzam and N. M. Bashara, "Ellipsometry and Polarized Light", *Elsevier* Science Pub Co (**1987**)

Other papers:

S. Y. Chou et al., "Nanoimprint lithography", *J. Vac. Sci. Technol. B* 14(6), Nov/Dec **1996**

G. Brusatin et al., "Direct pattern of photocurable glycidoxypropyltrimethoxysilane based sol–gel hybrid waveguides for photonic applications", *Materials Science and Engineering C* 27 (**2007**) 1022–1025

C. C. Wu and S. L. C. Hsu, "Thermo-curable epoxy systems for nanoimprint lithography", *J. Micromech. Microeng.* 20 (**2010**) 015006

B. Liu et al., "Nanolithography using spin-coatable ZrO_2 resist and its application to sub-10nm direct pattern transfer on compound semiconductors", *Nanotechnology* 19 (**2008**) 155303

K. Yoon et al., "Fabrication of polycrystalline TiO_2 nanopatterns by TiO_2 sol base imprint lithography", *Thin Solid Films* 518 (**2009**) 126–129

S. Gardin et al., "Photocatalytic Performance of Hybrid SiO_2-TiO_2 Films", *J. Phys. Chem. C* **2010**, *114,* 7646–7652

X. Le Guével et al., "Effect of titania content on the optical properties of dye-doped hybrid sol–gel coatings", *Optical Materials* 31 (**2008**) 451–454

M. Kumar et al., "The deposition of nanocrystalline TiO_2 thin film on silicon using Sol–Gel technique and its characterization", *Microelectronic Engineering* 87 (**2010**) 447–450

N.R. Mathews et al., "TiO_2 thin films – Influence of annealing temperature on structural, optical and photocatalytic properties", *Solar Energy* 83 (**2009**) 1499–1508

W. Que et al., "Effects of titanium content on properties of sol–gel silica–titania films via organically modified silane precursors", *J. Phys. D: Appl. Phys.* 34 (**2001**) 471–476

M. Vishwas et al., "Influence of surfactant and annealing temperature on optical properties of sol–gel derived nano-crystalline TiO_2 thin films", *Spectrochimica Acta Part A* 75 (**2010**) 1073–1077

W. Que and X. Hu, "Effects of titanium content on sol-gel hard optical films prepared in an organic-inorganic hybrid system", *J. Vac. Sci. Technol. A* 21(6), Nov/Dec **2003**

S. Dal Zilio et al., "Microlens arrays on large area UV transparent hybrid sol-gel materials fo optical tools", *Microelectronic Engineering* (**2009**)

N. Chaix ey al., "NIL processes and material characterization on transparent substrates for optical applications", *J. Vac. Sci. Techonol. B* 26(6), Nov/Dec **2008**

D. S. Mehta and K. Saxena, "Light out-coupling strategies in organic light emitting devices", Proc. of ASID'06, 8-12 Oct, New Delhi

R. Vogel and al., “Mesostructured Dye-Doped Titanium Dioxide for Micro-Optoelectronic Applications”, *CHEMPHYSCHEM* **2003**, 4, 595-603

M. Pagliaro et al., “Nanochemistry aspects of titania in dye-sensitized solar cells”, *Energy Environ. Sci.*, **2009**, 2, 838–844

ACKNOWLEDGEMENTS

I am grateful for the support of Microsystem Laboratory (Prof. J. Brugger) of École polytechnique fédérale de Lausanne and Dipartimento di Ingegneria Meccanica-Settore Materiali (Dott.essa Giovanna Brusatin) of Università degli Studi di Padova.

Many thanks are due to Dr. Vaida Auzelyte for her expertise, help, heartiness and patience. I also acknowledge Nicolas Schüwer for FTIR measurements, Mathieu Soutrenon for rheologhy characterization, Dr. Blake Erickson for AFM images and Philippe Langlet for ellipsometry simulations.

Moreover I would like to thank Dott.essa Giovanna Brusatin for giving me the opportunity to carry out the thesis abroad and its continuous willingness (even away) and competence, Dott.essa Gioia Della Giustina and Dott.essa Laura Brigo for their input and helpful discussions.

I am indebted with Mrs Erika Menamkat for the hospitality and affection show to me during the months that I spent in Switzerland.

A special thanks goes to my family for their financial and moral support and their love that they have always shown me.

Finally I would like to remind all people that believe in me and appreciate me as I am.